

# Data-Driven Dynamic Factor Modeling via Manifold Learning

Graeme Baker\*      Agostino Capponi†      J. Antonio Sidaoui‡

## Abstract

We propose a data-driven dynamic factor framework where a response variable  $y(t) \in \mathbb{R}^n$  depends on a high-dimensional set of covariates  $x(t) \in \mathbb{R}^m$ , without imposing any parametric model on the joint dynamics. Leveraging Anisotropic Diffusion Maps, a nonlinear manifold learning technique introduced by Singer & Coifman, our framework uncovers the joint dynamics of the covariates and responses in a purely data-driven way. We approximate the embedding dynamics using linear diffusions, and exploit Kalman filtering to predict the evolution of the covariates and response variables directly from the diffusion map embedding space. We generalize Singer’s convergence rate analysis of the graph Laplacian from the case of independent uniform samples on a compact manifold to the case of time series arising from Langevin diffusions in Euclidean space. Furthermore, we provide rigorous justification for our procedure by showing the robustness of approximations of the diffusion map coordinates by linear diffusions, and the convergence of ergodic averages under standard spectral assumptions on the underlying dynamics. We apply our method to the stress testing of equity portfolios using a combination of financial and macroeconomic factors from the Federal Reserve’s supervisory scenarios. We demonstrate that our data-driven stress testing method outperforms standard scenario analysis and Principal Component Analysis benchmarks through historical backtests spanning three major financial crises, achieving reductions in mean absolute error of up to 55% and 39% for scenario-based portfolio return prediction, respectively.

## 1 Introduction

The emerging field of data-driven dynamical systems aims to learn the potentially high-dimensional and nonlinear dynamical description of a data set without parametric assumptions. Some of the primary goals in this area include finding stochastic differential equation (SDE) descriptions of discretely sampled time series data, extracting interpretable stochastic models from experimental data, and finding simple linear descriptions for high-dimensional and nonlinear dynamical systems. Herein, we propose a data-driven approach to the problem of *dynamic factor modeling* in the *supervised learning* setting where a response variable  $y(t) \in \mathbb{R}^n$  depends on a high-dimensional set of covariates  $x(t) \in \mathbb{R}^m$ . Dynamic factor models typically find a state-space representation of a set of observed measurements, and operate under the premise that a few latent dynamic factors drive the co-movements of a multivariate time series. These latent factors themselves follow a time series process, commonly a vector auto-regressive (VAR) process, and restrictive assumptions are often imposed. (For an in-depth survey of classical dynamic factor models, we recommend [SW16].) In this work, we propose a data-driven dynamic factor framework which accounts for nonlinear joint covariate and response dynamics.

---

\*Department of Statistics, Columbia University, NY, USA [g.baker@columbia.edu](mailto:g.baker@columbia.edu).

†Department of Industrial Engineering and Operations Research, Columbia University, NY, USA [ac3827@columbia.edu](mailto:ac3827@columbia.edu).

‡Department of Industrial Engineering and Operations Research, Columbia University, NY, USA [j.sidaoui@columbia.edu](mailto:j.sidaoui@columbia.edu).

Standard Dynamic Factor Models usually uncover the latent factors from a single set of measurements  $x(t)$ . However, if one wants to use these latent factors as covariates under a supervised learning framework where  $y(t) = f(x(t)) + \varepsilon_t$ , these models do not jointly consider the variation of  $y(t)$  when uncovering the dynamic latent factors. As a consequence, the estimated sparse set of latent factors may not contain explanatory power for the responses. Rather than assuming a parametric model for the covariate dynamics, we leverage the geometry of the time series data and exploit Anisotropic Diffusion Maps (ADM), a nonlinear dimensionality reduction technique introduced in [SC08]. This allows us to learn the intrinsic dynamics of the high-dimensional covariate vector via lower-dimensional diffusion map embeddings, while jointly preserving much of the explanatory power of the time series responses. We define a state space *completely in terms of the diffusion map embeddings* that allows us to approximate the dynamics of the system using Kalman filtering, and perform response prediction and covariate sampling directly from the embedding space.

We treat the observation vector  $(x(t), y(t)) \in \mathbb{R}^{m+n}$  as the state of a dynamical system at time  $t$ . We assume the covariates and response variables are nonlinear functions of a true, possibly lower-dimensional, underlying state of the system  $\theta_t \in \mathbb{R}^d$ , which is assumed to satisfy a Langevin diffusion. These nonlinear functions restrict the trajectories of the observations to lie on some (unknown) manifold  $\mathcal{M}$ . Figure 1 displays a broad overview of our setting. Our framework relies on three key steps: (1) uncover latent dynamic factors, (2) estimate underlying dynamics from these factors, and (3) predict responses from learned functional relationships.

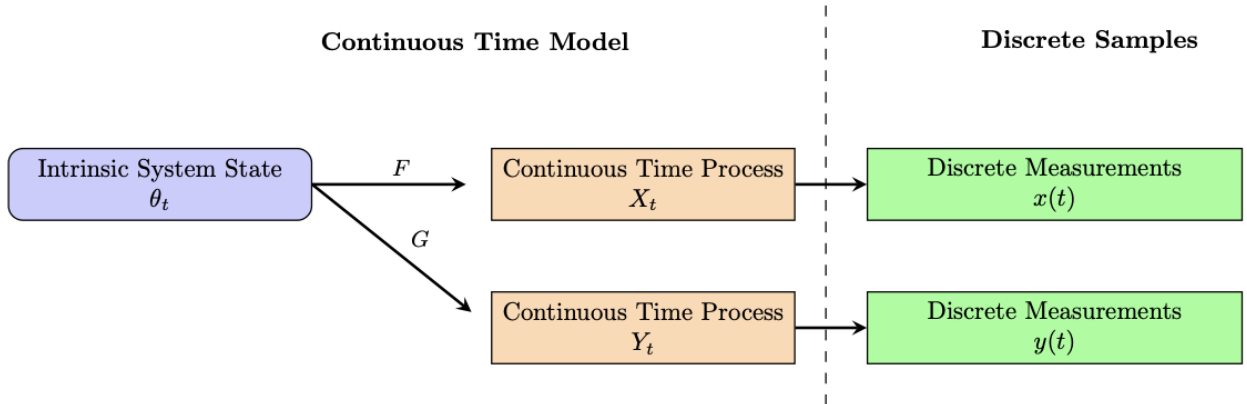


Figure 1: A diagram of the dynamical system setting.

Our framework relies on constructing dynamic diffusion coordinate embeddings of the observations that serve as proxies for the dynamics of  $\theta$ , combining state space modeling with diffusion maps. Commonly, dimensionality reduction methods, when applied to time series data, do not explicitly consider the temporal component in the data. This can be limiting in many applications, for instance, when dealing with high-dimensional financial market data where a portfolio manager (PM) might want to study how shocks to a given market factor propagate through time. By integrating Kalman filtering techniques with diffusion maps and extending the framework first introduced in [STS20], we construct dynamic diffusion coordinate embeddings which explicitly factor in the temporal component of the data. We construct our state space equations by leveraging a linear lifting operator that takes diffusion map embeddings back into the original measurement space.

The central mathematical contributions of our work are as follows: Applying concentration

inequalities for Markov processes, in Theorem 4.3 we generalize a result on the convergence of graph Laplacians from [Sin06] to the time series case, and show that the eigenfunctions of the Fokker–Planck operator associated with  $\theta$  can be learned. We provide rigorous justification for reconstructing points in the original data space via the lifting operator by establishing its convergence to an  $\mathbb{L}^2$ -projection with respect to the invariant measure of  $\theta$  (see Proposition 4.2). The rationale for utilizing diffusion maps and defining a state space framework completely in terms of these embeddings is the observation, first mentioned in [Coi+08], that the dynamics of the diffusion coordinate embeddings are *approximately linear*. Under standard spectral assumptions on the generator of  $\theta$ , we show in Subsection 4.3 that the approximation error using linear dynamics remains small when averaging over the data.

Since we approximate the intrinsic dynamics with a linear SDE in terms of the diffusion coordinate embeddings, our framework does not require us to discover the explicit joint dynamics of the observations  $(x(t), y(t))$ . Leveraging linear state-space equations, we devise a procedure to sample dynamic embeddings while conditioning on an information set defined in the original measurement space. It is well known that dimensionality reduction techniques give rise to the challenge of interpretability of the embeddings. In a framework such as ours that takes place completely in the embedding space, it is hence desirable to define fully interpretable conditioning events in the original measurement space. To define such a sampling procedure, we leverage the power of the linear lifting operator in a three step process: (1) lift statistics from the embedding space to the original measurement space, (2) condition on the desired information set in the covariate space and obtain the conditional distribution in terms of  $(x(t), y(t))$ , (3) restrict back to the embedding space with a pseudoinverse of the lifting operator. Our sampling procedure simultaneously learns the intrinsic geometry and dynamics from the data, and then *generates* sample paths for the diffusion coordinate embeddings and by extension of  $(x(t), y(t))$ . Of course, it is known that dimensionality reduction techniques do not necessarily preserve statistics in the data, hence approximating statistics in the measurement space with their lifted counterparts incurs some error. Our robustness results presented in Section 4 provide theoretical support for the applicability of our method.

We demonstrate the power of our framework for applications, focusing on problems from mathematical finance, where dynamical systems are ubiquitous. Continuous time processes, typically represented by SDEs, include interest rate models such as the Vasicek process, credit risk models such as Cox–Ingersoll–Ross, and derivatives pricing models such as Black–Scholes–Merton. Discrete time models are also widely present in financial applications; these include models for stochastic volatility such as ARCH and GARCH, and models for returns such as the standard autoregressive process. Strong parametric and modeling assumptions are often applied when fitting real-world data with stochastic processes.

Under comparably weak assumptions, our approach is applicable to a wide variety of problems. These include, for instance, asset pricing, where often one works with a high-dimensional “zoo” of candidate factors to explain the cross-section of stock returns. It is often desirable to construct a sparse set of factors, often latent, from the factor zoo in order to construct a model for the cross-section of returns. Our approach is well-suited for such a task as it produces lower-dimensional dynamic embeddings which propagate linearly, and also possess explanatory power comparable to the original high-dimensional set of factors. Another application is *nowcasting* (see [GRS08]), where one makes use of higher frequency/quality data to improve predictions on lower frequency/quality data. A third key application, with which we validate our framework via an empirical investigation, is financial stress testing and scenario analysis, which deals with predicting an asset or portfolio’s evolution conditional on a set of shocks to the risk factors that drive their value (see, for instance, [HL20]). Within the context of stress testing equity portfolios, we demonstrate the superiority of our framework over several comparison benchmarks including Principal Component Analysis (PCA)

via a series of historical rolling backtests. Our historical backtests span three major financial crisis periods and we demonstrate reductions in mean absolute error (MAE) of up to 55% and superior accuracy up to 77.78% of the time when utilizing our framework over the benchmarks.

The paper is organized as follows. Section 2 relates our work to the literature. Section 3 introduces our dynamic factor modeling framework and conditional sampling procedure. Section 4 presents key theoretical results, including convergence analysis of the graph Laplacian and the robustness of approximating the diffusion coordinates by linear diffusions. Section 5 describes the application of our method to financial stress testing: in 5.1 we describe the comparison benchmarks and 5.2 defines the historical backtesting procedure. Section 6 describes the data and the empirical results. We conclude in Section 7. Appendices A, B, C, D and E provide further details on the data, empirical results, implementation of benchmarks, and a lengthy calculation used for the analysis of the graph Laplacian.

## 2 Related Literature

Our paper contributes to the growing bodies of literature on data-driven stochastic systems, manifold learning, and dynamic factor modeling. Diffusion maps were introduced by [CL06] as a geometrically faithful dimensionality reduction technique. [Coi+08] present diffusion maps for feature extraction in high-dimensional stochastic systems, in particular, the first few eigenfunctions of the backward Fokker–Planck diffusion operator are proposed as a coarse-grained low-dimensional representation for the long-term evolution of a system. Our framework leverages the ADM algorithm first introduced in [SC08], and falls within the larger category of models that find linear reduced-order representations of high-dimensional nonlinear stochastic systems.

ADM recovers intrinsic parametrizations of independent and identically distributed (i.i.d.) data that have undergone a nonlinear transformation. The error analysis of ADM is based on a result from [Sin06] on the convergence of graph Laplacians, which we generalize from the case of uniform data on a compact manifold to data arising from a time series in Euclidean space. The heart of this analysis relies on a concentration inequality (called “the inequality of Chernoff” in [Sin06, paragraph before Equation (3.14)]) with the second moment of the summands as variance proxy. In [BH16, Appendix B.1], it is noted that Bernstein’s Inequality (see, for instance, [BLM13, Section 2.8]) is an applicable concentration inequality for the case of i.i.d. samples. In recent years, many concentration inequalities have been generalized for data arising from Markov chains (see, for instance [Ada08; Dou+11; Mia14; Pau15; FJS21]), and we will draw on this literature in Section 4.

As noted in the introduction, applying diffusion maps directly to time series data may be problematic since the data is not sampled uniformly and one should ideally take into account the temporal relationships in the data. Other works have also directly tackled the issue of explicitly incorporating the time dependencies into the diffusion coordinates or devised diffusion map-based models for multivariate time series. [STS20] propose a nonparametric framework for state-estimation of stochastic dynamical systems that are high-dimensional and evolve according to gradient flows with isotropic diffusion. Their framework combines diffusion maps with Kalman filtering and concepts from Koopman operator theory, and relies on the existence of a linear lifting operator. In Section 3.3, we extend and generalize this framework to admit two datasets, one of responses and one of covariates, to perform supervised learning tasks and ensure the estimated hidden states contain explanatory power for the responses. [ST22] present a data-driven approach for time series analysis that combines diffusion maps with contracting observers from control theory, and their main goal is to construct a low-dimensional representation of high-dimensional signals generated by dynamical systems without requiring strong modeling assumptions. [Lia+15] intro-

duce a method to analyze multivariate time series using diffusion maps on a parametric statistical manifold; the framework handles high-dimensional nonstationary signals that are subject to random interference and ambient noise, which could degrade the performance of more conventional methodologies.

Some of the aforementioned works, for instance, [Coi+08] and [STS20], make the assumption that the dynamics of the intrinsic latent state evolve according to a Langevin equation, a key assumption we carry forward into our work. In those works, it is suggested that the dynamics of the diffusion coordinates should approximately follow linear SDEs. Indeed, in Section 4, we establish a new robustness result showing that the approximation error using linear diffusions remains small when averaging over the data, and provided that some spectral assumptions are satisfied. When it comes to financial applications, it is worth noting that the class of Langevin diffusions encompasses a wide variety of stochastic processes ubiquitous in the finance literature (see Table 2), exemplified by the Ornstein-Uhlenbeck process. For the use of Langevin dynamics to model stock prices see, for instance, the early works [BC98; Can01].

An important financial application where dynamic factor models can yield powerful methodologies is financial stress testing and scenario analysis, which consists in predicting a portfolio’s profit & loss (P&L) when subsets of the risk factors that drive the portfolio’s value experience shocks. In [HL20], scenario analysis is embedded within a dynamic factor framework by defining a linear Gaussian state space model. There, derivatives portfolios are considered and the risk factors are low-dimensional, as is usually the case in stress testing. Our state space model, outlined in 3.3, allows one to define arbitrarily high-dimensional scenarios, and unlike the framework in [HL20] is purely data-driven and nonparametric, overcoming restrictive assumptions, like a VAR(1) process for the latent factors. Furthermore, our state space model is explicitly designed to admit two sets of observations (covariates and responses) and considers their joint dependence on the latent state as well as their joint dynamics, thus resulting in a supervised learning dynamic factor framework.

### 3 The Model

We propose a data-driven approach to dynamic factor modeling and conditional sampling for a supervised learning setting where *response variables* depend on a high-dimensional set of *covariates*. Rather than assuming a restrictive parametric model for the dynamics of the observations, we leverage the data-driven anisotropic diffusion maps (ADM) algorithm from [SC08] to learn the dynamics of a set of eigenfunctions associated with an intrinsic latent state. Motivated by the Kalman filtering framework of [STS20], we develop a sampling procedure to carry out scenario analysis in the original variable spaces, preserving the explanatory power of the observed data. We adopt the notations found in Table 1 throughout the remainder of the paper. We adopt the following conventions for stochastic processes:  $X_t$  (upper case Latin letter with subscript) is a continuous time process at time  $t$ ,  $x(t)$  (lower case Latin letter with bracketed argument) is a discrete time sample of  $X_t$ , and  $x_t$  (lower case Latin letter with subscript) is a linear state space approximation for  $x(t)$ . The convention for Greek letters will depend on context.

#### 3.1 Dynamical System Setting

Given integers  $m, n > 0$ , we model the *covariates*  $X = (X_t)_{t \geq 0}$  and *response variables*  $Y = (Y_t)_{t \geq 0}$  as continuous-time stochastic processes taking values in  $\mathbb{R}^m$  and  $\mathbb{R}^n$ , respectively. We model  $X$  and  $Y$  as nonlinear mappings of a latent stochastic process  $\theta = (\theta_t)_{t \geq 0}$ , which takes values in  $\mathbb{R}^d$  for some unknown dimension  $d$ . We introduce our key assumptions next.

Notation	Description
$\nabla$	gradient
$\Delta$	Laplacian
$I$	identity matrix
$C^2$	space of twice differentiable functions
$\mathbb{L}^2(\mu)$	space of square integrable functions with respect to a measure $\mu$
$\langle \cdot, \cdot \rangle_\mu$	$\mathbb{L}^2(\mu)$ inner product
$\  \cdot \ _{\mathbb{L}^2(\mu)}$	$\mathbb{L}^2(\mu)$ norm

Table 1: Frequently-used notations.

**Assumption 1** (Langevin Diffusion). *The latent variables  $\theta = (\theta_t)_{t \geq 0}$  satisfy a Langevin diffusion:*

$$d\theta_t = -\nabla U(\theta_t)dt + \sqrt{2}dW_t \quad (3.1)$$

where  $W = (W^1, \dots, W^d)$  is a Brownian motion in  $\mathbb{R}^d$  and  $U$  is a  $C^2$  potential function satisfying the following growth condition at infinity:

$$\lim_{\|w\| \rightarrow \infty} \left[ -\Delta U(w) + \frac{1}{2} |\nabla U(w)|^2 \right] = \infty. \quad (3.2)$$

The invariant measure for the dynamics of  $\theta$  is given by

$$\mu(dw) = \frac{1}{Z} \exp(-U(w))dw,$$

where  $Z$  is a normalizing constant (see, for instance, [BGL14, Section 1.15.7]). We let  $p(w) = \frac{1}{Z} \exp(-U(w))$  denote the density of  $\mu$ . Condition (3.2) ensures that the Fokker–Planck operator or generator associated with  $\theta$  given by

$$\mathcal{L} := \Delta - \nabla U \cdot \nabla$$

has a discrete spectrum, see [BGL14, Corollary 4.10.9].

**Assumption 2** (Manifold Hypothesis). *There exist  $C^2 \cap \mathbb{L}^2(\mu)$  functions  $F : \mathbb{R}^d \rightarrow \mathbb{R}^m$  and  $G : \mathbb{R}^d \rightarrow \mathbb{R}^n$  such that  $X_t = F(\theta_t)$  and  $Y_t = G(\theta_t)$  for all  $t \geq 0$ .*

*Remark 3.1.* Often, a Langevin diffusion is given with the coefficient  $\sqrt{2/\beta}$  in front of  $dW_t$ , where  $\beta > 0$  is a fixed constant. Here, we choose to absorb this additional degree of freedom into the unknown functions  $F$ ,  $G$ , and  $U$ .

Some vector calculus shows that the carré du champ operator for  $\mathcal{L}$ , denoted by  $\Gamma$ , and defined by  $\Gamma(f, g) = \frac{1}{2} (\mathcal{L}(fg) - f\mathcal{L}g - g\mathcal{L}f)$  satisfies  $\Gamma(f, g) = \nabla f \cdot \nabla g$ . Integration by parts gives

$$-\int_{\mathbb{R}^d} f\mathcal{L}g d\mu = -\int_{\mathbb{R}^d} g\mathcal{L}f d\mu = \int_{\mathbb{R}^d} \Gamma(f, g) d\mu = \int_{\mathbb{R}^d} \nabla f \cdot \nabla g d\mu. \quad (3.3)$$

Therefore, the spectrum of  $-\mathcal{L}$ , denoted  $0 = \lambda_0 \leq \lambda_1 \leq \dots$ , is contained in  $[0, \infty)$ . The diffusion maps algorithm uncovers the relationship between the latent variables and the observations by relying on the following fact: any  $f \in \mathbb{L}^2(\mu)$  can be decomposed as

$$f(w) = \sum_{k=0}^{\infty} a_k \varphi_k(w) \quad (3.4)$$

where  $(\varphi_k)_{k=0}^\infty$  is a complete orthonormal sequence of eigenfunctions for  $\mathcal{L}$  and for each  $k$

$$a_k = \langle f, \varphi_k \rangle_\mu = \int_{\mathbb{R}^d} f(w) \varphi_k(w) \mu(dw). \quad (3.5)$$

Our next and final assumption ensures that  $\lambda_0 = 0$  is a simple eigenvalue of  $-\mathcal{L}$ , and all of the other eigenvalues of  $-\mathcal{L}$  are bounded away from zero.

**Assumption 3** (Poincaré Inequality). *We assume there exists some  $C > 0$  so that for any  $f \in \mathbb{L}^2(\mu)$*

$$\text{Var}_\mu(f) \leq C \mathbb{E}_\mu[\|\nabla f\|_2^2].$$

If  $\varphi_k$  is an eigenfunction of  $\mathcal{L}$  with eigenvalue  $\lambda_k \neq 0$ , then equation (3.3) along with a Poincaré Inequality implies that  $\lambda_k \geq 1/C$ . In fact, the above Poincaré inequality is equivalent to the existence of a *spectral gap* for  $-\mathcal{L}$ , that is,  $\lambda_1 - \lambda_0 = \lambda_1 \geq 1/C$ . We remark that the term spectral gap is often employed in the diffusion maps literature to mean a gap in the spectrum other than between  $\lambda_0$  and  $\lambda_1$  (see, for instance, [Coi+08, Section 3.2]).

*Remark 3.2.* If  $\nabla^2 U \geq \rho I$  for some  $\rho > 0$ , then  $\mu$  satisfies a Poincaré inequality with  $C = 1/\rho$ . For instance, if  $U(x) = \frac{1}{2}x^T A x$  with  $A$  positive definite, then  $\mu$  is a non-degenerate Gaussian, the smallest eigenvalue of  $A$  gives the spectral gap  $\rho$ , and  $1/\rho$  is in fact the best Poincaré constant. However, this condition is not necessary, for instance, the two-sided exponential (a.k.a. Laplace) distribution  $\frac{1}{2}e^{-|x|}$  on  $\mathbb{R}$  satisfies a Poincaré inequality with  $C = 4$ .

Itô's formula yields the dynamics for a  $C^2$  function of  $\theta$ , such as  $X$  or  $Y$ . For instance,  $X = (X^1, \dots, X^m)$  satisfies (in components):

$$\begin{aligned} dX_t^j &= (-\nabla F_j(\theta_t) \cdot \nabla U(\theta_t^i) + \Delta F_j(\theta_t)) dt + \sqrt{2} \nabla F_j(\theta_t) \cdot dW_t \\ &= \mathcal{L}F(\theta_t) dt + \sqrt{2} \nabla F_j(\theta_t) \cdot dW_t \\ &= \mathcal{L}F(\theta_t) dt + \sqrt{2} \|\nabla F_j(\theta_t)\|_2 \cdot dB_t^j, \quad j = 1, \dots, m, \end{aligned} \quad (3.6)$$

where  $B^j$  is a Brownian motion by Lévy's Theorem (see, for instance, a similar derivation for the case of Bessel processes in [KS14, Proposition 3.3.21]). And similarly, writing  $Y = (Y^1, \dots, Y^n)$  we have  $dY_t^j = \mathcal{L}G(\theta_t) dt + \sqrt{2} \nabla G_j(\theta_t) \cdot dW_t$ , and so on. These SDEs admit the flexibility to capture many of the standard models of mathematical finance, as shown in Table 2. For illustrative purposes, we will work with a low-dimensional example which gives rise to Ornstein–Uhlenbeck (OU) and Cox–Ingersoll–Ross (CIR) processes:

**Example 3.3** (OU and CIR Processes). Suppose that  $U$  is given by  $U(w) = \frac{1}{2}(w_1^2 + w_2^2)$  for  $w \in \mathbb{R}^2$ . In this case,  $\theta$  is a 2-dimensional Ornstein–Uhlenbeck process satisfying  $d\theta_t = -\theta_t dt + \sqrt{2} dW_t$ , the Fokker–Planck operator satisfies  $\mathcal{L}f(w) = \Delta f(w) - w \cdot \nabla f(w)$ , and the invariant distribution  $\mu$  is  $N(0, I)$ . The Hermite polynomials  $(h_k)_{k \geq 0}$  are defined by

$$h_k(x) = \frac{(-1)^k}{\sqrt{k!}} \exp\left(\frac{x^2}{2}\right) \frac{d^k}{dx^k} \exp\left(-\frac{x^2}{2}\right), \quad x \in \mathbb{R}.$$

The first several Hermite polynomials are given by  $h_0 = 1$ ,  $h_1(x) = x$ , and  $h_2(x) = \frac{1}{\sqrt{2}}(x^2 - 1)$ . Note that  $\mathcal{L}h_k(w_1) = -kh_k(w_1)$  and  $h'_k(w_1) = \sqrt{k}h_{k-1}(w_1)$  for  $w_1 \in \mathbb{R}$ . An orthonormal basis for

$\mathbb{L}^2(\mu)$  is given by the family  $(h_{i,j})_{i,j \geq 0}$  where  $h_{i,j}(w) := h_i(w_1)h_j(w_2)$  for any  $w \in \mathbb{R}^2$ . Consider the case where  $X_t = (\theta_t^1)^2 + (\theta_t^2)^2$  so that

$$dX_t = -2 [(\theta_t^1)^2 + (\theta_t^2)^2 - 2] dt + 2\sqrt{2}\theta_t^1 dW_t^1 + 2\sqrt{2}\theta_t^2 dW_t^2 = -2(X_t - 2)dt + 2\sqrt{2X_t}dB_t,$$

where  $B$  is a standard Brownian motion, by Lévy's Theorem.  $X$  is a CIR process, a popular model for non-negative data such as interest rates, typically. We may take  $Y_t = \theta_t^1$ , so that  $Y$  is a 1-dimensional OU process. We note for later use that  $d\langle X, Y \rangle_t = 4Y_t dt$ .

$U$	$F$	$X$
linear	exponential	Black–Scholes–Merton
linear	$\ \cdot\ _2$	Bessel
quadratic	linear	Ornstein–Uhlenbeck/Vasicek
quadratic	quadratic	Cox–Ingersoll–Ross (CIR)
quadratic	power	constant elasticity of variance (CEV)

Table 2: Common stochastic processes from mathematical finance which can be written in the form  $X_t = F(\theta_t)$  with  $d\theta_t = -\nabla U(\theta_t)dt + \sqrt{2}dW_t$ . These may all be checked using Itô's formula, see for instance, [JYC09, Sections 2.6 and 6.4] for the necessary computations in the case of CIR and CEV processes. Note also that a linear  $U$  does not satisfy the growth condition (3.2); however, these processes can be approximated locally.

*Remark 3.4.* In [SC08], diffusion maps were used to uncover the dynamics of  $\theta$  when the components  $\theta^1, \dots, \theta^d$  are *independent* homogeneous diffusions of the form  $d\theta_t^i = b^i(\theta_t^i)dt + \sigma^i(\theta_t^i)dW_t^i$  with drifts  $b^1, \dots, b^d$  and non-degenerate diffusion coefficients  $\sigma^1, \dots, \sigma^d$ . In this case, one may apply a Lamperti Transformation (see [KS14, Chapter 5, Exercise 2.20]) to map the diffusion coefficients to constants, provided some integrability and boundedness assumptions hold on  $b^i$  and  $\sigma^i$ . Specifically, for each  $i$ , let  $g^i$  be an antiderivative of  $1/\sigma^i$  and define  $\tilde{\theta}_t^i = g^i(\theta_t^i)$ . Then Itô's lemma gives

$$d\tilde{\theta}_t^i = \left( \frac{b^i(\theta_t^i)}{\sigma^i(\theta_t^i)} - \frac{(\sigma^i)'(\theta_t^i)}{2} \right) dt + dW_t^i$$

While the functions  $U, F, G$  and the dimension  $d$  are unobserved, the quadratic covariation processes of  $X$  and  $Y$  yield information about the Jacobians of  $F$  and  $G$ :

$$\begin{aligned} d\langle X^j, X^k \rangle_t &= 2\nabla F_j(\theta_t) \cdot \nabla F_k(\theta_t)dt, \quad j, k = 1, \dots, m \\ d\langle Y^j, Y^k \rangle_t &= 2\nabla G_j(\theta_t) \cdot \nabla G_k(\theta_t)dt, \quad j, k = 1, \dots, n. \end{aligned}$$

To illustrate, let  $w, \tilde{w} \in \mathbb{R}^d$  and set  $x = F(w)$  and  $\tilde{x} = F(\tilde{w})$ . Denoting the Jacobian matrix for  $F$  by  $J_F$ , a Taylor approximation as in [SC08] gives

$$\|w - \tilde{w}\|^2 = \frac{1}{2}(x - \tilde{x})^T \left( (J_F J_F^T)^{-1}(x) + (J_F J_F^T)^{-1}(\tilde{x}) \right) (x - \tilde{x}) + O(\|x - \tilde{x}\|^4) \quad (3.7)$$

The first term is a *modified Mahalanobis distance*. Hence, distances in the latent space can be approximated using observations of  $X$  and/or  $Y$  along with estimates of the quadratic covariation processes. In the next subsection, we follow this insight to uncover the eigenvalues and eigenfunctions of the Fokker–Planck operator associated with the dynamics of  $\theta$ .

### 3.2 Data-Driven Embedding

Following [SC08], we describe the anisotropic diffusion maps algorithm which is used to uncover the evolution of the latent coordinates. Let  $Z = H(\theta)$  be a  $C^2 \cap \mathbb{L}^2(\mu)$  mapping of  $\theta$ , and suppose we are given a data set of  $N + 1$  discrete-time observations of  $Z$ , denoted  $(z(t_i))_{i=0}^N$ . Depending on the application at hand, and the size and quality of the data sets, we may for instance take  $Z = X$ ,  $Z = Y$ , or  $Z = (X, Y)$ . To fix notation, we consider the situation here where  $Z = (X, Y)$  so that  $H = (F, G) : \mathbb{R}^d \rightarrow \mathbb{R}^{m+n}$ . We assume that the data has been mean-centered.

Motivated by the Taylor approximation (3.7) in the previous subsection, we consider the modified Mahalanobis distance between  $z_i$  and  $z_j$ :

$$d(z(t_i), z(t_j)) := \frac{1}{2}(z(t_i) - z(t_j))^T (C^{-1}(t_i) + C^{-1}(t_j))(z(t_i) - z(t_j)),$$

where  $C(t_i)$  denotes the instantaneous quadratic covariation matrix of  $z(t_i)$ . In Section 5, we approximate  $C(t_i)$  by its sample average in a trailing window. For strictly positive financial data, one can also use an estimator such as the one presented in [CE95].

We construct a distance matrix for the data  $\mathbf{D} \in \mathbb{R}^{N+1} \times \mathbb{R}^{N+1}$  with entries  $\mathbf{D}_{ij} = d(z(t_i), z(t_j))$ . We pass the entries of  $\mathbf{D}$  through the Radial Basis Function (RBF) kernel  $\exp(-d(\cdot, \cdot)/2\varepsilon)$  with parameter  $\varepsilon > 0$  to obtain an adjacency matrix  $\mathbf{W}$ :

$$\mathbf{W}_{ij} = \exp\left(-\frac{d(z(t_i), z(t_j))}{2\varepsilon}\right).$$

A popular choice for practitioners is to choose  $\varepsilon$  as the median of all distances between data points (see [STS20] or Subsection 6.2). Another methodology (see [Sin+09, Figure 3]) is to choose  $\varepsilon$  in a region where the Log-Log plot of the sum of all entries of  $\mathbf{W}$  versus  $\varepsilon$  is linear. In any case,  $\mathbf{W}$  is then normalized to create a stochastic matrix  $\mathbf{P}$  (which is in fact doubly-stochastic as it is symmetric):

$$\mathbf{P}_{ij} = \frac{\mathbf{W}_{ij}}{\sum_{j=0}^N \mathbf{W}_{ij}}.$$

In Theorem 4.3, we show that the *graph Laplacian*  $\mathbf{P} - I$  approximates the Fokker-Planck operator  $\mathcal{L}$  in the following sense: if  $(z(t_i))_{i=0}^N = (H(\theta(t_i)))_{i=0}^N$  where  $\theta$  satisfies the dynamics in Assumption 1, and if  $f : \mathbb{R}^{m+n} \rightarrow \mathbb{R}$  is such that  $f \circ H \in \mathbb{L}^2(\mu)$  then the  $i$ th row of  $(\mathbf{P} - I)$  applied to the vector  $[f(z(t_0)), \dots, f(z(t_N))]$  satisfies

$$\sum_{j=0}^N \mathbf{P}_{ij} f(z(t_j)) - f(z(t_i)) = \varepsilon \mathcal{L}(f \circ H)(\theta(t_i)) + O(\varepsilon^2)$$

with high probability. This is the key insight of diffusion maps: if  $f$  is an eigenvector of  $\mathbf{P}$  with eigenvalue  $\kappa$  (note that  $\mathbf{P} - I$  and  $\mathbf{P}$  share eigenvectors), then  $f \circ H$  is approximately an eigenfunction of  $\mathcal{L}$ . Using the approximation  $\mathbf{P} \approx I + \varepsilon \mathcal{L} \approx \exp(\varepsilon \mathcal{L})$ , an estimate for the associated eigenvalue of  $-\mathcal{L}$  is given by the spectral mapping  $\lambda = -\varepsilon^{-1} \log \kappa > 0$ . Since the spectrum of  $\mathcal{L}$  is discrete, one can hope to approximate functions of the latent state  $\theta$ , using truncations of the eigenfunction expansion (3.4). This motivates using the eigenvectors of  $\mathbf{P}$  as *diffusion coordinates*, a geometrically faithful representation of the underlying system states. We denote the ordered eigenvalues and an associated basis of  $\mathbb{R}^{N+1}$ -orthonormal eigenvectors of  $\mathbf{P}$  by

$$1 = \kappa_0 \geq \dots \geq \kappa_N \geq 0, \quad \text{and} \quad \psi_0, \dots, \psi_N.$$

As our data is mean-centered, we discard the first eigenvector (a constant vector corresponding to eigenvalue 1) and keep eigenvectors 1 through  $\ell$ , for some  $\ell > 0$ . Practitioners commonly choose  $\ell$  to correspond to the eigenvalue preceding the largest drop-off  $\kappa_i - \kappa_{i+1}$  (see, for instance, Subsection 6.2 or [Coi+08, Subsection 3.2]). In the context of Example 3.3, a higher value of  $\ell$  corresponds to a set of polynomials with higher maximum degree.

**Definition 3.5.** The *diffusion coordinates* at each time  $t_i$  are given by  $\psi(t_i) := [\psi_1(t_i), \dots, \psi_\ell(t_i)]$ .

Following, [STS20], we approximate the observed data by a *lifting operator*  $z(t_i) = \mathbf{H}\psi(t_i)$ , which is given in coordinates by

$$z_j(t_i) \approx \sum_{k=1}^{\ell} \mathbf{H}_{j,k} \psi_k(t_i), \quad j = 1, 2, \dots, m$$

where  $\mathbf{H}_{j,k} = \langle z_j, \psi_k \rangle_{\text{data}} := (N+1)^{-1} \sum_{i=0}^N z_j(t_i) \psi_k(t_i)$ . We note the analogy to (3.5), the  $\mathbb{L}^2(\mu)$ -projection of  $Z_t^j = H(\theta_t)$  onto an  $\mathcal{L}$ -eigenfunction  $\varphi_k$ . In Proposition 4.2, we consider  $N^{-1/2} \mathbf{H}_{j,k}$  for large  $N$ , which is asymptotically normal.

*Remark 3.6.* Notice that  $\langle \cdot, \cdot \rangle_{\text{data}}$  is defined in [STS20] without the normalization by  $N+1$ . Note also that the diffusion coordinates themselves are of order  $O(N^{-1/2})$ , as they are the coordinates of  $\mathbb{R}^{N+1}$ -orthonormal vectors. These scaling factors are of no consequence for the state-space model presented in the next subsection, since the diffusion coordinates are treated as hidden variables and may be rescaled as one wishes.

Next, we consider the dynamics of the eigenfunctions of  $\mathcal{L}$ , which we will approximate using diffusion coordinates. Suppose that  $\varphi_1, \dots, \varphi_\ell$  satisfy  $\mathcal{L}\varphi_i = -\lambda_i \varphi_i$  for  $i = 1, \dots, \ell$ . Just as with (3.6), Itô's lemma gives

$$\begin{aligned} d\varphi_i(\theta_t) &= -\nabla U(\theta_t) \cdot \nabla \varphi_i(\theta_t) dt + \Delta \varphi_i(\theta_t) dt + \sqrt{2} \nabla \varphi_i(\theta_t) \cdot dW_t \\ &= \mathcal{L}\varphi_i(\theta_t) dt + \sqrt{2} \|\nabla \varphi_i(\theta_t)\|_2 dB_t^i \\ &= -\lambda_i \varphi_i(\theta_t) dt + \sqrt{2} \|\nabla \varphi_i(\theta_t)\|_2 dB_t^i, \end{aligned} \tag{3.8}$$

where  $B^i$  is a Brownian motion and we have applied Lévy's Theorem for the second equality. Note also that for  $i \neq j$  we have

$$d\langle \varphi_i(\theta_t), \varphi_j(\theta_t) \rangle_t = 2 \nabla \varphi_i(\theta_t) \cdot \nabla \varphi_j(\theta_t) dt$$

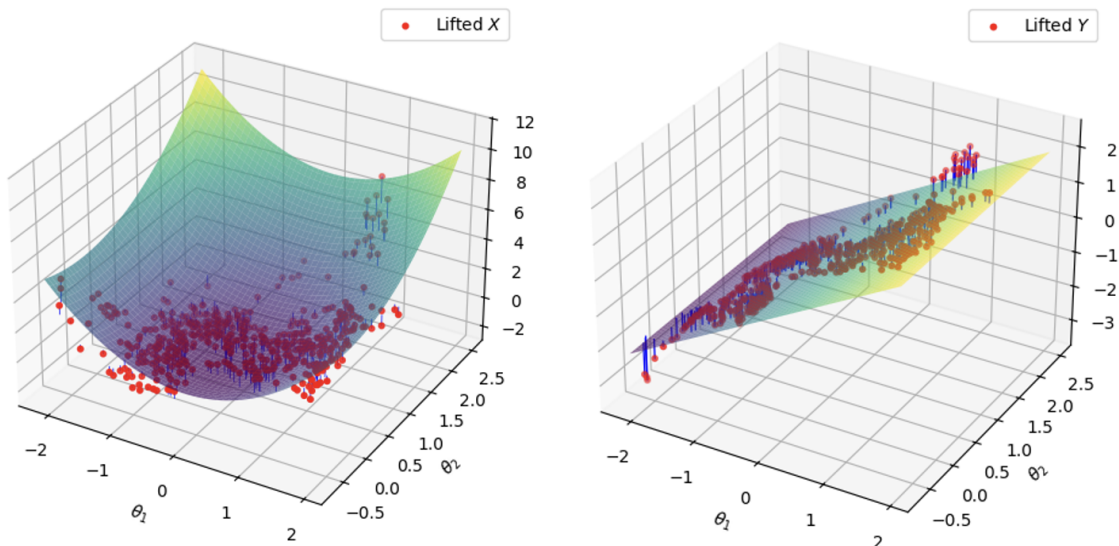
The right hand side is twice the *carré du champ* operator for  $\mathcal{L}$  applied to  $\varphi_i$  and  $\varphi_j$ . The identity (3.3) gives

$$\int \nabla \varphi_i(w) \cdot \nabla \varphi_j(w) \mu(dw) = - \int \varphi_i(w) \mathcal{L}\varphi_j(w) \mu(dw) = 0,$$

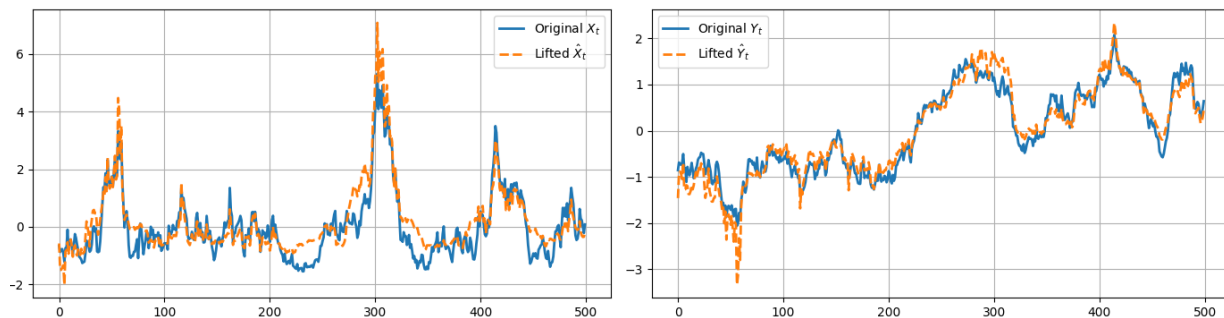
by orthogonality of eigenfunctions. The above analysis suggests that the dynamics of the eigenvectors  $\psi(t)$  of  $\mathbf{P}$  can be approximated using uncorrelated processes with linear drifts determined by the associated eigenvalues. Indeed, this is justified rigorously in Subsection 4.3. Along with the lifting operator  $\mathbf{H}$ , this motivates the use of a linear state space model and Kalman filter as described in the next subsection.

Before turning to our data-driven methodology, we return to Example 3.3 and illustrate the use of diffusion maps on synthetic data. We perform a simulation of the observation vector  $z(t) = (x(t), y(t))$  composed of 500 discrete-time samples of the processes  $X$  and  $Y$ , respectively. The data

has been mean-centered and the covariation process is approximated using a windowed covariance matrix, with a trailing window of size 50. Since we have access to the true  $\theta$  and the ground-truth Hermite polynomial eigenfunctions, we can assess how well the diffusion coordinates recover the eigenfunctions of  $\mathcal{L}$ , as well as the reconstruction quality of the  $X$  and  $Y$  processes via the lifting operator  $\mathbf{H}$ , using the dominant 10 diffusion map eigenvectors. Figures 2a and 2b below display the reconstructed  $X$  and  $Y$  processes both in terms of time series and hypersurfaces.

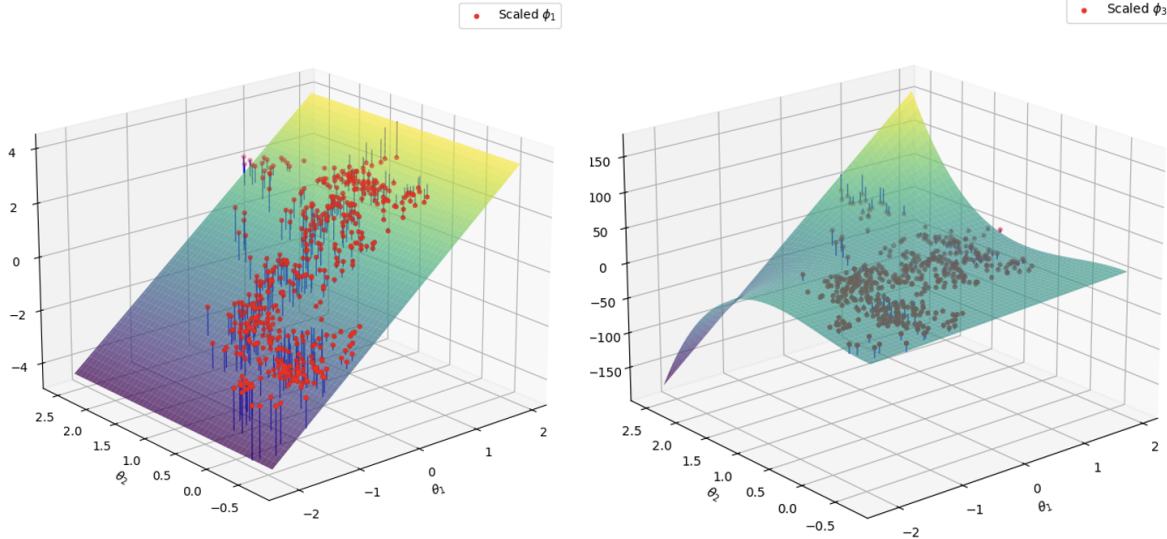


(a) True  $X_t$  (left) and  $Y_t$  (right) surfaces as a function of  $\theta_t$  and stem plots of the lifted reconstructions via  $\mathbf{H}\psi(t)$ .

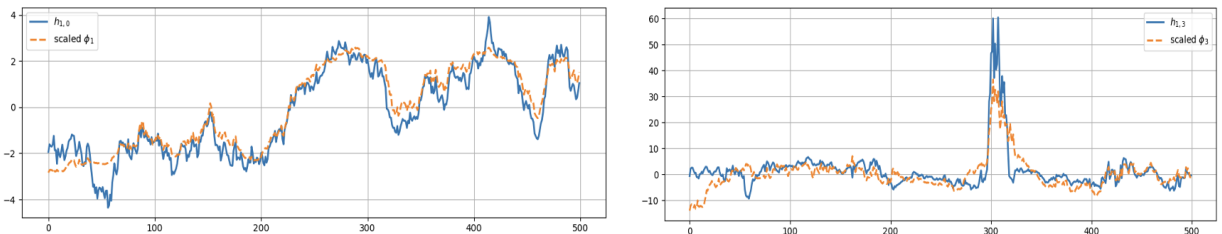


(b) True  $X_t$  (left) and  $Y_t$  (right) as a function of time and the lifted time series via  $\mathbf{H}\psi(t)$ .

Similarly, Figures 2c and 2d below display two ground-truth Hermite eigenfunctions of the backward Fokker-Planck operator  $\mathcal{L}$  and their approximation via the diffusion map eigenvectors, both in terms of time series and hypersurfaces. The observed fit is satisfactory in these cases; however, we note that the diffusion maps algorithm may be learning a *different* basis than these Hermite eigenfunctions (even restricting to polynomials, there are an uncountable number of such bases due to the rotational invariance of the Gaussian density).



(c) Hermite polynomials  $h_{1,0}$  (left) and  $h_{1,3}$  (right) surfaces as a function of  $\theta_t$  alongside stem plots of  $\psi_1(t)$  and  $\psi_3(t)$  respectively.



(d) Hermite polynomials  $h_{1,0}$  (left) and  $h_{1,3}$  (right) as a function of time against the time series  $\psi_1(t)$  and  $\psi_3(t)$  respectively.

Figure 2: Eigenfunction recovery and path reconstructions for the simulation of Example 3.3

### 3.3 Joint Diffusion Kalman Filter

We describe here our linear state space approximation for the dynamics of the diffusion coordinates. Assuming that the gradients in (3.8) are constant, [STS20] define a state-space model, dubbed the Diffusion Kalman Filter (DKF), for the case where the data arises from a single data set  $(x(t_i))_{i=0}^N$  (see Appendix A). We now modify DKF for a supervised learning framework to incorporate information in the series of the dependent variables  $y(t_i)$ , which depend jointly with  $x(t_i)$  on  $\theta(t_i)$ . If one were to use the estimated diffusion coordinates from DKF as developed in [STS20], a simple OLS regression of the dependent variables on these coordinates will show that most of the explanatory power of the original covariates  $x(t_i)$  for the dependent variables is lost (see, for instance, Appendix B for the regression of individual stock returns on a high-dimensional set of macroeconomic covariates). Thus, it is important to extend DKF to also account for the variation in the dependent variable in order for the diffusion coordinates to preserve explanatory power. We call this approach the Joint Diffusion Kalman Filter (JDKF). In this supervised learning framework, we adopt the dynamical system setting from Subsection 3.1:

$$d\theta_t = -\nabla U(\theta_t) + \sqrt{2}dW_t \in \mathbb{R}^d,$$

$$X_t = F(\theta_t) \in \mathbb{R}^m, \text{ and } Y_t = G(\theta_t) \in \mathbb{R}^n.$$

Following the procedure in Subsection 3.2, the diffusion coordinates  $\psi(t_i)$  are computed jointly on samples of  $(X, Y)$ , denoted  $(x(t_i), y(t_i))_{i=0}^N$ , and  $x$  and  $y$  can be similarly reconstructed by the linear lifts:

$$\begin{aligned} x(t_i) &\approx \mathbf{H}^x \psi(t_i) \\ y(t_i) &\approx \mathbf{H}^y \psi(t_i) \end{aligned}$$

where  $\mathbf{H}_{i,j}^x = \langle x_i, \psi_j \rangle_{\text{data}}$  and  $\mathbf{H}_{i,j}^y = \langle y_i, \psi_j \rangle_{\text{data}}$ . Let  $\Lambda$  denote the transition matrix for the linear dynamics containing the mapped eigenvalues  $-\varepsilon^{-1} \log \kappa_1, \dots, -\varepsilon^{-1} \log \kappa_\ell$  on its diagonal.

Going forward, we denote variables in our linear state space using lower case letters and subscripts taking values in  $\mathbb{Z}_{\geq 0}$  (e.g.  $x_t$  and  $\psi_t$ ). As with DKF, we consider a state transition equation where  $\psi_t$  evolves over time according to the linear dynamics

$$\psi_{t+1} = \mathbf{A}\psi_t + w_t, \quad w_t \sim \mathcal{N}(0, \mathbf{Q}) \quad (3.9)$$

where  $\psi_t \in \mathbb{R}^\ell$  is the latent state vector at time  $t$ ;  $\mathbf{A} = I - \Lambda \in \mathbb{R}^{\ell \times \ell}$  is the state transition matrix; and  $\mathbf{Q} \in \mathbb{R}^{\ell \times \ell}$  is the process noise covariance. We observe two variables,  $x_t$  (the discrete time covariate samples) and  $y_t$  (the discrete time response samples) and postulate the following two measurement state-space equations:

$$\begin{aligned} x_t &= \mathbf{H}^x \psi_t + v_{x,t} \\ y_t &= \mathbf{H}^y \psi_t + v_{y,t} \end{aligned} \quad (3.10)$$

where  $v_{x,t} \sim \mathcal{N}(0, \mathbf{R}_x)$  and  $v_{y,t} \sim \mathcal{N}(0, \mathbf{R}_y)$  with cross-covariance  $\mathbf{R}_{xy}$  model noise due to reconstruction error. We estimate  $\mathbf{R}_x$  and  $\mathbf{R}_y$  and construct estimates  $\hat{\psi}_{t+1} = \mathbb{E}[\psi_{t+1} | \{x_i, y_i\}_{i=0}^t]$  using the EM algorithm described below:  $\mathbf{A} = I - \Lambda$  is computed from applying diffusion maps jointly on  $(x(t_i), y(t_i))_{i=0}^N$ , and  $\mathbf{Q}$  is computed as the empirical covariance matrix of the resulting diffusion coordinates.

An important special case is the linear multi-factor model, with  $G = \mathbf{B} \circ F$  where  $\mathbf{B}$  is a matrix of regression coefficients (also known as factor loadings). In this case, we compute  $\Lambda$  and  $\mathbf{H}^x$  using  $(x(t_i))_{i=0}^N$  and postulate:

$$\begin{aligned} Y_t &= G(\theta_t) = \mathbf{B} \circ F(\theta_t) = \mathbf{B}X_t, \\ y_t &= \mathbf{B}\mathbf{H}^x \psi_t + v_{y,t}. \end{aligned}$$

Note that  $v_{y,t}$  here is a noise *correlated* with  $v_{x,t}$  through  $\mathbf{B}$ . Concretely, for a *linear factor model* of the form  $y_t = \mathbf{B}x_t + \varepsilon_{y,t}$ , where  $\varepsilon_{y,t}$  represents Gaussian idiosyncratic noise, we can cast the state space equation for  $y_t$  in terms of  $\psi_t$  as follows:

$$y_t = \mathbf{B}x_t + \varepsilon_{y,t} = \mathbf{B}(\mathbf{H}^x \psi_t + v_{x,t}) + \varepsilon_{y,t} = \mathbf{B}\mathbf{H}^x \psi_t + \underbrace{(\mathbf{B}v_{x,t} + \varepsilon_{y,t})}_{v_{y,t}}$$

In this linear case, we additionally aim to estimate  $\mathbf{B}$  and we have the following state-space representation in terms of  $\psi_t$ :

### Special Case: Linear Multi-Factor Model

State-Space Equations:

$$\begin{aligned}x_t &= \mathbf{H}^x \psi_t + v_{x,t} \\y_t &= \mathbf{B} \mathbf{H}^x \psi_t + v_{y,t} \\ \psi_{t+1} &= \mathbf{A} \psi_t + w_t\end{aligned}$$

$\mathbf{A} = I - \Lambda$  is computed using anisotropic diffusion maps on covariates  $(x(t_i))_{i=0}^N$ . We estimate  $\mathbf{B}$ ,  $\mathbf{R}$ , and estimate  $\hat{\psi}_{t+1} = \mathbb{E}[\psi_{t+1} | \{x_1, \dots, x_t\}]$  using the EM algorithm.

We now aim to estimate the unknown parameters in the state-space using the standard EM algorithm. The procedure involves alternating between:

1. E-step: Run the Kalman filter to estimate the latent state  $\psi_t$ .
2. M-step: Update the parameters  $\mathbf{R}_x$ ,  $\mathbf{R}_y$ , and the cross-covariance  $\mathbf{R}_{xy}$  (and  $\mathbf{B}$  in the linear case) based on the current estimates of  $\psi_t$ .

#### 3.3.1 E-Step: Kalman Filter with Joint Observations

The Kalman filter is used to estimate the latent state  $\psi_t$  and the corresponding state covariance  $P_{t|t}$ . In our supervised learning framework, we define the joint observation vector:

$$z_t = \begin{bmatrix} x_t \\ y_t \end{bmatrix} = \begin{bmatrix} \mathbf{H}^x \\ \mathbf{H}^y \end{bmatrix} \psi_t + \begin{bmatrix} v_{x,t} \\ v_{y,t} \end{bmatrix}$$

Note that in the *linear case*, we would replace  $\mathbf{H}^y$  with  $\mathbf{B} \mathbf{H}^x$ . The steps of the Kalman filter are as follows:

1. Prediction Step:

$$\hat{\psi}_{t|t-1} = \mathbf{A} \hat{\psi}_{t-1|t-1}, \quad P_{t|t-1} = \mathbf{A} P_{t-1|t-1} \mathbf{A}^\top + \mathbf{Q}$$

2. Innovation (Residual):

$$e_t = z_t - \mathbf{H}^z \hat{\psi}_{t|t-1}$$

where:

$$\mathbf{H}^z = \begin{bmatrix} \mathbf{H}^x \\ \mathbf{H}^y \end{bmatrix}$$

and the joint noise covariance is:

$$\mathbf{R} = \begin{bmatrix} \mathbf{R}_x & \mathbf{R}_{xy} \\ \mathbf{R}_{xy}^\top & \mathbf{R}_y \end{bmatrix}$$

3. Innovation Covariance:

$$S_t = \mathbf{H}^z P_{t|t-1} \mathbf{H}^{z\top} + \mathbf{R}$$

4. Kalman Gain:

$$K_t = P_{t|t-1} \mathbf{H}^{z\top} S_t^{-1}$$

5. Update Step:

$$\hat{\psi}_{t|t} = \hat{\psi}_{t|t-1} + K_t e_t, \quad P_{t|t} = (I - K_t \mathbf{H}^{z\top}) P_{t|t-1}$$

6. Log-Likelihood Contribution:

$$\mathcal{L}^{(t)} = -\frac{1}{2} \left( \log |S_t| + e_t^\top S_t^{-1} e_t + (n + m) \log 2\pi \right)$$

After running the Kalman filter, we apply the Rauch–Tung–Striebel (RTS) smoother [RTS65]:

1. Initialize at  $T$ :

$$\hat{\psi}_{T|T} = \hat{\psi}_{T|T}, \quad P_{T|T} = P_{T|T}$$

2. Backward pass for  $t = T - 1, \dots, 1$ :

$$\begin{aligned} J_t &= P_{t|t} \mathbf{A}^\top P_{t+1|t}^{-1} \\ \hat{\psi}_{t|T} &= \hat{\psi}_{t|t} + J_t \left( \hat{\psi}_{t+1|T} - \hat{\psi}_{t+1|t} \right) \\ P_{t|T} &= P_{t|t} + J_t (P_{t+1|T} - P_{t+1|t}) J_t^\top \end{aligned}$$

### 3.3.2 M-Step: Parameter Updates

After running the Kalman filter, we update the parameters  $\mathbf{R}_x$ ,  $\mathbf{R}_y$ , and  $\mathbf{R}_{xy}$  (and  $\mathbf{B}$  in the linear case) based on the current estimates of  $\psi_t$ .

1. Update  $\mathbf{R}_x$  using the residuals from the smoothed estimates  $\hat{\psi}_{t|T}$ :

$$\mathbf{R}_x = \frac{1}{T} \sum_{t=1}^T \left( x_t - \mathbf{H}^x \hat{\psi}_t \right) \left( x_t - \mathbf{H}^x \hat{\psi}_t \right)^\top$$

2. Update  $\mathbf{R}_y$  using the residuals from the smoothed estimates  $\hat{\psi}_{t|T}$ :

$$\mathbf{R}_y = \frac{1}{T} \sum_{t=1}^T \left( y_t - \mathbf{H}^y \hat{\psi}_t \right) \left( y_t - \mathbf{H}^y \hat{\psi}_t \right)^\top$$

3. Update  $\mathbf{R}_{xy}$  using the residuals from the smoothed estimates  $\hat{\psi}_{t|T}$ :

$$\mathbf{R}_{xy} = \frac{1}{T} \sum_{t=1}^T \left( x_t - \mathbf{H}^x \hat{\psi}_t \right) \left( y_t - \mathbf{H}^y \hat{\psi}_t \right)^\top$$

4. *In the linear case*, update  $\mathbf{B}$  via least squares regression on the lifted smoothed estimates  $\hat{\psi}_{t|T}$ :

$$\mathbf{B} = \left( \sum_{t=1}^T y_t (\mathbf{H}^x \hat{\psi}_t)^\top \right) \left( \sum_{t=1}^T \mathbf{H}^x \hat{\psi}_t (\mathbf{H}^x \hat{\psi}_t)^\top \right)^{-1}$$

### 3.3.3 EM Algorithm

---

**Algorithm 1** EM Algorithm Iteration
 

---

- 1: **Initialize** the parameters  $\mathbf{R}_x$ ,  $\mathbf{R}_y$ , and  $\mathbf{R}_{xy}$  (and  $\mathbf{B}$  in the linear case).
  - 2: **Set** tolerance  $\varepsilon$  and maximum iterations  $N_{\max}$ .
  - 3: **Initialize** log-likelihood  $\mathcal{L}^{(0)} \leftarrow -\infty$ , iteration counter  $k \leftarrow 0$ .
  - 4: **while** not converged and  $k < N_{\max}$  **do**
  - 5:     **E-step:** Run Joint Diffusion Kalman filter using current estimates of  $\mathbf{R}_x$ ,  $\mathbf{R}_y$  and  $\mathbf{R}_{xy}$ .
  - 6:     **Output:** Estimate  $\psi_t$  and compute the log-likelihood  $\mathcal{L}^{(k+1)}$ .
  - 7:     **M-step:** Update  $\mathbf{R}_x$ ,  $\mathbf{R}_y$ , and  $\mathbf{R}_{xy}$  using the smoothed estimates of  $\psi_t$ .
  - 8:     **Convergence check:**
  - 9:     **if**  $\frac{|\mathcal{L}^{(k+1)} - \mathcal{L}^{(k)}|}{|\mathcal{L}^{(k)}|} < \varepsilon$  **then**
  - 10:         **Converged:** Stop the algorithm.
  - 11:     **else**
  - 12:          $k \leftarrow k + 1$
  - 13:     **end if**
  - 14: **end while**
- 

We have added an extra layer with the measurement equation for the dependent variables to maintain the explanatory power in the embeddings and taken this into account via the modified state-space. JDKF thus gives us diffusion coordinates that propagate linearly and preserve much of the original explanatory power from the full high-dimensional set of covariates. Figure 3 displays a broad flow map of the JDKF procedure. In the next subsection, we describe the conditional sampling procedure.

### 3.4 Sampling $\psi_{t+1}$ Conditional on Information from $(x_{t+1}, y_{t+1})$

When implementing the Joint Diffusion Kalman Filter, we seek to sample diffusion coordinates conditional on information in the original measurement spaces of  $x_{t+1}$  and  $y_{t+1}$ , where this information is typically that a subset of coordinates of  $x_{t+1}$  (and/or  $y_{t+1}$ ) are fixed to some pre-determined values. To do this, we can leverage the power of the linear lifting operator to go back and forth between the measurement and embedding spaces. Given the setup in equations (3.9) and (3.10), we desire to sample  $\hat{\psi}_{t+1}$  given  $\hat{\psi}_t$  while conditioning on a subset of coordinates of the reconstructed  $(x_{t+1}, y_{t+1})$ , or equivalently  $(\mathbf{H}^x \hat{\psi}_{t+1}, \mathbf{H}^y \hat{\psi}_{t+1})$  being fixed to specific values. Let  $\psi_t$  be the latent state at time  $t$ . Recall the state transition model is given by:

$$\psi_{t+1} = \mathbf{A}\psi_t + w_t$$

where  $\mathbf{A}$  is the state transition matrix and  $w(t) \sim \mathcal{N}(0, \mathbf{Q})$  is the process noise with covariance  $\mathbf{Q}$ . The filtered observation estimates are given from the observation equation by:

$$\begin{aligned} \hat{x}_{t+1} &= \mathbf{H}^x \hat{\psi}_{t+1} \\ \hat{y}_{t+1} &= \mathbf{H}^y \hat{\psi}_{t+1} \end{aligned}$$

where  $\mathbf{H}^x$  and  $\mathbf{H}^y$  are the lifting operators that map the latent state to the observation spaces.

Now, given the current state  $\psi_t$ , the predicted mean and covariance of the next state  $\psi_{t+1}$  are:

$$\begin{aligned} \mu_{\psi_{t+1}} &= \mathbf{A}\psi_t \\ \Sigma_{\psi_{t+1}} &= \mathbf{Q} \end{aligned}$$

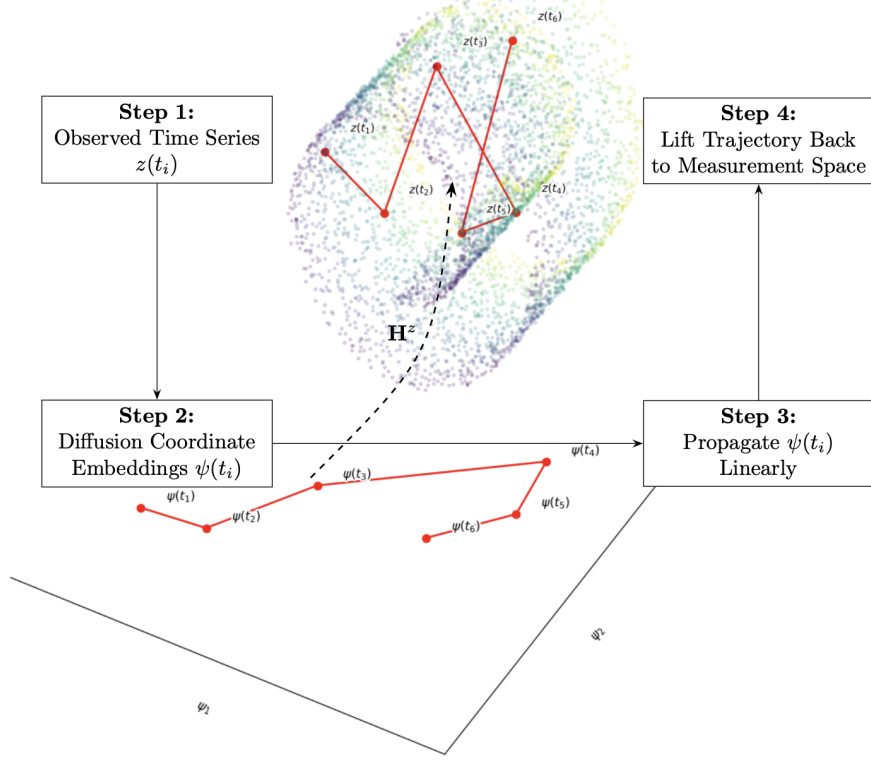


Figure 3: A flow map of the Joint Diffusion Kalman Filter (JDKF) procedure.

The predicted mean and covariance of the reconstructed observation  $(x_{t+1}, y_{t+1}) = (\mathbf{H}^x \psi_{t+1}, \mathbf{H}^y \psi_{t+1})$  are:

$$\begin{aligned} \mu_{(x_{t+1}, y_{t+1})} &= (\mathbf{H}^x \mu_{\psi_{t+1}}, \mathbf{H}^y \mu_{\psi_{t+1}}) = (\mathbf{H}^x \mathbf{A} \psi_t, \mathbf{H}^y \mathbf{A} \psi_t) \\ \Sigma_{(x_{t+1}, y_{t+1})} &= (\mathbf{H}^x \Sigma_{\psi_{t+1}} \mathbf{H}^{xT} \quad \mathbf{H}^y \Sigma_{\psi_{t+1}} \mathbf{H}^{yT}) = (\mathbf{H}^x \mathbf{Q} \mathbf{H}^{xT} \quad \mathbf{H}^y \mathbf{Q} \mathbf{H}^{yT}) \end{aligned}$$

Now, to condition on the subset of coordinates, let  $(x_{t+1}, y_{t+1})$  be partitioned into two parts:  $(x_{t+1}, y_{t+1})^{(1)}$  and  $(x_{t+1}, y_{t+1})^{(2)}$ , where  $(x_{t+1}, y_{t+1})^{(1)}$  are the coordinates we condition on, and  $(x_{t+1}, y_{t+1})^{(2)}$  are the coordinates we want to sample. Suppose  $(x_{t+1}, y_{t+1})^{(1)}$  is fixed to some vector  $\mathbf{c}$ . We can express  $(x_{t+1}, y_{t+1})$  as being distributed as:

$$\begin{pmatrix} (x_{t+1}, y_{t+1})^{(1)} \\ (x_{t+1}, y_{t+1})^{(2)} \end{pmatrix} \sim \mathcal{N} \left( \begin{pmatrix} \mu_{(x_{t+1}, y_{t+1})}^{(1)} \\ \mu_{(x_{t+1}, y_{t+1})}^{(2)} \end{pmatrix}, \begin{pmatrix} \Sigma_{(x_{t+1}, y_{t+1})}^{(11)} & \Sigma_{(x_{t+1}, y_{t+1})}^{(12)} \\ \Sigma_{(x_{t+1}, y_{t+1})}^{(21)} & \Sigma_{(x_{t+1}, y_{t+1})}^{(22)} \end{pmatrix} \right)$$

The conditional distribution of  $(x_{t+1}, y_{t+1})^{(2)}$  given  $(x_{t+1}, y_{t+1})^{(1)} = \mathbf{c}$  is then:

$$(x_{t+1}, y_{t+1})^{(2)} \mid (x_{t+1}, y_{t+1})^{(1)} = \mathbf{c} \sim \mathcal{N}(\mu_{\text{cond}}, \Sigma_{\text{cond}})$$

where

$$\begin{aligned} \mu_{\text{cond}} &= \mu_{(x_{t+1}, y_{t+1})}^{(2)} + \Sigma_{(x_{t+1}, y_{t+1})}^{(21)} (\Sigma_{(x_{t+1}, y_{t+1})}^{(11)})^{-1} (\mathbf{c} - \mu_{(x_{t+1}, y_{t+1})}^{(1)}) \\ \Sigma_{\text{cond}} &= \Sigma_{(x_{t+1}, y_{t+1})}^{(22)} - \Sigma_{(x_{t+1}, y_{t+1})}^{(21)} (\Sigma_{(x_{t+1}, y_{t+1})}^{(11)})^{-1} \Sigma_{(x_{t+1}, y_{t+1})}^{(12)} \end{aligned}$$

Next, to sample  $\psi_{t+1}$  conditioned on the fixed values for a subset of coordinates in the observation spaces, we need to convert the conditional mean and covariance from the observation spaces back to the latent space. Let  $\mathbf{H}_2^x$  and  $\mathbf{H}_2^y$  be the rows of  $\mathbf{H}^x$  and  $\mathbf{H}^y$  corresponding to the free indices (the coordinates we want to sample), and let  $\mathbf{H}_1^x$  and  $\mathbf{H}_1^y$  be the rows of  $\mathbf{H}^x$  and  $\mathbf{H}^y$  corresponding to the fixed indices. We can solve the linear system to find the corresponding conditional mean and covariance in the latent space:

$$\begin{aligned}\mu_{\text{cond,diff}} &= (\mathbf{H}_2^{x+} \mu_{\text{cond}}, \mathbf{H}_2^{y+} \mu_{\text{cond}}) \\ \Sigma_{\text{cond,diff}} &= (\mathbf{H}_2^{x+} \Sigma_{\text{cond}} (\mathbf{H}_2^{x+})^T \quad \mathbf{H}_2^{y+} \Sigma_{\text{cond}} (\mathbf{H}_2^{y+})^T)\end{aligned}$$

where  $\mathbf{H}_2^{x+}$  and  $\mathbf{H}_2^{y+}$  are the Moore-Penrose pseudo-inverses of  $\mathbf{H}_2^x$  and  $\mathbf{H}_2^y$ . Finally, we sample from the conditional multivariate normal distribution to get  $\psi_{t+1}$  given the conditional information in the original space:

$$\hat{\psi}_{t+1} \sim \mathcal{N}(\mu_{\text{cond,diff}}, \Sigma_{\text{cond,diff}})$$

## 4 Convergence of Averages and Robustness of Approximations

The works [STS20; ST22] leverage the algorithm put forth in [SC08] to learn the eigenvalues of  $\mathcal{L}$ , to estimate the dynamics of the eigenfunctions, and to approximate the observations using a linear lift. The Kalman filtering framework of [STS20] is the motivation for the Joint Diffusion Kalman Filter and conditional sampling procedure developed in Subsections 3.3 and 3.4. However, there are some mathematical questions that need to be addressed to make this procedure rigorous. Under the assumptions in Subsection 3.1, we show in this section that it is admissible to learn the eigenvalues and the lift from time series data. In particular, a Poincaré Inequality (Assumption 3) implies that initialization errors are forgotten, and time averages converge (see Subsection 4.1). In Subsection 4.2, we bound the approximation error of the eigenfunctions of  $\mathcal{L}$  by the diffusion map eigenvectors using a concentration inequality. Furthermore, in Subsection 4.3 we quantify the error of approximating the eigenfunction dynamics using linear diffusions, demonstrating robustness.

At the heart of the error analysis for diffusion maps and related algorithms is the consideration of empirical averages of the form

$$S_N = \frac{1}{N+1} \sum_{i=0}^N V(\theta(t_i)). \quad (4.1)$$

For instance, in the setting of [Sin06],  $(\theta(t_i))_{i=0}^N$  are independent uniform samples from a compact Riemannian manifold  $\mathcal{M}$ , and the graph Laplacian is shown to approximate the Laplace–Beltrami operator  $\Delta_{\mathcal{M}}$ , that is, the following holds for smooth  $f$  and a point  $\theta(t_i)$  fixed:

$$\frac{\sum_{j \neq i} \exp\left(-\frac{\|\theta(t_i) - \theta(t_j)\|^2}{2\varepsilon}\right) f(\theta(t_j))}{\sum_{j \neq i} \exp\left(-\frac{\|\theta(t_i) - \theta(t_j)\|^2}{2\varepsilon}\right)} \rightarrow \frac{\mathbb{E}\left[\exp\left(-\frac{\|\theta - \theta(t_i)\|^2}{2\varepsilon}\right) f(\theta)\right]}{\mathbb{E}\left[\exp\left(-\frac{\|\theta - \theta(t_i)\|^2}{2\varepsilon}\right)\right]} = f(\theta(t_i)) + \frac{\varepsilon}{2} \Delta_{\mathcal{M}} f(\theta(t_i)) + O(\varepsilon^2). \quad (4.2)$$

The first arrow denotes convergence of the numerator and denominator to their averages by the law of large numbers, and these averages undergo Taylor expansions to give the error estimate in  $\varepsilon$ . Error analysis in the number of samples is then carried out by showing concentration of the empirical averages around their expectation.

In our setting, the summands in (4.1) arise not from independent samples, but from a sampled Langevin diffusion, which yields a Markov chain. In this case, the convergence of  $S_N$  to the expectation  $\mathbb{E}_\mu[V]$  as  $N \rightarrow \infty$  is an *ergodic property*, which is guaranteed for  $V \in \mathbb{L}^2(\mu)$  under our assumption of a Poincaré inequality or (equivalently) a spectral gap. If the Langevin diffusion is started in equilibrium, i.e.  $\theta_0 \sim \mu$ , then  $(\theta(t_i))_{i=0}^N$  is a stationary sequence and  $\mathbb{E}_{\theta_0 \sim \mu}[S_N] = \mathbb{E}_\mu[V]$  for any  $N \geq 0$ . In this case, the fluctuations  $\sqrt{N}S_N$  converge as  $N \rightarrow \infty$  to a Gaussian distribution by the celebrated Kipnis–Varadhan Central Limit Theorem [KV86]. A fast rate of convergence to equilibrium for Markov chains is a desirable property in the context of Markov chain Monte Carlo algorithms, and many central limit theorem results are collected in the survey paper [RR04]. For continuous time averages, we refer the reader to [CCG12], where the trend to equilibrium is studied under weaker assumptions than ours (for instance, some laws with sub-exponential tails are shown to be ergodic). In general, the rate of convergence depends both on the integrability of  $V$  and the weight of the tails of  $\mu$ . To fix notation, throughout the remainder of this section we consider a constant fixed step size  $\Delta t = t_i - t_{i-1}$  and set  $t_0 = 0$ .

#### 4.1 Short-Term Equilibration and Long-Term Convergence

We collect here some results on Markov chains which hold under Assumption 3, and apply these results to the sampled Markov process  $(\theta(t_i))_{i=0}^N$ . For any  $t \geq 0$ , consider the operator  $P_t$  which acts on  $f \in \mathbb{L}^2(\mu)$  by  $P_t f(x) = \mathbb{E}[f(\theta_t) | \theta_0 = x]$ . Some calculus gives

$$\partial_t \|P_t f\|_{\mathbb{L}^2(\mu)}^2 = \partial_t \int_{\mathbb{R}^d} (P_t f)^2 d\mu = 2 \int_{\mathbb{R}^d} P_t f \mathcal{L} P_t f d\mu = -2 \int_{\mathbb{R}^d} \Gamma(P_t f, P_t f) d\mu \leq -\frac{2}{C} \|P_t f\|_{\mathbb{L}^2(\mu)}^2,$$

where we have used Assumption 3 for the inequality. The differential form of Grönwall’s Inequality yields  $\|P_t f\|_{\mathbb{L}^2(\mu)}^2 \leq \exp(-2t/C) \|f\|_{\mathbb{L}^2(\mu)}^2$ . Hence,  $P_t f$  converges to equilibrium in  $\mathbb{L}^2$  exponentially fast. In fact, this property is equivalent to a Poincaré Inequality (see for instance [BGL14, Theorem 4.2.5]). In the next lemma, we exploit this fact to bound the deviation of observables from their values at equilibrium when  $\theta_0$  is initialized at some  $\mu_0$  which is absolutely continuous with respect to the equilibrium measure  $\mu$ . In practice, this error can be diminished by discarding an initial *burn-in* period (as we have done in Subsection 5.2). Similar results hold in other  $\mathbb{L}^p$ -spaces by Riesz–Thorin Interpolation (see, for instance, [Rud12, Proposition 3.17] and the application to MCMC methods in [FJS21, Theorem 12]), but we restrict to the  $\mathbb{L}^2$  case to reduce notation.

**Lemma 4.1.** *Suppose  $\theta_0 \sim \mu_0$  where  $\mu_0$  admits a Radon–Nikodym derivative with respect to the invariant measure  $\mu$  such that  $\|\frac{d\mu_0}{d\mu} - 1\|_{\mathbb{L}^2(\mu)} < \infty$ , and let  $\mu_t$  denote the distribution of  $\theta_t$ . If  $f \in \mathbb{L}^2(\mu)$  then for  $t \geq 0$ ,*

$$\mathbb{E}_{\theta_0 \sim \mu_0} [f(\theta_t)] \leq \mathbb{E}_\mu[f] + \exp(-\lambda_1 t) \left\| \frac{d\mu_0}{d\mu} - 1 \right\|_{\mathbb{L}^2(\mu)} \|f\|_{\mathbb{L}^2(\mu)}$$

*Proof.* We have that

$$\begin{aligned} \mathbb{E}_{\theta_0 \sim \mu_0} [f(\theta_t)] &= \int_{\mathbb{R}^d} f(w) \left( 1 + \frac{d\mu_t}{d\mu}(w) - 1 \right) \mu(dw) \\ &\leq \mathbb{E}_\mu[f] + \left\| \frac{d\mu_t}{d\mu} - 1 \right\|_{\mathbb{L}^2(\mu)} \|f\|_{\mathbb{L}^2(\mu)} \\ &\leq \mathbb{E}_\mu[f] + \exp(-\lambda_1 t) \left\| \frac{d\mu_0}{d\mu} - 1 \right\|_{\mathbb{L}^2(\mu)} \|f\|_{\mathbb{L}^2(\mu)} \end{aligned}$$

where we have used Hölder's Inequality for the first inequality, and the  $\mathbb{L}^2$ -exponential convergence of  $P_t$  for the second (recall that the spectral gap and first non-zero eigenvalue of  $-\mathcal{L}$  satisfy  $C = 1/\lambda_1$ ).  $\square$

Next, we turn to the long-term behavior of the Markov chain  $(\theta(t_i))_{i=0}^N$ . As a particular application, we focus on the empirical sums

$$\mathbf{H}_{j,k} = \langle z_j, \psi_k \rangle_{\text{data}} := \frac{1}{N+1} \sum_{i=0}^N z_j(t_i) \psi_k(t_i)$$

which define the lifting operator  $\mathbf{H}$ . In light of Remark 3.6, we will assume that  $\psi_k$  has been rescaled so that  $(N+1)^{-1} \sum_{i=0}^N \psi_k(t_i) = \mathbb{E}_\mu[\varphi_k(\theta)]$ . Recall that  $z_j(t_i) = F^j(\theta(t_i))$  and we have assumed mean-centering:  $\mathbb{E}_\mu[F^j] = 0$ . Setting  $a_{jk} = \langle F^j, \varphi_k \rangle_\mu$ , the triangle inequality gives

$$|\mathbf{H}_{j,k} - a_{jk}| \leq \frac{1}{N+1} \left| \sum_{i=0}^N F^j(\theta(t_i)) (\psi_k(t_i) - \varphi_k(\theta(t_i))) \right| + \frac{1}{N+1} \left| \sum_{i=0}^N \{F^j(\theta(t_i)) \varphi_k(\theta(t_i)) - a_{jk}\} \right|.$$

The first sum concerns the approximation of the eigenfunctions of  $\mathcal{L}$  by diffusion coordinates, which is addressed in the next subsection. Focusing on the second term, we shall apply the Kipnis–Varadhan Central Limit Theorem [KV86]. We state the result with  $\theta_0 \sim \mu$ ; however, under suitable assumptions on  $F^j \varphi_k$  similar results hold even when the Markov chain is started from a deterministic initial condition (see, for instance, [DL01; DL03; CP12; CCG12]).

**Proposition 4.2** ([KV86]). *Suppose  $\theta_0 \sim \mu$  and there exists  $g$  such that  $F^j \varphi_k = \sqrt{I - P_{\Delta t}} g$ . Then the weak convergence*

$$\frac{1}{\sqrt{N}} \sum_{i=0}^N \{F^j(\theta(t_i)) \varphi_k(\theta(t_i)) - a_{jk}\} \implies \mathcal{N}(0, \sigma^2) \text{ as } N \rightarrow \infty$$

holds, where  $\sigma^2$  satisfies

$$\sigma^2 = \lim_{N \rightarrow \infty} \frac{1}{N} \text{Var}_\mu \left( \sum_{i=0}^N F^j(\theta(t_i)) \varphi_k(\theta(t_i)) \right) = \int_{-1}^1 \frac{1+\lambda}{1-\lambda} \rho_{F^j \varphi_k}(\mathrm{d}\lambda) < \infty$$

and  $\rho_{F^j \varphi_k}$  is the spectral measure of  $F^j \varphi_k$ .

In the context of Example 3.3,  $F^j \varphi_k$  is a polynomial and  $\sigma^2$  can be computed using knowledge of the Hermite eigenfunctions.

## 4.2 Error Analysis of the Graph Laplacian

The ADM approach of [SC08] relies on the approximation of the Fokker–Planck operator by the graph Laplacian. Suppose  $(\theta(t_i))_{i=0}^N$  are i.i.d. samples from  $\mu$ , let  $f \in \mathbb{L}^2(\mu)$ , and set  $z(t_i) = H(\theta_i)$ . Then an analogous argument to (4.2) (see [SC08, Equation (30)] along with extra accounting for a factor of 2 from differences in some definitions given there) yields

$$\sum_{j=0}^N \mathbf{P}_{ij} f(z(t_j)) \rightarrow \frac{\mathbb{E}_\mu \left[ \exp \left( -\frac{\|\theta - \theta(t_i)\|^2}{2\varepsilon} \right) f \circ H(\theta) \right]}{\mathbb{E}_\mu \left[ \exp \left( -\frac{\|\theta - \theta_j\|^2}{2\varepsilon} \right) \right]} = f \circ H(\theta(t_i)) + \varepsilon \mathcal{L}(f \circ H)(\theta(t_i)) + O(\varepsilon^2)$$

as  $N \rightarrow \infty$ , where  $\mathbf{P}$  is the stochastic matrix described in Subsection 3.2. This suggests that an eigenvector of  $\mathbf{P} - I$  is close to an eigenfunction of  $\mathcal{L}$  on the support of the samples  $(\theta(t_i))_{i=0}^N$ .

Our aim in this section is to generalize this approximation for the case when  $(\theta(t_i))_{i=0}^N$  is a time series corresponding to a sampled Langevin diffusion, and to quantify the error using a concentration inequality. We begin by fixing some notation. Fix  $f \in \mathbb{L}^2(\mu)$ ,  $w \in \mathbb{R}^d$ , and let

$$u(\theta) = \exp\left(-\frac{\|\theta - w\|^2}{2\varepsilon}\right) f(\theta) \quad \text{and} \quad v(\theta) = \exp\left(-\frac{\|\theta - w\|^2}{2\varepsilon}\right). \quad (4.3)$$

Setting  $w = \theta(t_i)$ , we have that

$$\sum_{j=0}^N \mathbf{P}_{ij} f(z(t_j)) = \frac{\sum_{j=0}^N u(\theta(t_j))}{\sum_{j=0}^N v(\theta(t_j))}$$

The following theorem demonstrates concentration of the right hand side around  $\mathbb{E}_\mu[u]/\mathbb{E}_\mu[v]$ .

**Theorem 4.3.** *Suppose that Assumptions 1, 2, and 3 hold. Let  $f \in \mathbb{L}^2(\mu)$ , fix  $w \in \mathbb{R}^d$ , and define  $u, v$  by (4.3). Then*

$$\mathbb{P}_{\theta_0 \sim \mu} \left( \left| \frac{\sum_{j=0}^N u(\theta(t_j))}{\sum_{j=0}^N v(\theta(t_j))} - \frac{\mathbb{E}_\mu[u]}{\mathbb{E}_\mu[v]} \right| > \alpha \right) \leq 2 \exp \left( \frac{-(1 - \exp(-\lambda_1 \Delta t))(N+1)p(w)\alpha^2}{10C\alpha p(w) + 2^{-d+2}\pi^{-d/2}\varepsilon^{-d/2}(\varepsilon\|\nabla f(w)\|^2 + O(\varepsilon^2))} \right)$$

where  $C$  depends on  $\|u\|_\infty$ .

*Remark 4.4.* If  $\theta$  is initialized at  $\mu_{-r}$  with  $\|\frac{d\mu_{-r}}{d\mu} - 1\|_{\mathbb{L}^2(\mu)} < \infty$ , then Lemma 4.1 may be applied after discarding a burn-in period of length  $r$ . This yields an extra factor of  $1 + \exp(-\lambda_1 r) \|\frac{d\mu_{-r}}{d\mu} - 1\|_{\mathbb{L}^2(\mu)}$  on the right hand side of the above inequality.

*Proof.* We adapt the argument from [Sin06, Section 3] to samples  $(\theta(t_i))_{i=0}^N$  from the Langevin diffusion (3.1). In this case,  $(\theta(t_i))_{i=0}^N$  forms a reversible Markov chain with spectral gap  $1 - \exp(-\lambda_1 \Delta t)$ . We will show an upper bound for the right tail in the desired inequality. The left tail follows similarly and the statement of the theorem holds by a union bound. If we let

$$V(\theta(t_j)) = \frac{\mathbb{E}_\mu[v]u(\theta(t_j)) - \mathbb{E}_\mu[u]v(\theta(t_j)) + \alpha\mathbb{E}_\mu[v](\mathbb{E}_\mu[v] - v(\theta(t_j)))}{\mathbb{E}_\mu[v]^2}.$$

then we see that

$$\mathbb{P}_{\theta_0 \sim \mu} \left( \frac{\sum_{j=0}^N u(\theta(t_j))}{\sum_{j=0}^N v(\theta(t_j))} - \frac{\mathbb{E}_\mu[u]}{\mathbb{E}_\mu[v]} > \alpha \right) = \mathbb{P}_{\theta_0 \sim \mu} \left( \sum_{j=0}^N V(\theta(t_j)) > \alpha(N+1) \right)$$

Note that  $\mathbb{E}_\mu[V] = 0$  and  $V$  is bounded in absolute value by some constant  $C$  which depends on  $\|u\|_\infty$ . We seek to apply a concentration inequality which will capture the second moment of  $V$  in the variance proxy. The version of Bernstein's Inequality for Markov chains given in [Paul15, Theorem 3.3] gives

$$\mathbb{P}_{\theta_0 \sim \mu} \left( \left| \frac{\sum_{j=0}^N u(\theta(t_j))}{\sum_{j=0}^N v(\theta(t_j))} - \frac{\mathbb{E}_\mu[u]}{\mathbb{E}_\mu[v]} \right| > \alpha \right) \leq 2 \exp \left( \frac{-(1 - \exp(-\lambda_1 \Delta t))(N+1)\alpha^2}{4 \text{Var}_\mu(V) + 10C\alpha} \right)$$

A lengthy computation (which is relegated to Appendix C) shows that

$$\text{Var}_\mu(V) = \frac{2^{-d}\pi^{-d/2}\varepsilon^{-d/2}(\varepsilon\|\nabla f(w)\|^2 + O(\varepsilon^2))}{p(w)}$$

and the conclusion of the theorem follows.  $\square$

### 4.3 Approximating the Eigenfunctions by Independent Linear Equations

Let  $\varphi = (\varphi_1, \dots, \varphi_\ell)$  be a vector of  $\mathcal{L}$ -eigenfunctions with eigenvalues  $0 > -\lambda_1 \geq \dots \geq -\lambda_\ell$  such that  $\mathcal{L}\varphi_i = -\lambda_i\varphi_i$  for  $i = 1, \dots, \ell$ . In Subsection 3.2, we saw that

$$\begin{aligned} d\varphi_i(\theta_t) &= -\nabla U(\theta_t) \cdot \nabla \varphi_i(\theta_t) dt + \Delta \varphi_i(\theta_t) dt + \sqrt{2} \nabla \varphi_i(\theta_t) \cdot dW_t \\ &= \mathcal{L}\varphi_i(\theta_t) dt + \sqrt{2} \|\nabla \varphi_i(\theta_t)\|_2 dB_t^i \\ &= -\lambda_i \varphi_i(\theta_t) dt + \sqrt{2} \|\nabla \varphi_i(\theta_t)\|_2 dB_t^i, \end{aligned} \tag{4.4}$$

where  $B^i$  is a Brownian motion, and for  $i \neq j$  we have

$$d\langle \varphi_i(\theta_t), \varphi_j(\theta_t) \rangle_t = 2 \nabla \varphi_i(\theta_t) \cdot \nabla \varphi_j(\theta_t) dt.$$

If  $\theta_0$  is initialized according to the invariant measure  $\mu$ , then

$$\begin{aligned} \mathbb{E}_{\theta_0 \sim \mu} [\langle \varphi_i(\theta_t), \varphi_j(\theta_t) \rangle_t] &= \mathbb{E}_{\theta_0 \sim \mu} \left[ \int_0^t 2 \nabla \varphi_i(\theta_s) \cdot \nabla \varphi_j(\theta_s) ds \right] \\ &= 2t \int_{\mathbb{R}^d} \Gamma(\varphi_i(z), \varphi_j(z)) \mu(dz) \\ &= -2t \int_{\mathbb{R}^d} \varphi_i(z) \mathcal{L} \varphi_j(z) \mu(dz) \\ &= 2\lambda_j t \int_{\mathbb{R}^d} \varphi_i(z) \varphi_j(z) \mu(dz) = 0 \end{aligned} \tag{4.5}$$

where the third equality holds by identity (3.3), the fourth uses the fact that  $\varphi_j$  is an eigenfunction, and the final equality holds by the orthogonality of eigenfunctions. If  $\theta_0$  is started out of equilibrium, then by the argument of Lemma 4.1, it holds that  $\varphi_i(\theta_t)$  and  $\varphi_j(\theta_t)$  are close to being uncorrelated after an initial burn-in period:

**Corollary 4.5.** *Suppose  $\theta_0 \sim \mu_0$  where  $\|\frac{d\mu_0}{d\mu} - 1\|_{\mathbb{L}^2(\mu)} < \infty$ . Then, for  $i, j \in \{1, \dots, \ell\}$  with  $i \neq j$  and  $0 \leq s \leq t$  we have that*

$$\begin{aligned} &|\mathbb{E}_{\theta_0 \sim \mu_0} [\langle \varphi_i(\theta_t), \varphi_j(\theta_t) \rangle_t - \langle \varphi_i(\theta_s), \varphi_j(\theta_s) \rangle_s]| \\ &\leq \lambda_1^{-1} (\exp(-\lambda_1 s) - \exp(-\lambda_1 t)) \left\| \frac{d\mu_0}{d\mu} - 1 \right\|_{\mathbb{L}^2(\mu)} \|\nabla \varphi_i \cdot \nabla \varphi_j\|_{\mathbb{L}^2(\mu)}. \end{aligned}$$

*Proof.* For  $u \geq 0$ , let  $\mu_u$  denote the law of  $\theta_u$ . We have that

$$\begin{aligned} &|\mathbb{E}_{\theta_0 \sim \mu_0} [\langle \varphi_i(\theta_t), \varphi_j(\theta_t) \rangle_t - \langle \varphi_i(\theta_s), \varphi_j(\theta_s) \rangle_s]| \\ &= \left| 2 \int_s^t \int_{\mathbb{R}^d} \nabla \varphi_i(w) \cdot \nabla \varphi_j(w) \left( 1 + \frac{d\mu_u}{d\mu}(w) - 1 \right) \mu(dw) du \right| \\ &\leq 2 \int_s^t \left| \int_{\mathbb{R}^d} \nabla \varphi_i(w) \cdot \nabla \varphi_j(w) \mu(dw) \right| du + 2 \int_s^t \left| \int_{\mathbb{R}^d} \nabla \varphi_i(w) \cdot \nabla \varphi_j(w) \left( \frac{d\mu_u}{d\mu}(w) - 1 \right) \mu(dw) \right| du \end{aligned}$$

The first term is null by (4.5). As seen previously,  $\|\frac{d\mu_u}{d\mu} - 1\|_{\mathbb{L}^2(\mu)} \leq \exp(-\lambda_1 u) \|\frac{d\mu_0}{d\mu} - 1\|_{\mathbb{L}^2(\mu)}$ . Applying this along with Hölder's Inequality to the second term above and integrating in time gives the desired inequality.  $\square$

In [STS20], the gradients  $\|\nabla\varphi_i(\theta_t)\|_2$ , for  $i = 1, \dots, \ell$  are assumed to be constant, so that the SDE for  $\varphi_i(\theta_t)$  is linear-Gaussian and a Kalman filtering framework may be applied. As another corollary of Lemma 4.1, we show next that the approximation error between the contractive dynamics (4.4) and a linear SDE can remain small. For  $i = 1, \dots, \ell$ , let  $\xi^1, \dots, \xi^\ell$  satisfy

$$d\xi_t^i = -\lambda_i \xi_t^i dt + \sqrt{2}\gamma_i dB_t^i$$

where  $\gamma_1, \dots, \gamma_\ell > 0$  are fixed constants,  $B^1, \dots, B^\ell$  are the same Brownian motions which drive  $\varphi^1(\theta_t), \dots, \varphi^\ell(\theta_t)$ , and we fix a deterministic initial condition  $(\xi_0^1, \dots, \xi_0^\ell) \in \mathbb{R}^\ell$ .

**Corollary 4.6.** *Suppose  $\theta_0 \sim \mu_0$  where  $\|\frac{d\mu_0}{d\mu} - 1\|_{\mathbb{L}^2(\mu)} < \infty$ . For  $i \in \{1, \dots, \ell\}$  the following holds:*

$$\begin{aligned} & \mathbb{E}_{\theta_0 \sim \mu_0} [(\varphi_i(\theta_t) - \xi_t^i)^2] \\ & \leq \exp(-2\lambda_i t) \left( \mathbb{E}_{\theta_0 \sim \mu_0} [(\varphi_i(\theta_0) - \xi_0^i)^2] + 2t \mathbb{E}_\mu [(\|\nabla\varphi_i\|_2 - \gamma_i)^2] + \alpha(t) \right) \end{aligned} \quad (4.6)$$

where

$$\alpha(t) = \lambda_1^{-1} (1 - \exp(-\lambda_1 t)) \left\| \frac{d\mu_0}{d\mu} - 1 \right\|_{\mathbb{L}^2(\mu)} \mathbb{E}_\mu [(\|\nabla\varphi_i\|_2 - \gamma_i)^4]^{1/2}.$$

*Remark 4.7.* Setting  $\gamma_i = \mathbb{E}_\mu[\|\nabla\varphi_i\|_2]$  minimizes  $\mathbb{E}_\mu [(\|\nabla\varphi_i\|_2 - \gamma_i)^2]$  yielding  $\text{Var}_\mu(\|\nabla\varphi_i\|_2)$ .

*Proof.* By Itô's formula, the squared error at time  $t \geq 0$  satisfies

$$\begin{aligned} (\varphi_i(\theta_t) - \xi_t^i)^2 &= (\varphi_i(\theta_0) - \xi_0^i)^2 + 2 \int_0^t (\varphi_i(\theta_u) - \xi_u^i) (d\varphi_i(\theta_u) - d\xi_u^i) + \int_0^t d\langle \varphi_i(\theta_\cdot) - \xi_\cdot^i \rangle_u \\ &= (\varphi_i(\theta_0) - \xi_0^i)^2 - 2\lambda_1 \int_0^t (\varphi_i(\theta_u) - \xi_u^i)^2 du + M_t + 2 \int_0^t (\|\nabla\varphi_i(\theta_u)\|_2 - \gamma_i)^2 du, \end{aligned}$$

where  $M_t = 2 \int_0^t (\varphi_i(\theta_u) - \xi_u^i) (\|\nabla\varphi_i(\theta_u)\|_2 - \gamma_i) dB_u^i$  is a local martingale term, which we assume to be a true martingale (this can be verified depending on the dynamics of  $\theta$ , for instance, it holds in the case of Example 3.3 where  $\theta$  is an OU process and  $\varphi_i$  is a Hermite polynomial). Taking expectations and applying Fubini's Theorem yields

$$\mathbb{E} [(\varphi_i(\theta_t) - \xi_t^i)^2] = (\varphi_i(\theta_0) - \xi_0^i)^2 - 2\lambda_1 \int_0^t \mathbb{E} [(\varphi_i(\theta_u) - \xi_u^i)^2] du + 2 \int_0^t \mathbb{E} [(\|\nabla\varphi_i(\theta_u)\|_2 - \gamma_i)^2] du. \quad (4.7)$$

For  $u \geq 0$ , let  $\mu_u$  denote the law of  $\theta_u$ . By Lemma 4.1, we have

$$\begin{aligned} & \mathbb{E}_{\theta_0 \sim \mu_0} [(\|\nabla\varphi_i(\theta_u)\|_2 - \gamma_i)^2] \\ & \leq \mathbb{E}_\mu [(\|\nabla\varphi_i\|_2 - \gamma_i)^2] + \exp(-\lambda_1 u) \left\| \frac{d\mu_0}{d\mu} - 1 \right\|_{\mathbb{L}^2(\mu)} \mathbb{E}_\mu [(\|\nabla\varphi_i\|_2 - \gamma_i)^4]^{1/2} \end{aligned}$$

The final result follows from integrating in time, substituting into (4.7), and applying the integral form of Grönwall's Inequality.  $\square$

## 5 Model Validation

We now turn to an application of our framework to financial stress testing and scenario analysis of equity portfolios. As in [CRR86], we consider a standard macroeconomic multi-factor model where stock returns respond to unexpected changes in economy-wide factors. We stress our portfolios using the supervisory scenarios specified in [Boa22]. It is important to note that even unconditionally uncorrelated factors can display moderate dependence, for instance, factors can be uncorrelated and yet exhibit significant conditional dependence when a subset of them is learned. As a result the distribution of these factors conditional on an extreme scenario can display strong dependence.

Rather than selecting a handful of macro variables to explain stock returns, we incorporate **all** covariates in our stress-testing framework and instead allow the diffusion mapping to uncover the lower-dimensional intrinsic state  $\theta$  that is driving the joint dynamics while jointly preserving most of the explanatory power of the higher-dimensional set. This allows for a more realistic scenario analysis where a Portfolio Manager (PM) can incorporate his beliefs about the state of the world rather than limiting defining a scenario in terms of three or four variables.<sup>1</sup>

The standard multi-factor model assumes that the (excess) return of an asset  $j$  at time  $t$ , denoted as  $Y_{j,t}$ , can be expressed as a linear function of a set of  $p$  common factors  $X_{1,t}, X_{2,t}, \dots, X_{p,t}$  and a firm-specific error term  $\varepsilon_{j,t}$ :

$$Y_{j,t} = \beta_{1,j}X_{1,t} + \beta_{2,j}X_{2,t} + \dots + \beta_{p,j}X_{p,t} + \varepsilon_{j,t}$$

where  $Y_{j,t}$  is the return (excluding dividends) of asset  $j$  at time  $t$ ;  $X_{i,t}$  represents the value of the  $i$ -th factor at time  $t$ , where  $i = 1, \dots, p$  for  $p$  factors;  $\beta_{i,j}$  represents the (time-independent) loading or sensitivity of asset  $j$ 's returns to factor  $i$ ;  $\varepsilon_{j,t}$  is the idiosyncratic (or specific) error term for asset  $j$  at time  $t$ , which is assumed to have a mean of zero and be uncorrelated across assets and time. We use this as our observation equation in the JDKF framework, which can be written in vector-matrix form as:

$$\mathbf{Y}_t = \mathbf{B}\mathbf{X}_t + \varepsilon_t$$

where  $\mathbf{Y}_t$  is the  $n \times 1$  vector of excess returns at time  $t$  (where  $n$  is the number of assets),  $\mathbf{X}_t$  is the  $p \times 1$  vector of factor realizations at time  $t$ ,  $\mathbf{B} = (\beta_1, \beta_2, \dots, \beta_p)$  is the  $n \times p$  matrix of factor loadings, where each column  $\beta_i = (\beta_{i,1}, \beta_{i,2}, \dots, \beta_{i,n})^\top$  represents the loadings of all assets on factor  $i$ , and  $\varepsilon_t = (\varepsilon_{1,t}, \varepsilon_{2,t}, \dots, \varepsilon_{n,t})^\top$  is the  $n \times 1$  vector of idiosyncratic errors. We note that this linear multi-factor model is the *special case in our JDKF framework* where  $G = \mathbf{B} \circ F$  described in Section 3.3, where we recall that under this situation, the diffusion coordinates are computed only on the observations  $x(t)$  and there is only a lifting operator  $\mathbf{H}^x$  from the diffusion coordinate space to the space of the observed common factors.

### 5.1 Scenario Analysis Models

We consider several benchmark models for conducting the scenario analysis and stress tests. The main premise in scenario analysis models for financial portfolios is that there is a set of risk factors that drive a given asset or portfolio's value. The goal is then to estimate a given portfolio's return under different scenarios that involve applying shocks or stresses to some or all of the risk factors. In our macroeconomic multi-factor model described above, for instance, the risk factors

---

<sup>1</sup>Note that the goal of this paper is not to come up with the best factors (in terms of explanatory power) to explain stock returns or the best factor model, but to illustrate the power of our data-driven framework to stress test portfolios where the risk factors are a function of a high-dimensional vector of characteristics.

are the set of macroeconomic covariates  $\{X_{i,t}\}_{i=1}^p$ . There are several types of scenarios in stress testing models, including hypothetical scenarios chosen by the PM or historical scenarios that have happened throughout financial crises. Figure 4 displays the classic scenario analysis framework and the various types of risk factors, scenarios, and risk metrics that PMs typically deal with in conducting stress tests.

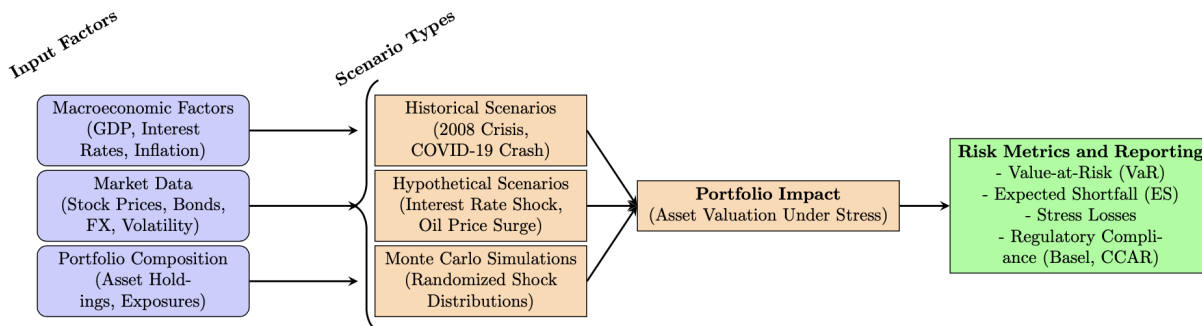


Figure 4: Diagram of the scenario analysis framework.

### 5.1.1 Standard Scenario Analysis

Standard Scenario analysis (SSA) for financial portfolios aims to compute a portfolio's profit and loss (P&L) or overall return under various combinations of stresses to a sub-collection of the risk factors that drive the portfolio's valuation. It is well known that scenario portfolio numbers calculated under SSA can be quite inaccurate for a wealth of reasons. First, post-stress P&L is computed under the assumption that the un-stressed factors are set to zero; meaning they remain unchanged under stresses to the other factors, however, there is often clear statistical dependence among factors, and in particular conditional dependence. Applying a stress to a sub-collection of factors at a given time period  $t$  should also have dynamic propagation effects through future time periods. A good stress test must not only take into account cross-factor dependencies but also the joint dynamics of the common factors themselves to assess how a stress propagates through time considering dynamic factor correlations. Furthermore, scenario analysis often involves dealing with latent (unobserved) factors that may actually be intrinsically driving the dynamics. Finally, one of the chief drawbacks of SSA is its lack of backtesting to validate the accuracy of scenario-conditional P&L, since SSA does not explicitly impose a probability model on the factors, it does not naturally lend itself to backtesting. In [HL20], a standard linear Gaussian state space model for the dynamics of the risk factors is proposed and scenario analysis is married with dynamic factor models. A dynamic factor model for scenario analysis has the advantage that it now allows for backtesting the performance of a stress test for a given portfolio. However, when considering equity portfolios where the assets are modeled with a high-dimensional set of common factors and their joint dynamics are highly nonlinear, such a standard state space model no longer applies.

In concrete terms, under the standard multi-factor model for stock returns, if  $\mathbf{X}_t \in \mathbb{R}^p$  is the  $p$ -dimensional vector of common factors, we define  $\mathcal{S}$  to be the set containing the indices of the factors in a scenario (the factors we intend to stress), and thus  $\mathcal{S}^C$  is the index set of those factors we leave un-stressed and which are not in our scenario. SSA then stresses the components of  $\mathbf{X}_{\mathcal{S},t}$  according to a given scenario (e.g. +20 on the S&P index, -2 on the CPI index, and +5 on the US Dollar/Euro exchange rate), and keeps the components in  $\mathbf{X}_{\mathcal{S}^C,t}$  unchanged (i.e. equal to their current value). The new portfolio P&L or overall return  $V_t$  is then computed with  $\mathbf{Y}_t$  determined

by the scenario and the multi-factor model. By leaving  $\mathbf{X}_{\mathcal{S},t}$  unchanged, SSA implicitly assumes that  $\mathbb{E}[\mathbf{X}_{\mathcal{S}^C,t+1}|\mathcal{F}_t, \mathbf{X}_{\mathcal{S},t+1}] = 0$ , here  $\mathcal{F}_t$  denotes a filtration with information up to time  $t$ .

1. Let  $\Delta\mathbf{X}_{\mathcal{S},t+1} = \mathbf{X}_{\mathcal{S},t+1} - \mathbf{X}_{\mathcal{S},t}$  denote the  $t + 1$  scenario stress vector  $\in \mathbb{R}^{|\mathcal{S}|}$ .
2. Compute the SSA factor change vector,  $\Delta\mathbf{X}_{t+1}^{\text{SSA}}$  as:

$$\Delta\mathbf{X}_{i,t+1}^{\text{SSA}} = \begin{cases} \Delta\mathbf{X}_{\mathcal{S},t+1}, & \text{for } i \in \mathcal{S} \\ 0, & \text{for } i \in \mathcal{S}^C \end{cases}$$

3. Obtain the predicted factor vector under SSA

$$\mathbf{X}_{t+1}^{\text{SSA}} = \mathbf{X}_t + \Delta\mathbf{X}_{t+1}^{\text{SSA}}$$

4. From the fitted matrix of factor loadings  $\tilde{\mathbf{B}}$ , fit via a multivariate regression, predict post-stress asset returns as:

$$\mathbf{Y}_{t+1}^{\text{SSA-stress}} = \tilde{\mathbf{B}}\mathbf{X}_{t+1}^{\text{SSA}}$$

We summarize the SSA procedure in the following algorithm, which we will then feed into a historical rolling window backtest in the next section. We let  $s$  denote the size of the rolling window. Note that the fitted matrix of factor loadings,  $\tilde{\mathbf{B}}$  is treated as an input in this algorithmic format. We denote with  $x_{t-s:t} \in \mathbb{R}^{s \times p}$  the matrix of common factors from time  $t - s$  up to  $t$ , and with  $y_{t-s:t} \in \mathbb{R}^{s \times n}$  the matrix of asset returns from time  $t - s$  up to  $t$ . We take  $x_{\text{actual},\mathcal{S},t+1}$  to be the realized historical scenario.

---

**Algorithm 2** SSA Portfolio Simulation

---

**Require:**  $x_{t-s:t}, x_{t+1}, \tilde{\mathbf{B}}$  (fitted from  $(y_{t-s:t}, x_{t-s:t})$ )

- 1: Set  $x_{\mathcal{S},t+1} = x_{\text{actual},\mathcal{S},t+1}$  and  $x_{\mathcal{S}^C,t+1} = x_{\mathcal{S}^C,t}$  to form  $x_{t+1,\text{SSA}}$
  - 2: Compute  $y_{t+1,\text{SSA}}$  from fitted equation  $y_t = \tilde{\mathbf{B}}x_t$  given  $x_{t+1,\text{SSA}}$
  - 3: Compute the  $1/N$  (or Markowitz) weights  $w$
  - 4: Compute portfolio return  $\hat{V}_{t+1,\text{SSA}} = w \cdot y_{t+1,\text{SSA}}$
- 

### 5.1.2 Static PCA

We employ a PCA-based benchmark to assess the impact of stressed scenarios on asset returns. This benchmark is closer to SSA in that we do not impose model dynamics on the PC components, here, we consider the projection of the vector of factor stresses onto the space spanned by the PC components computed from the factor changes. Unlike SSA however, the un-stressed factors are not assumed to remain unchanged and their co-movement is given from the projection. Given a factor matrix  $\mathbf{X} \in \mathbb{R}^{T \times p}$  and a return matrix  $\mathbf{Y} \in \mathbb{R}^{T \times n}$ , the static PCA procedure comprises a series of steps. First, we estimate the linear multi-factor regression model, then we project the factor changes onto principal components, apply stress scenarios, and predict the corresponding returns from the fitted factor model.

#### 1. Preprocessing and Centering.

First we compute the differenced factor matrix containing the time  $t$  factor changes:

$$\Delta\mathbf{X}_t = \mathbf{X}_t - \mathbf{X}_{t-1}.$$

We compute the mean of the differenced data, defined as  $\mu_{\Delta\mathbf{X}} = \frac{1}{T} \sum_{t=1}^T \Delta\mathbf{X}_t$ , and subtract it to obtain the centered factors upon which we will apply PCA:

$$\tilde{\mathbf{X}}_t = \Delta\mathbf{X}_t - \mu_{\Delta\mathbf{X}}.$$

## 2. Estimation of the Multivariate Regression Model.

We fit the multivariate regression model to obtain  $\tilde{\mathbf{B}}$ :

$$\mathbf{Y}_t = \mathbf{X}_t\mathbf{B} + \varepsilon_t,$$

## 3. Principal Component Analysis (PCA).

For each specified PCA dimension  $d$ , we compute the PCA transformation of the centered factors on  $\tilde{\mathbf{X}}_t$ :

$$\mathbf{X}_{\text{PCA}} = U\Sigma V^T.$$

and extract the principal component loading matrix:

$$W = V^T.$$

## 4. Applying Stressed Scenarios in PCA Space.

We define the unstressed scenario by setting the un-stressed factors equal to their current value at time  $t$  (meaning no change as in SSA):

$$\mathbf{X}_{t+1,i}^{\text{scenario}} = \mathbf{X}_{t,i}, \quad \forall i \notin \mathcal{S}.$$

For the specified set of stressed scenario variables  $\mathcal{S}$ , set the  $t+1$  values equal to their realized historical level, meaning we consider the true historical stress:

$$\mathbf{X}_{t+1,i}^{\text{scenario}} = \mathbf{X}_{t+1,i}, \quad \forall i \in \mathcal{S}.$$

Compute the perturbation vector (whose elements corresponding to un-stressed factors will be zero and those corresponding to the stressed factors will be equal to the true historical change):

$$\Delta\mathbf{X} = \mathbf{X}_{t+1}^{\text{scenario}} - \mathbf{X}_t.$$

Center the perturbation vector:

$$\Delta\tilde{\mathbf{X}} = \Delta\mathbf{X} - \mu_{\Delta\mathbf{X}}.$$

Project the stress perturbation onto the PCA component space:

$$\text{proj}_{\text{PCA}} = W(W^T\Delta\tilde{\mathbf{X}}).$$

Obtain the perturbed scenario factor vector:

$$\mathbf{X}_{t+1}^{\text{PCA-stress}} = \mathbf{X}_t + \text{proj}_{\text{PCA}} + \mu_{\Delta\mathbf{X}}.$$

## 5. Prediction of Stressed Returns.

Using the estimated regression factor loading matrix  $\tilde{\mathbf{B}}$ , we predict the asset returns under the stressed scenario:

$$\mathbf{Y}_{t+1}^{\text{PCA-stress}} = \mathbf{X}_{t+1}^{\text{PCA-stress}}\tilde{\mathbf{B}}.$$

We summarize the static PCA procedure in the following algorithm, which we will feed into our historical rolling window backtest in the next section. We let  $s$  denote the size of the rolling window. Note that the fitted matrix of factor loadings,  $\tilde{\mathbf{B}}$  is treated as an input in this algorithmic format. We denote with  $x_{t-s:t} \in \mathbb{R}^{s \times p}$  the matrix of common factors from time  $t - s$  up to  $t$ , and with  $y_{t-s:t} \in \mathbb{R}^{s \times n}$  the matrix of asset returns from time  $t - s$  up to  $t$ . We take  $x_{\text{actual}, \mathcal{S}, t+1}$  to be the realized historical scenario. For notational brevity, in the algorithm below we also assume that the mean of the factor changes,  $\mu_{\Delta \mathbf{X}}$ , is already added back into  $\text{proj}_{\text{PCA}}$

---

**Algorithm 3** Static PCA Portfolio Simulation

---

**Require:**  $x_{t-s:t}, x_{t+1}, \tilde{\mathbf{B}}$  (fitted from  $(y_{t-s:t}, x_{t-s:t})$ )

- 1: Apply PCA on the (pre-processed) differenced data  $\Delta x_{t-s:t}$
  - 2: Set  $x_{\mathcal{S}, t+1} = x_{\text{actual}, \mathcal{S}, t+1}$  and  $x_{\mathcal{S}^c, t+1} = x_{\mathcal{S}^c, t}$  to form  $\tilde{x}_{t+1}$
  - 3: Obtain the change vector  $\Delta x_t = \tilde{x}_{t+1} - x_t$
  - 4: Compute the projection of the centered  $\Delta x_t$  onto the PCA component space:  $\text{proj}_{\text{PCA}}$
  - 5: Obtain the perturbed scenario vector  $x_{t+1, \text{Static PCA}} = x_t + \text{proj}_{\text{PCA}}$
  - 6: Compute  $y_{t+1, \text{Static PCA}}$  from fitted equation  $y_t = \tilde{\mathbf{B}}x_{t+1, \text{Static PCA}}$
  - 7: Compute the  $1/N$  (or Markowitz) weights  $w$
  - 8: Compute portfolio return  $\hat{V}_{t+1, \text{Static PCA}} = w \cdot y_{t+1, \text{Static PCA}}$
- 

### 5.1.3 Dynamic PCA

A natural comparison benchmark against method is a dynamic version of Principal Component Analysis (PCA), which provides a simpler alternative to the arguably more complex Diffusion Mapping. Recalling that an empirical covariance matrix  $\mathbb{C}$  can be decomposed as  $\mathbb{C} = \mathbf{\Gamma} \mathbf{\Lambda} \mathbf{\Gamma}^\top$ , where  $\mathbf{\Gamma}$  is the matrix of eigenvectors (columns) and  $\mathbf{\Lambda}$  is a diagonal matrix of eigenvalues, we define the following PCA-based linear Gaussian state space model as a competing benchmark:

$$\textbf{Observation Equation: } \mathbf{X}_t = \mathbf{\Gamma} \mathbf{Z}_t + \varepsilon_t, \quad \varepsilon_t \sim \mathcal{N}(0, \mathbf{R}),$$

where  $\mathbf{X}_t$  is the observed data vector at time  $t$ ;  $\mathbf{Z}_t$  is the latent state vector (principal component embeddings) at time  $t$ ;  $\mathbf{\Gamma}$  is the eigenvector matrix (computed from PCA on the data) serving as the observation (loading) matrix; and  $\varepsilon_t$  is a Gaussian observation noise with covariance matrix  $\mathbf{R}$ .

$$\textbf{State Equation: } \mathbf{Z}_t = \mathbf{A} \mathbf{Z}_{t-1} + \eta_t, \quad \eta_t \sim \mathcal{N}(0, \mathbf{Q}),$$

where  $\mathbf{Z}_t$  is the latent state vector (principal component embeddings) at time  $t$ ;  $\mathbf{A}$  is the transition matrix governing the dynamics of the principal component embeddings; and  $\mathbf{Q}$  is the process noise covariance matrix.

1. We estimate the transition matrix  $\mathbf{A}$  by fitting a VAR(1) process to the PC components computed from the data.
2. From the state space representation we then implement the standard Kalman filter (see Appendix D) to obtain our dynamic estimates  $\mathbf{Z}_t$  of the PC embeddings. In our empirical experiments we select the dimension of the PC embeddings as  $d = 5$  such that  $> 99\%$  of the variance in our data is explained by them.
3. Once we have obtained our estimates for  $\mathbf{Z}_t$ , we perform conditional sampling given a scenario to obtain the stressed factor vector. The conditional sampling procedure closely follows that

outlined in Section 3.4 with the exception that we replace the lifting operator matrix with  $\mathbf{\Gamma}$  and the diffusion coordinates with  $\mathbf{Z}_t$ :

$$\begin{aligned}\mu_{\text{cond, PCA}} &= \mathbf{\Gamma}_{\mathcal{S}C}^+ \mu_{\text{cond}} \\ \Sigma_{\text{cond, PCA}} &= \mathbf{\Gamma}_{\mathcal{S}C}^+ \Sigma_{\text{cond}} (\mathbf{\Gamma}_{\mathcal{S}C}^+)^T\end{aligned}$$

we then sample from the conditional multivariate normal distribution to get  $\mathbf{Z}_{t+1}$  given the scenario in the original space:

$$\mathbf{Z}_{t+1} \mid \mathbf{Z}_t, \mathbf{X}_{\mathcal{S},t} \sim \mathcal{N}(\mu_{\text{cond, PCA}}, \Sigma_{\text{cond, PCA}})$$

We obtain  $K$  Monte Carlo conditional samples:

$$\{\mathbf{Z}_{t+1}^{(k)} \mid \mathbf{Z}_t, \mathbf{X}_{\mathcal{S},t}\}_{k=1}^K$$

4. For each conditional Monte Carlo sample, predict post-stress asset returns under the dynamic PCA stress using the fitted matrix of factor loadings  $\tilde{\mathbf{B}}$ :

$$\mathbf{Y}_{t+1, \text{Dynamic PCA}}^{(k)} = \tilde{\mathbf{B}} \mathbf{\Gamma}^T \mathbf{Z}_{t+1}^{(k)}$$

5. Obtain the dynamic PCA post-stress returns by taking the average across all Monte Carlo predictions:

$$\mathbf{Y}_{t+1, \text{Dynamic PCA}} = \frac{1}{K} \sum_{k=1}^K \mathbf{Y}_{t+1, \text{Dynamic PCA}}^{(k)}$$

We summarize the dynamic PCA procedure post-Kalman filter fitting, in the following algorithm, which we will feed into a historical rolling window backtest in the next section. We let  $s$  denote the size of the rolling window. Note that the fitted matrix of factor loadings,  $\tilde{\mathbf{B}}$ , the matrix of eigenvectors  $\mathbf{\Gamma}$ , and the time  $t$  Kalman filter estimate  $z_t$  for the latent state are all treated as inputs in this algorithmic format. We denote with  $x_{t-s:t} \in \mathbb{R}^{s \times p}$  the matrix of common factors from time  $t-s$  up to  $t$ , and  $y_{t-s:t} \in \mathbb{R}^{s \times n}$  the matrix of asset returns from time  $t-s$  up to  $t$ .

---

**Algorithm 4** Dynamic PCA Portfolio Simulation

---

**Require:**  $K, z_t, x_{t+1}, \mathbf{\Gamma}, \tilde{\mathbf{B}}$  (fitted from  $(y_{t-s:t}, x_{t-s:t})$ )

- 1: **for**  $k \leftarrow 1$  to  $K$  **do**
  - 2:   Generate  $z_{t+1}^{(k)} \mid (z_t, x_{\mathcal{S},t+1})$
  - 3:   Compute  $y_{t+1, \text{Dynamic PCA}}^{(k)} = \tilde{\mathbf{B}} \mathbf{\Gamma}^T z_{t+1}^{(k)}$
  - 4:   Compute the  $1/N$  (or Markowitz) weights  $w^{(k)}$
  - 5:   Compute portfolio return  $V_{t+1, \text{Dynamic PCA}}^{(k)} = w^{(k)} \cdot y_{t+1, \text{Dynamic PCA}}^{(k)}$
  - 6: **end for**
  - 7: Compute  $\hat{V}_{t+1, \text{Dynamic PCA}} = K^{-1} \sum_{i=1}^K V_{t+1, \text{Dynamic PCA}}^{(k)}$
-

#### 5.1.4 JDKF

Unlike SSA, the key advantage of our JDKF framework is that it accounts for dynamic correlations among the factors to compute conditional portfolio return under a given stress scenario, all this without imposing any parametric model on the joint factor dynamics. The conditional sampling procedure described in Section 3.4 allows us to sample dynamic diffusion coordinates  $\psi_t$  conditional on a scenario in the observation space,  $\mathbf{X}_{\mathcal{S},t}$ . Under the multi-factor model for asset returns, the multivariate regression equation becomes our observation equation, so that we operate under the following state space:

$$\begin{aligned} \text{Observation Equations: } \mathbf{Y}_t &= \mathbf{B}\mathbf{X}_t + \varepsilon_t = \mathbf{B}\mathbf{H}_X\psi_t + v_{Y,t}, & v_{Y,t} &\sim \mathcal{N}(0, \mathbf{R}_Y), \\ \mathbf{X}_t &= \mathbf{H}_X\psi_t + v_{X,t}, & v_{X,t} &\sim \mathcal{N}(0, \mathbf{R}_X) \end{aligned}$$

where  $\mathbf{X}_t$  is the observed data vector at time  $t$ ;  $\psi_t$  is the latent state vector (diffusion coordinates) at time  $t$ ;  $\mathbf{H}_X$  is the linear lifting operator (computed from applying diffusion maps on the data); and  $v_{Y,t}$  is a Gaussian observation noise with covariance matrix  $\mathbf{R}_Y$ , correlated with  $v_{X,t}$ .

$$\text{State Equation: } \psi_{t+1} = \mathbf{A}\psi_t + \eta_t, \quad \eta_t \sim \mathcal{N}(0, \mathbf{Q}),$$

where  $\psi_t$  is the latent state vector (diffusion coordinate) at time  $t$ ;  $\mathbf{A}$  is the transition matrix governing the dynamics of the principal component embeddings; and  $\mathbf{Q}$  is the process noise covariance matrix.

1. We first apply diffusion maps on the common factors data matrix  $\mathbf{X} \in \mathbb{R}^{T \times p}$  and obtain the matrix of diffusion coordinates  $\psi \in \mathbb{R}^{T \times \ell}$ . We then obtain the lifting operator  $\mathbf{H}_X = \mathbf{X}^T \psi \in \mathbb{R}^{p \times \ell}$  and the transition matrix  $\mathbf{A} = (I + \Lambda) \in \mathbb{R}^{\ell \times \ell}$ . Recall that  $\ell$  denotes the dimension of the diffusion coordinate space, which we choose from observing the largest eigenvalue drop when the diffusion maps algorithm is applied on the factor data.
2. From the state space equations, we then estimate the JDKF parameters, which include  $\mathbf{B}$ ,  $\mathbf{R}_X$ ,  $\mathbf{R}_Y$ , and  $\mathbf{R}_{XY}$  by fitting the joint Kalman filter as outlined in Section 3.3 to obtain filtered dynamic diffusion coordinate estimates  $\psi_t^{\text{JDKF}}$ , from which we also obtain  $\mathbf{X}_t^{\text{JDKF}} = \mathbf{H}_X \psi_t^{\text{JDKF}}$ .
3. Using the estimated diffusion coordinates from the JDKF  $\psi_t^{\text{JDKF}}$ , we then perform conditional sampling given the scenario in the factor observation space. Recall that we split our time  $t$  factor vector  $\mathbf{X}_t$  into two parts,  $\mathbf{X}_{\mathcal{S},t}$  and  $\mathbf{X}_{\mathcal{S}^c,t}$  based on the stressed and un-stressed factors. Following the conditional sampling procedure outlined in Section 3.4:

$$\begin{aligned} \mu_{\text{cond,diff}} &= \mathbf{H}_{\mathcal{S}^c}^+ \mu_{\text{cond}} \\ \Sigma_{\text{cond,diff}} &= \mathbf{H}_{\mathcal{S}^c}^+ \Sigma_{\text{cond}} (\mathbf{H}_{\mathcal{S}^c}^+)^T \end{aligned}$$

we then sample from the conditional multivariate normal distribution to get  $\psi_{t+1}$  given the scenario in the original space:

$$\psi_{t+1} \mid \psi_t, \mathbf{X}_{\mathcal{S},t} \sim \mathcal{N}(\mu_{\text{cond,diff}}, \Sigma_{\text{cond,diff}})$$

We obtain  $K$  Monte Carlo conditional samples:

$$\{\psi_{t+1}^{(k)} \mid \psi_t, \mathbf{X}_{\mathcal{S},t}\}_{k=1}^K$$

4. For each conditional Monte Carlo sample, predict post-stress asset returns under the JDKF stress directly from the fitted observation equation:

$$\mathbf{Y}_{t+1,\text{JDKF}}^{(k)} = \mathbf{B}\mathbf{H}_X\psi_{t+1}^{(k)}$$

5. Obtain the JDKF post-stress returns by taking the average across all Monte Carlo predictions:

$$\mathbf{Y}_{t+1,\text{JDKF}} = \frac{1}{K} \sum_{k=1}^K \mathbf{Y}_{t+1,\text{JDKF}}^{(k)}$$

We summarize the JDKF procedure post-Kalman filter fitting, in the following algorithm, which we will feed into a historical rolling window backtest in the next section. We let  $s$  denote the size of the rolling window. Note that the fitted matrix of factor loadings,  $\mathbf{B}$ , the linear lifting operator  $\mathbf{H}_X$ , and the time  $t$  Kalman filter estimate  $\psi_t$  for the latent state are all treated as inputs to the algorithm. We denote with  $x_{t-s:t} \in \mathbb{R}^{s \times p}$  the matrix of common factors from time  $t - s$  up to  $t$ , and  $y_{t-s:t} \in \mathbb{R}^{s \times n}$  the matrix of asset returns from time  $t - s$  up to  $t$ .

---

**Algorithm 5** JDKF Portfolio Simulation

---

**Require:**  $K, \hat{\psi}_t, \mathbf{B}, \mathbf{H}_x, x_{t+1}$

- 1: **for**  $k \leftarrow 1$  to  $K$  **do**
  - 2:   Generate  $\hat{\psi}_{t+1}^{(k)} \mid (\hat{\psi}_t, x_{\mathcal{S},t+1})$
  - 3:   Compute  $y_{t+1,\text{JDKF}}^{(k)} = \mathbf{B}\mathbf{H}_x\hat{\psi}_{t+1}^{(k)}$
  - 4:   Compute the  $1/N$  (or Markowitz) weights  $w^{(k)}$
  - 5:   Compute portfolio return  $V_{t+1,\text{JDKF}}^{(k)} = w^{(k)} \cdot y_{t+1,\text{JDKF}}^{(k)}$
  - 6: **end for**
  - 7: Compute  $\hat{V}_{t+1,\text{JDKF}} = K^{-1} \sum_{i=1}^K V_{t+1,\text{JDKF}}^{(k)}$
- 

## 5.2 Historical Backtesting

To validate our model with data, we conduct several historical backtests covering major periods of financial crisis and set our scenarios equal to the actual realized historical scenarios, such that for a given factor  $i \in \mathcal{S}$  in our scenario, the magnitude of the stress would be  $\Delta \mathbf{X}_t^i = \mathbf{X}_t^i - \mathbf{X}_{t-1}^i$ . For each of the historical backtests, we implement JDKF and the comparison benchmarks of SSA, Static PCA, and Dynamic PCA, described in Section 5.1. We then compare the conditional (on the scenario) predicted portfolio returns of JDKF, SSA, Static PCA, and Dynamic PCA relative to the realized time  $t$  portfolio return. On each period of our backtest, we consider a PM who has access to a universe of  $N$  stocks and constructs his portfolio weights via the  $1/N$  equal weighting rule. On each period then, the PM predicts the portfolio return conditional on the scenario under each model.

Historical backtesting involves estimating the performance of a given model *if it had been employed in the past*. Historical backtesting is very well suited for evaluating the performance of scenario analysis models, especially during historical periods of financial stress. The main idea is to attempt to predict portfolio return conditional on a scenario that we have observed in the past. More concretely, if at a given time period  $t$  we know the historical magnitude of the stress  $\Delta \mathbf{X}_t^i$  for our scenario-defining factors  $i \in \mathcal{S}$ , can we accurately predict the co-movements in the un-stressed factors  $i \notin \mathcal{S}$ ? Of course, the portfolio return is a function of the factors and so from these we compute the conditional scenario portfolio return. Hence the goal of our historical backtest is to assess

how well JDKF captures the dynamic correlation among the factors that are driving a portfolio’s overall return as compared to the other benchmarks. Our historical backtesting algorithm, which we describe in detail below, calls on the already defined algorithms in Section 5.1 for each model and treats them as function calls.

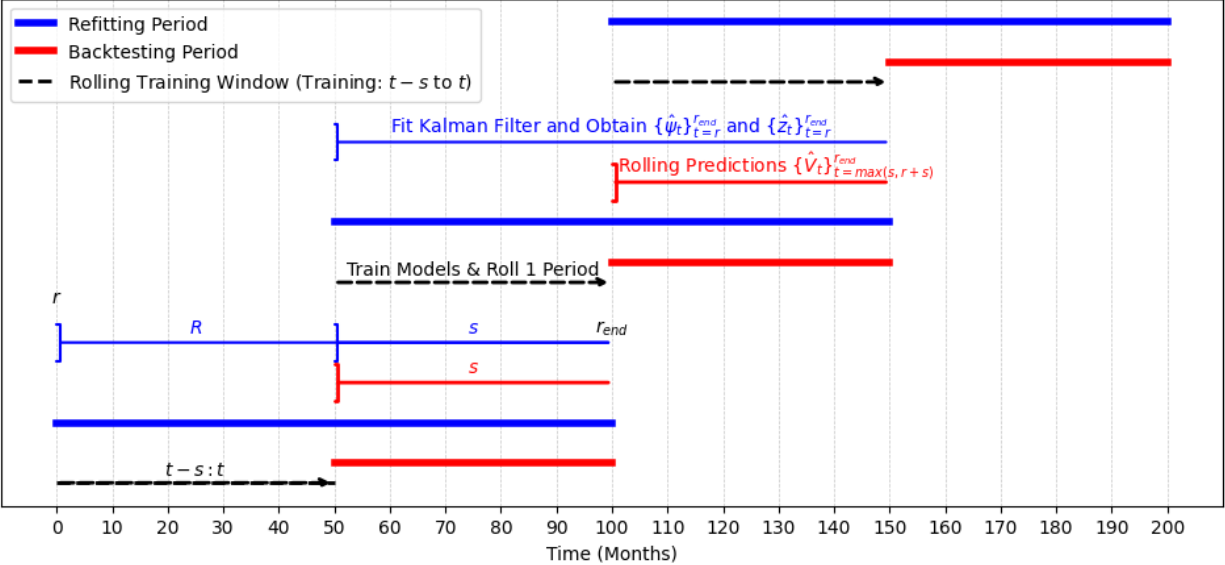


Figure 5: Flow of the historical rolling backtest: periodic re-fitting & rolling training window

Our historical backtest, **Algorithm 6** below is composed of two phases, the *refitting period* for periodic re-fitting of the Kalman filters in JDKF and Dynamic PCA, and the *backtesting period* for the rolling one-step-ahead predictions of portfolio return. Figure 5 displays a schematic representation of our backtesting design. First, for JDKF and Dynamic PCA, we periodically refit the Kalman filters based on a fixed refitting period  $R$ , for the rolling window training, we select a fixed window size of  $s$ . The idea is to start the Kalman filters with lead time  $R$  and run them through the end of the backtesting period. During the backtesting period, we retrieve the necessary inputs already estimated from the Kalman filters, primarily the filtered estimates for the diffusion coordinates and PC components, and train our models on a one-step-ahead rolling basis, training on data from  $t - s : t$  and predicting portfolio return one test period out.

The reason our backtesting design has an additional phase for refitting the Kalman filters, is so that we can avoid refitting the Kalman filter every time the training window rolls one period ahead. The rationale is the well-known burn-in period phenomenon observed in the Kalman filter. The burn-in period refers to the initial phase of the Kalman filter algorithm during which the estimates might not yet accurately reflect the system state. Allowing the filter to run through the burn-in period allows the algorithm to converge to a more stable set of state estimates. For this very reason, we start up the filter with a lead before the backtesting period and let it run for some time in order for the estimates to stabilize.

---

**Algorithm 6** Historical Rolling Back-Test SSA vs JDKF with Periodic Re-Fitting

---

**Require:**  $s, T, K, R$

- ▷  $s = \#$  periods in rolling window for model training
- ▷  $T = \#$  periods in the data
- ▷  $K = \#$  Monte-Carlo samples used to estimate factor model-based scenario Portfolio Return
- ▷  $R = \#$  months before re-fitting the Kalman filter
- ▷  $r$  is the start index for refitting
- ▷  $r_{\text{end}}$  is the end index for refitting

- 1: **for**  $r \leftarrow 0 : R : T - 1$  **do**
- 2:      $r_{\text{end}} = \min(r + R + s, T)$
- 3:     Fit JDKF parameters  $(\Lambda, \mathbf{H}^x, \mathbf{R}_x, \mathbf{R}_y, \mathbf{R}_{xy}, \mathbf{Q}, \mathbf{B})$  from  $(x_{r:r_{\text{end}}}, y_{r:r_{\text{end}}})$
- 4:     Fit Dynamic PCA Kalman Filter parameters  $(\mathbf{A}, \mathbf{\Gamma}, \mathbf{R}, \mathbf{Q})$  from  $(x_{r:r_{\text{end}}}, y_{r:r_{\text{end}}})$
- 5:     **for**  $t \leftarrow \max(s, r + s)$  to  $r_{\text{end}}$  **do**
- 6:         **Retrieve Precomputed Kalman Filter Estimates**
- 7:         Retrieve  $\hat{\psi}_t, \hat{z}_t$  from Kalman filter estimates
- 8:         **Estimate Multivariate Regression Model**
- 9:         Fit  $\tilde{\mathbf{B}}$  using  $(y_{t-s:t}, x_{t-s:t})$
- 10:         **Compute Portfolio Simulations**
- 11:          $\hat{V}_{t+1, \text{JDKF}} \leftarrow \text{JDKF\_Simulation}(K, \psi_t, \mathbf{B}, \mathbf{H}_x, x_{t+1}) \dots (\text{Algorithm 5})$
- 12:          $\hat{V}_{t+1, \text{Dynamic PCA}} \leftarrow \text{DynamicPCA\_Simulation}(K, z_t, \tilde{\mathbf{B}}, \mathbf{\Gamma}, x_{t+1}) \dots (\text{Algorithm 4})$
- 13:          $\hat{V}_{t+1, \text{Static PCA}} \leftarrow \text{StaticPCA\_Simulation}(x_{t-s:t}, x_{t+1}, \tilde{\mathbf{B}}) \dots (\text{Algorithm 3})$
- 14:          $\hat{V}_{t+1, \text{SSA}} \leftarrow \text{SSA\_Simulation}(x_t, x_{t+1}, \tilde{\mathbf{B}}) \dots (\text{Algorithm 2})$
- 15:         Compute true portfolio return  $V_{t+1, \text{TRUE}}$
- 16:         **Compute Errors**
- 17:          $E_{\text{JDKF}, t+1} = |\hat{V}_{t+1, \text{JDKF}} - \hat{V}_{t+1, \text{TRUE}}|$
- 18:          $E_{\text{Dynamic PCA}, t+1} = |\hat{V}_{t+1, \text{Dynamic PCA}} - \hat{V}_{t+1, \text{TRUE}}|$
- 19:          $E_{\text{Static PCA}, t+1} = |\hat{V}_{t+1, \text{Static PCA}} - \hat{V}_{t+1, \text{TRUE}}|$
- 20:          $E_{\text{SSA}, t+1} = |\hat{V}_{t+1, \text{SSA}} - \hat{V}_{t+1, \text{TRUE}}|$
- 21:     **end for**
- 22: **end for**

---

In all of our experiments in Section 6.2, we use  $K = 10,000$  Monte Carlo simulations of conditional portfolio returns for the probabilistic models JDKF and Dynamic PCA. Since we are working under the special linear multi-factor model case of our JDKF framework, for each refitting period we estimate  $\mathbf{B}$  via ordinary least squares (OLS) and  $\mathbf{R}$  as the empirical covariance of the OLS residuals; furthermore, we estimate  $\mathbf{V}$  as the empirical covariance matrix of the common factors. Given the time series of portfolio return predictions  $\hat{V}_t$  and absolute errors  $E_t$  for each model from running the historical backtests, we then consider two main metrics for assessing model performance. Following the literature, as in [HL20], we consider the Mean Absolute Error (MAE) for each model defined as:

$$\frac{1}{T_{\text{test}}} \sum_{t=1}^{T_{\text{test}}} |\hat{V}_t - V_{t, \text{TRUE}}|$$

where  $T_{\text{test}}$  is the number of time periods for each test financial crisis. We also consider the percentage accuracy of JDKF against the comparison benchmarks, defined as the percentage of time JDKF yielded a predicted portfolio return closer to the truth, expressed as:

$$\frac{\sum_{t=1}^{T_{\text{test}}} \mathbb{1}_{\{E_{\text{JDKF},t}/E_{\text{bench},t} < 1\}}}{T_{\text{test}}} \times 100 \text{ where } E_t = |\hat{V}_t - V_{t,\text{TRUE}}|$$

We also employ standard Value-at-Risk (VaR) exceptions tests to statistically test whether the predicted portfolio returns  $\hat{V}_{t,\text{JDKF}}$  from the backtest are consistent with the realized  $V_{t,\text{TRUE}}$ . As is standard practice in risk management, and using  $V_t$  as the random variable representing portfolio return, the time  $t$  level- $\alpha$  VaR, which is an  $\mathcal{F}_t$ -measurable random variable, is defined for  $\alpha \in (0, 1)$  as:

$$\mathbb{P}(V_t \leq \text{VaR}_t(\alpha) | \mathcal{F}_t) = 1 - \alpha$$

In short, the time  $t$  VaR at level  $\alpha$  is simply the  $(1 - \alpha)$ -quantile of the distribution of the portfolio return conditional on  $\mathcal{F}_t$ . Now, a VaR exception is defined as the event that the realized portfolio return is below  $\text{VaR}_t(\alpha)$ , as is standard practice, one can then define an indicator variable:

$$\mathbb{1}_t(\alpha) = \begin{cases} 1 & , \text{ if } V_t < \text{VaR}_t(\alpha) \\ 0 & , \text{ otherwise} \end{cases}$$

Our backtest gives us a sequence of empirical VaR exception indicators  $\hat{\mathbb{1}}_t(\alpha)$  from the empirical distribution of the JDKF portfolio return predictions. Following [Kup95], under the null hypothesis that JDKF is correct,  $\sum_{t=1}^T \hat{\mathbb{1}}_t(\alpha)$  follows a Binomial distribution with  $T$  trials and success probability  $1 - \alpha$ , from which a two-sided binomial test follows with test statistic:

$$Z_T = \frac{\sum_{t=1}^T \hat{\mathbb{1}}_t(\alpha) - T(1 - \alpha)}{\sqrt{T\alpha(1 - \alpha)}}$$

which we use to test the null hypothesis.

## 6 Model Estimation using Real Data

### 6.1 Data Description

We model the series of stock returns via a classical macroeconomic factor model with the 124 FRED-MD macro-level factors from [MN16] plus the 8 macroeconomic factors from [GW08]. This gives us a total of  $D=132$  common factors. We utilize the curated data version as provided from [CRR86], which applies some standard transformations to the macro factors to ensure we deal with stationary time series (see Appendix E for the transformation details). The monthly stock returns data is obtained from CRSP. The time period considered is 1967-2016. We consider stocks trading in the NYSE, NASDAQ, and the American Stock Exchange. For each financial crisis period in our backtests, we maximize the size of the universe of firms by using the largest number of firms present throughout the entire time span of the considered period. We select four periods for out-of-sample prediction:

1. July 1990 - Mar 1991. We fit the Kalman filters only once with sufficient lead time before the start of the crisis. We re-train for each rolling window time step on all data available from  $t - s : t$  and predict conditional portfolio return for each of the 8 periods (months) in the backtesting phase. This period captures to the oil price shock of 1990, debt accumulation, and consumer pessimism present during those times. For this period, we have a universe of  $N=1,200$  firms.

2. Mar 2001 - Nov 2001. We fit the Kalman filters only once with sufficient lead time before the start of the crisis. We re-train for each rolling window time step on all data available from  $t - s : t$  and predict conditional portfolio return for each of the 8 periods in the backtesting phase. This period captures the dot-com bubble and the 9/11 attacks. For this period we have a universe of  $N=1,344$  firms.
3. Dec 2007 - June 2009. We fit the Kalman filters only once, with sufficient lead time before the start of the crisis period. We re-train for each rolling window time step on all data available from  $t - s : t$  and predict conditional portfolio return for each of the 18 periods in the backtesting phase. This period contains the subprime mortgage crisis. For this period we have a universe of  $N=1,409$  firms.
4. June 2004-December 2016, where we periodically refit the Kalman filter every 50 months and predict conditional portfolio return for each of the 150 periods within the crisis; we have three backtesting periods, each of length 50, corresponding exactly as in Figure 5. This period captures the 2007-2009 housing crisis and this test was conducted to allow for a large training set and a large out-of-sample test set to allow for a more robust binomial VAR exceptions test. For this period we have a universe of  $N=1,776$  firms.

For our empirical tests, we consider a portfolio manager who on each period uses the  $1/N$  rule to construct the weights of his portfolio. To define our scenarios, we consider the following macroeconomic variables, which roughly correspond to the FED’s 2022 variables for their supervisory scenarios. These variables are taken as our subset  $\mathcal{S}$  of the common factors that will define the stress variables in the historical backtests:

Table 3: Scenario Stress Macroeconomic Variables

Variable Name	Description
S&P 500	S&P’s Common Stock Price Index: Composite
CPIAUCSL	CPI: All Items
EXSZUSx	Switzerland / U.S. Foreign Exchange Rate
EXJPUSx	Japan / U.S. Foreign Exchange Rate
EXUSUKx	U.S. / U.K. Foreign Exchange Rate
EXCAUSx	Canada / U.S. Foreign Exchange Rate
FEDFUNDS	Effective Federal Funds Rate
RPI	Real Personal Income
UNRATE	Civilian Unemployment Rate
TB3MS	3-Month Treasury Bill Rate
GS5	5-Year Treasury Rate
GS10	10-Year Treasury Rate
AAA	Moody’s Seasoned Aaa Corporate Bond Yield
BAA	Moody’s Seasoned Baa Corporate Bond Yield
VXOCLSx	CBOE S&P 100 Volatility Index: VXO

## 6.2 Stress Test Analysis Data

We conduct a historical backtest as outlined in Algorithm 6 for each one of the financial crises. For each backtest, in addition to reporting the performance metrics MAE and percentage accuracy, we also display the time series plots of the predicted conditional portfolio returns for each one of the

models along with the true historical portfolio returns, where we re-emphasize that each portfolio is constructed with the  $1/N$  rule. An important note is that for Static PCA, we perform each backtest for every possible PC component dimension and select the best performing one in terms of MAE. We begin with the richest of the four backtests, spanning June 2004-December 2016, where we have 150 prediction periods. As mentioned earlier, in this backtest we periodically refit the Kalman filters every 50 months. Figure 6 displays the time series of the conditional predictions from the backtest. We note that for a few months, Dynamic PCA yielded predictions that were significantly far off from the truth, we removed some of these outlier predictions from the plot to preserve the visibility of all the other time series displayed. We display a gray bar over each month where Dynamic PCA yielded such an outlier prediction.

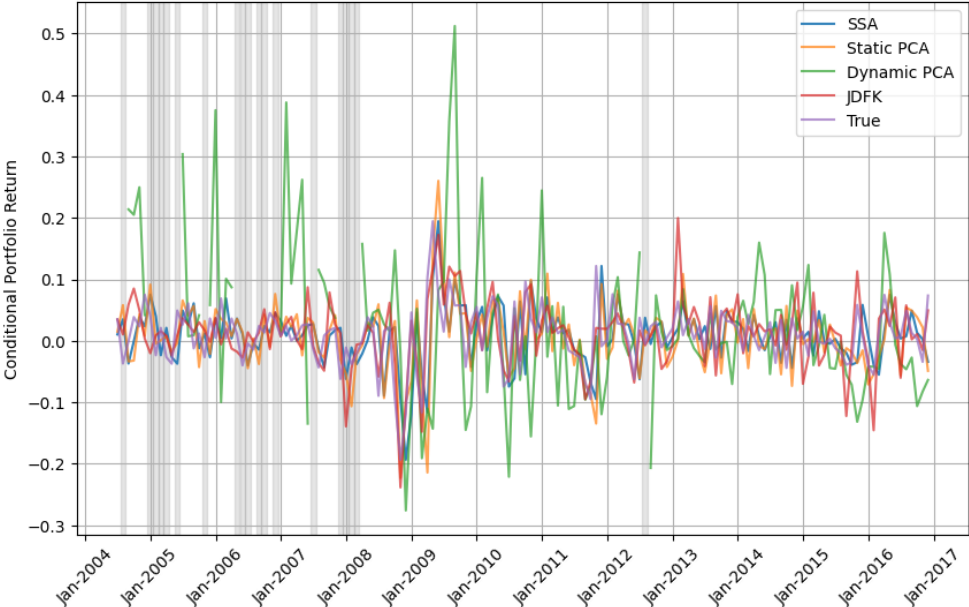


Figure 6: True and conditionally predicted portfolio returns spanning 150 prediction periods. June 2004-December 2016

We report the MAE for each model in Table 6. We find that JDKF achieves a significantly lower MAE than all of the other benchmarks, and a 35.86% reduction over the MAE achieved by SSA, which is the second best performing benchmark in terms of MAE. In terms of percentage accuracy, as shown in Table 7, over the 150 predicted periods, JDKF performs better than SSA 66% of the time, better than Dynamic PCA 66.67% of the time, and better than Static PCA 76.67% of the time. Notice that even though Static PCA achieved a slightly higher MAE than SSA (about 5.9% higher), the percentage of time that JDKF performs better than Static PCA is lower than that of SSA. This indicates that, while on average SSA achieves a slightly lower absolute error, Static PCA is more consistent in yielding predictions closer to JDKF. This is suggestive of SSA exhibiting more frequent large deviations, whereas Static PCA, despite its slightly higher MAE, yields predictions that are more stable relative to JDKF across the 150 prediction periods.

As is common practice, we also assess whether the realized portfolio values are consistent with the conditionally predicted portfolio values via a 95% VaR exceptions test on the predictions obtained under JDKF. We have already seen that JDKF is superior to all comparison benchmarks not only in terms of MAE, but also in terms of percentage accuracy, now we statistically assess the null hypothesis that JDKF is the correct model via the two-sided binomial VaR exceptions test,

and obtain the following results:

<b>Metric</b>	<b>Value</b>
VaR Threshold ( $\alpha = 0.05$ )	-0.0691
Actual Exceptions	7
Expected Exceptions	7.5
Binomial Test p-value	0.99

Table 4: 95% Value at Risk (VaR) Exceptions Results

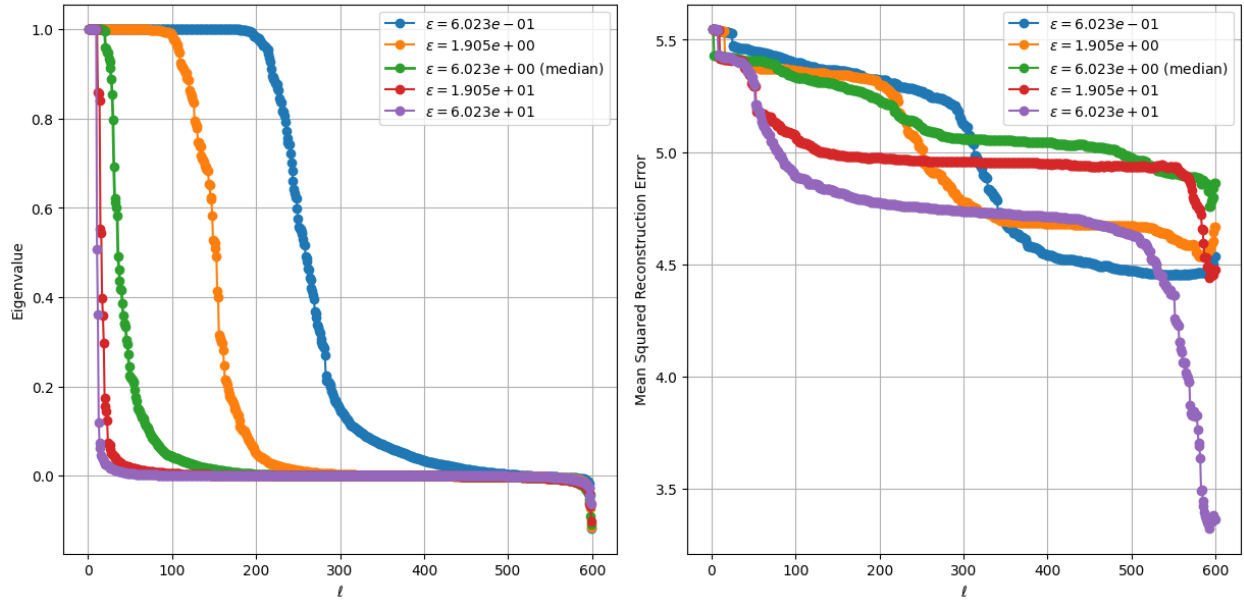
we also report the results for a 99% VaR exceptions two-sided binomial test:

<b>Metric</b>	<b>Value</b>
VaR Threshold ( $\alpha = 0.01$ )	-0.1468
Actual Exceptions	1
Expected Exceptions	1.5
Binomial Test p-value	0.99

Table 5: 99% Value at Risk (VaR) Exceptions Results

Note that for both the 95% VaR exceptions test in Table 4 and the 99% VaR exceptions test in Table 5 there is no strong evidence to reject the null hypothesis that JDKF is correct. Meaning that the VaR estimates from JDKF appear statistically consistent with the expected distribution. In both cases the number of observed exceptions is in line with the expected exceptions. For the 95% test we observe 7 exceptions with an expected 7.5, JDKF is slightly conservative but certainly well within an acceptable range. This indicates JDKF is not displaying systematic under or over-estimation of risk.

We now proceed to perform similar backtests on the other shorter periods of financial turmoil, which contain a very small number of prediction periods. Note that there are more periods of recessions in our data sample, but we decided to begin in 1990 to have a reasonable training window size. As mentioned earlier, for each of these shorter crisis periods, we fit the Kalman filter once starting a few months before the beginning of the interval to overcome the burn-in period. For the diffusion mapping, throughout all backtests (including the already discussed June 2004-December 2016), we made the empirical choice of  $\ell = 39$  for the diffusion coordinate embedding dimension and set  $\varepsilon$  to the median  $d(x(t_i), x(t_j))$ , based on the decay of the spectrum of the  $\mathbf{P}$  matrix, displayed in Figure 7a for different choices of  $\varepsilon$ . The rate of spectrum decay generally determines how well the manifold structure has been captured, slower decay requires more eigenvectors to represent the data, while faster decay usually suggests fewer dimensions are sufficient. We also display in Figure 7b the mean squared reconstruction error (using the lifting operator  $\mathbf{H}^x$ ) for the diffusion maps computed on the macroeconomic factors for different choices of  $\ell$  and  $\varepsilon$ , our choice of  $\varepsilon$  balances a lower error than that for smaller  $\varepsilon$  with a better capture of the manifold structure than that for larger  $\varepsilon$ , as evidenced by Figure 7a, where the larger  $\varepsilon$  capture mostly noise. These choices of  $\ell$  and  $\varepsilon$  are fixed throughout the historical backtests and was obtained by inspecting the point where we observe the largest pairwise consecutive drop in the ordered eigenvalues obtained from applying the diffusion map to the entire time series of macroeconomic factors.

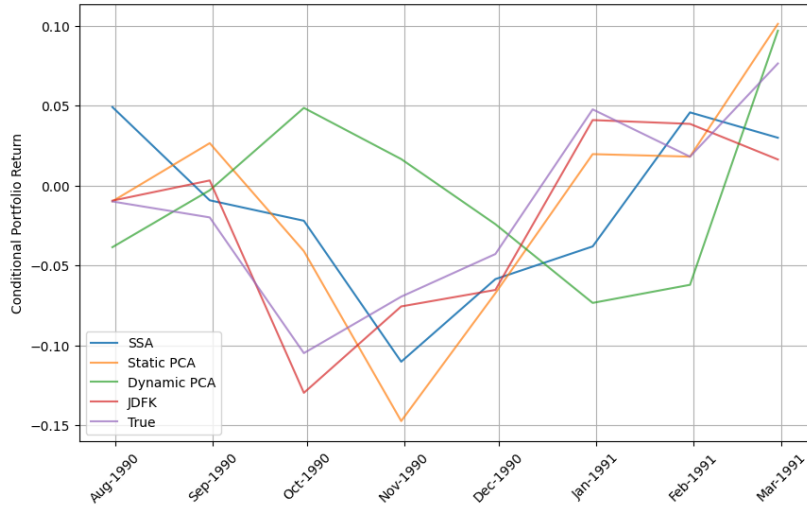


(a) Diffusion Map Spectrum: Eigenvalues of the Markov Matrix  $\mathbf{P}$  for different choices of  $\varepsilon$  as a function of the diffusion coordinate embedding dimension  $l$

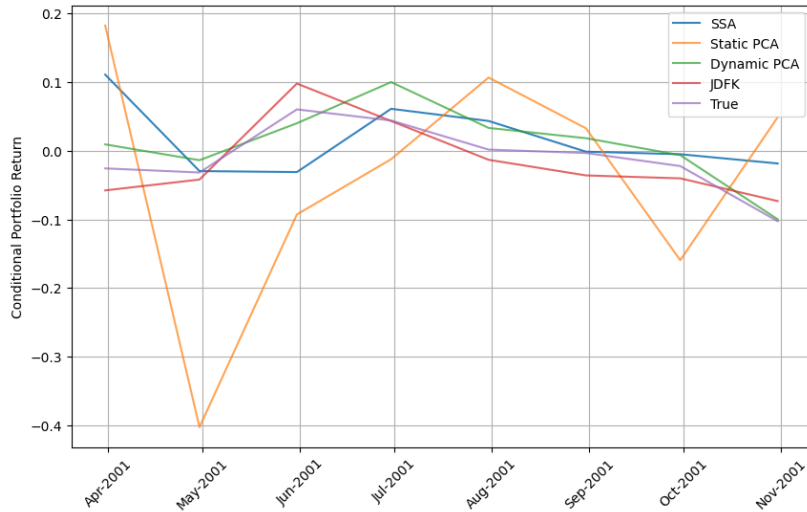
(b) Mean Squared Reconstruction Error: Mean Squared Error from reconstructing diffusion coordinates via the lifting operator  $\mathbf{H}^x$  for different choices of  $\varepsilon$  as a function of the diffusion coordinate embedding dimension  $l$

Figure 7: Diffusion Map Spectrum and Reconstruction Error of the Macroeconomic Factors

Figure 8 displays the conditional predicted portfolio returns under each model as well as the truth for each of the three shorter crisis periods. Again, we note that for Dec 2007-June 2009, Dynamic PCA yielded outlier predictions during the first few periods, which we removed from the plot in panel 8c for visibility purposes, and marked those periods with a gray bar. Analyzing the panel 8a for the Oil Price Shock crisis from July 1990-March 1991, it is striking to observe the consistency of the movements between JDKF and the true portfolio return. Focusing on the sharp downturn from September to October 1990, followed by the consistent increase from October 1990 to January 1991, JDKF correctly anticipates the fall and rise, indicating that the dynamic correlation among the common factors is being captured from our sampling procedure. SSA and Static PCA for instance, seem to identify the sudden fall and subsequent steady rise but with a clear delay. Dynamic PCA struggles to capture any consistent trends from the true portfolio returns, this is highly indicative that neither the structure of the common factors nor their dynamics are well explained by linear models (PCA, and VAR(1)). Furthermore, as shown in Table 6, JDKF achieves the lowest MAE out of all benchmarks, followed closely by Static PCA. While it is true that Static PCA is a close competitor of JDKF in terms of MAE, Table 7 shows that JDKF achieves higher accuracy than Static PCA 62.5% of the time, indicating that JDKF is more consistent in capturing month-to-month fluctuations.



(a)



(b)



(c)

Figure 8: Historical back-tests during major financial crises. (a) July 1990 - March 1991: True and Conditionally Predicted Portfolio Returns Spanning the Oil Price Shock of 1990, Debt Accumulation, Consumer Pessimism. (b) March 2001 - November 2001: True and Conditionally Predicted Portfolio Returns Spanning the Dot-Com Bubble, 9/11 Attacks (c) December 2007 - June 2009: True and Conditionally Predicted Portfolio Returns Spanning the Subprime Mortgage Crisis.

For the period encapsulating the Dot-Com Bubble and the 9/11 attacks, displayed in panel 8b, it is notable that from April to July 2001, the time series for the true portfolio return follows a zig-zag pattern followed by a slight downward trend thereafter, which is captured by JDKF and notably also by Dynamic PCA. Indeed JDKF outperforms all metrics in terms of MAE as per Table 6, but Dynamic PCA is a close competitor with respect to this metric. Even still, JDKF achieves approximately a 12.75% reduction in MAE over Dynamic PCA. Another notable fact from this backtest is that, unlike in the Oil Price shock crisis, Dynamic PCA is performing significantly better than Static PCA in terms of MAE and also time series trend consistency. This could be suggestive of dynamics during this period that are not highly nonlinear and are perhaps also well captured by linear models.

Finally, it is during the Mortgage crisis period from December 2007 to June 2009, displayed in panel 8c, where JDKF significantly outperforms all benchmarks by a wide margin in terms of both performance metrics. A visually striking indication of JDKF’s superiority can be observed during the months of October 2008 to March 2009, where there is a sharp spike down in the true portfolio return, which then roughly recovers towards the end of February 2009. JDKF is the only model to accurately capture this trend, again indicating that JDKF is successfully uncovering the joint dynamics of the factors driving the portfolio’s return and the conditional sampling procedure is uncovering their dynamic correlations. SSA again appears to predict spikes with a delay and Dynamic PCA completely confuses the temporal trends. Table 6 shows JDKF achieving a 39.17% reduction over the MAE achieved by Static PCA, which was the second best performing benchmark in terms of MAE. JDKF, as shown in Table 7 also achieves higher accuracy than Static PCA 72.22% of the time. The significantly higher MAE achieved by Dynamic PCA, combined with the obvious confusion in capturing the temporal trend of the true portfolio return and the fact that it performed relatively well during the Dot-Com Bubble, is suggestive of more nonlinearities present in the data during the Subprime Mortgage Crisis, which are being successfully picked up by JDKF due to the diffusion map embeddings.

These backtests provide solid evidence that taking the joint dynamics of the common factors into account result in more accurate scenario analysis. Furthermore, JDKF has provided a simple data-driven framework to define high-dimensional scenarios that are fully interpretable and embed them in a dynamic scenario analysis seamlessly without losing much explanatory power. We summarize the complete MAE numbers in the figures above in the following table:

Time Period	JDKF	SSA	Dynamic PCA	Static PCA
July 1990 - Mar 1991	<b>.0206</b>	.0462	.0658	.0332
Mar 2001 - Nov 2001	<b>.0219</b>	.0490	.0251	.1523
Dec 2007 - June 2009	<b>.0441</b>	.0750	1.017	.0725
Jun 2004 - Dec 2016	<b>.0304</b>	.0474	.2615	.0502

Table 6: MAE for JDKF and Benchmark Models Across Different Time Periods

As defined earlier, we also compute the proportion of time the ratio  $E_{\text{JDKF},t}/E_{\text{SSA},t}$  is less than 100%, which indicates the proportion of time JDKF gave a more accurate scenario portfolio return than SSA. And we similarly compute the proportion of time JDKF is more accurate than the PCA-based benchmarks. The proportions for all of the financial crisis periods against the benchmark models are listed in the following table:

<b>Time Period</b>	$E_{\text{JDKF},t}/E_{\text{SSA},t}$	$E_{\text{JDKF},t}/E_{\text{DynamicPCA},t}$	$E_{\text{JDKF},t}/E_{\text{StaticPCA},t}$
July 1990 - Mar 1991	62.5%	62.5%	62.5%
Mar 2001 - Nov 2001	62.5%	50%	100%
Dec 2007 - June 2009	72.22%	77.78%	72.22%
Jun 2004 - Dec 2016	66%	66.67%	76.67%

Table 7: Percentage of times JDKF predictions have a higher accuracy, measured by the absolute value error  $E_t$ . We consider four different financial crisis periods.

## 7 Conclusions

We have proposed a novel data-driven framework for dynamic factor modeling within a supervised learning setting where one observes both, a dataset of responses  $y(t) \in \mathbb{R}^n$ , and a high-dimensional set of covariates  $x(t) \in \mathbb{R}^m$ . Our framework requires no knowledge of the observation dynamics and is versatile enough that it can simultaneously handle the two sets of observations. The key assumption is that the intrinsic state  $\theta$  follows a Langevin equation with certain spectral properties, which we demonstrate is not too restrictive, particularly for financial applications. We uncover the joint dynamics of the covariates and responses in a purely data-driven way via lower-dimensional covariate embeddings that retain explanatory power while exhibiting simple linear dynamics.

We combine anisotropic diffusion maps with Kalman filtering to infer the latent dynamic covariate embeddings, and predict the response variable directly from the diffusion map embedding space. We develop a conditional sampling procedure that accounts for dynamic correlations between covariates when conditioning on fixed values for a subset of them, and note that the procedure is general enough that it allows for conditioning on subsets of responses as well. Our approach is justified via theoretical results on the convergence of anisotropic diffusion maps as well as the robustness of approximating the learned diffusion coordinates by linear SDEs. The former result applies concentration inequalities for Markov processes to generalize the arguments of [Sin06; SC08] to the time series case; the latter adapts arguments typically seen in literature on Markov chain Monte Carlo methods.

We study an application of our framework to financial stress testing, where we consider the special case of a linear multi-factor model. Our historical backtests demonstrate the superiority of our methodology in capturing dynamic correlations between the macroeconomic factors driving the return of equity portfolios. We make use of several comparison benchmarks, including the standard approach to scenario analysis and PCA-based models. We demonstrate through our empirical experiments that working on the diffusion coordinate space indeed uncovers the dynamics of the common factors and captures nonlinearities in the data during historical periods of financial stress.

While the primary application of our framework in this paper has been financial stress testing, it is important to emphasize the rich set of applications where our framework can be employed. First, our dynamic factor modeling framework is well-suited for asset pricing problems, where one seeks to construct a sparse set of dynamic factors from a high-dimensional factor zoo that possess high explanatory power for the cross-section of stock returns. Another application of our framework is to the problem of nowcasting, where one seeks to utilize a higher-frequency dataset to improve predictions on lower-frequency data. Our data-driven framework gives rise to a broad set of new possibilities, especially when one wishes to make minimal modeling and parametric assumptions on observed data.

## References

- [Ada08] R. Adamczak. “A tail inequality for suprema of unbounded empirical processes with applications to Markov chains”. *Electronic Journal of Probability* 13 (Jan. 2008).
- [BC98] J.-P. Bouchaud and R. Cont. “A Langevin approach to stock market fluctuations and crashes”. *The European Physical Journal B-Condensed Matter and Complex Systems* 6.4 (1998), pp. 543–550.
- [BGL14] D. Bakry, I. Gentil, and M. Ledoux. *Analysis and Geometry of Markov Diffusion Operators*. Vol. 348. Grundlehren der mathematischen Wissenschaften. Cham: Springer International Publishing, 2014.
- [BH16] T. Berry and J. Harlim. “Variable bandwidth diffusion kernels”. *Applied and Computational Harmonic Analysis* 40.1 (Jan. 2016), pp. 68–96.
- [BLM13] S. Boucheron, G. Lugosi, and P. Massart. *Concentration Inequalities: A Nonasymptotic Theory of Independence*. Oxford University Press, Feb. 2013.
- [Boa22] Board of Governors of the Federal Reserve System. *2022 Stress Test Scenarios*. Tech. rep. Board of Governors of the Federal Reserve System publication. Feb. 2022.
- [Can01] E. Canessa. “Langevin Dynamics of Financial Systems: A Second-Order Analysis”. *The European Physical Journal B* 22 (2001), pp. 123–127.
- [CCG12] P. Cattiaux, D. Chafai, and A. Guillin. “Central limit theorems for additive functionals of ergodic Markov diffusions processes”. *ALEA* 9.2 (2012), pp. 337–382.
- [CE95] M. Chesney and R. J. Elliott. “Estimating the instantaneous volatility and covariance of risky assets”. *Applied Stochastic Models and Data Analysis* 11.1 (1995), pp. 51–58.
- [CL06] R. R. Coifman and S. Lafon. “Diffusion maps”. *Applied and Computational Harmonic Analysis* 21.1 (2006), pp. 5–30.
- [Coi+08] R. R. Coifman et al. “Diffusion maps, reduction coordinates, and low-dimensional representation of stochastic systems”. *Multiscale Modeling & Simulation* 7.2 (2008), pp. 842–864.
- [CP12] C. Cuny and M. Peligrad. “Central Limit Theorem Started at a Point for Stationary Processes and Additive Functionals of Reversible Markov Chains”. *Journal of Theoretical Probability* 25.1 (Mar. 2012), pp. 171–188.
- [CPZ20] L. Chen, M. Pelger, and J. Zhu. *Internet Appendix for Deep Learning in Asset Pricing*. Available at SSRN: <https://ssrn.com/abstract=3600206>. Sept. 2020.
- [CRR86] N.-F. Chen, R. Roll, and S. A. Ross. “Economic Forces and the Stock Market”. *The Journal of Business* 59.3 (1986), pp. 383–403.
- [DL01] Y. Derriennic and M. Lin. “The central limit theorem for Markov chains with normal transition operators, started at a point”. *Probability Theory and Related Fields* 119.4 (Apr. 2001), pp. 508–528.
- [DL03] Y. Derriennic and M. Lin. “The central limit theorem for Markov chains started at a point”. *Probability Theory and Related Fields* 125.1 (Jan. 2003), pp. 73–76.
- [Dou+11] R. Douc et al. “Consistency of the maximum likelihood estimator for general hidden Markov models”. *The Annals of Statistics* 39.1 (Feb. 2011).

- [FJS21] J. Fan, B. Jiang, and Q. Sun. “Hoeffding’s Inequality for General Markov Chains and Its Applications to Statistical Learning”. *Journal of Machine Learning Research* 22 (2021), pp. 1–35.
- [GRS08] D. Giannone, L. Reichlin, and D. Small. “Nowcasting: The real-time informational content of macroeconomic data”. *Journal of Monetary Economics* 55.4 (May 2008), pp. 665–676.
- [GW08] A. Goyal and I. Welch. “A Comprehensive Look at the Empirical Performance of Equity Premium Prediction”. *The Review of Financial Studies* 21.4 (2008), pp. 1455–1508.
- [HL20] M. B. Haugh and O. R. Lacedelli. “Scenario Analysis for Derivatives Portfolios via Dynamic Factor Models”. *Quantitative Finance* 20.9 (2020), pp. 1471–1490.
- [JYC09] M. Jeanblanc, M. Yor, and M. Chesney. *Mathematical Methods for Financial Markets*. London: Springer London, 2009.
- [KS14] I. Karatzas and S. Shreve. *Brownian Motion and Stochastic Calculus*. New York, NY: Springer, 2014.
- [Kup95] P. H. Kupiec. “Techniques for Verifying the Accuracy of Risk Measurement Models”. *The Journal of Derivatives* 3.2 (1995), pp. 73–84.
- [KV86] C. Kipnis and S. R. S. Varadhan. “Central limit theorem for additive functionals of reversible Markov processes and applications to simple exclusions”. *Communications in Mathematical Physics* 104.1 (Mar. 1986), pp. 1–19.
- [Lia+15] W. Lian et al. “Multivariate time-series analysis and diffusion maps”. *Signal Processing* 116 (Nov. 2015), pp. 13–28.
- [Mia14] B. Miasojedow. “Hoeffding’s inequalities for geometrically ergodic Markov chains on general state space”. *Statistics & Probability Letters* 87 (Apr. 2014), pp. 115–120.
- [MN16] M. W. McCracken and S. Ng. “FRED-MD: A Monthly Database for Macroeconomic Research”. *Journal of Business & Economic Statistics* 34.4 (2016), pp. 574–589.
- [Pau15] D. Paulin. “Concentration inequalities for Markov chains by Marton couplings and spectral methods”. *Electronic Journal of Probability* 20.79 (2015), pp. 1–32.
- [RR04] G. O. Roberts and J. S. Rosenthal. “General state space Markov chains and MCMC algorithms”. *Probability Surveys* 1 (2004), pp. 20–71.
- [RTS65] H. Rauch, F. Tung, and C. Striebel. “Maximum likelihood estimates of linear dynamic systems”. *AIAA Journal* 55.8 (1965), pp. 1445–1450.
- [Rud12] D. Rudolf. “Explicit error bounds for Markov chain Monte Carlo”. *Dissertationes Mathematicae* 485 (2012), pp. 1–93.
- [SC08] A. Singer and R. R. Coifman. “Non-linear independent component analysis with diffusion maps”. *Applied and Computational Harmonic Analysis* 25.2 (2008), pp. 226–239.
- [Sin+09] A. Singer et al. “Detecting intrinsic slow variables in stochastic dynamical systems by anisotropic diffusion maps”. *Proceedings of the National Academy of Sciences* 106.38 (Sept. 2009), pp. 16090–16095.
- [Sin06] A. Singer. “From graph to manifold Laplacian: The convergence rate”. *Applied and Computational Harmonic Analysis* 21.1 (July 2006), pp. 128–134.

- [ST22] T. Shnitzer and R. Talmon. “Manifold learning with contracting observers for data-driven time-series analysis”. *Journal of Machine Learning Research* 23.77 (2022), pp. 1–41.
- [STS20] T. Shnitzer, R. Talmon, and J.-J. Slotine. “Diffusion Maps Kalman Filter for a Class of Systems with Gradient Flows”. *The Koopman Operator in Systems and Control: Concepts, Methodologies, and Applications*. Springer, 2020, pp. 359–382.
- [SW16] J. H. Stock and M. W. Watson. “Dynamic Factor Models, Factor-Augmented Vector Autoregressions, and Structural Vector Autoregressions in Macroeconomics”. *Handbook of Macroeconomics, Volume 2A*. Elsevier B.V., 2016, pp. 415–525.

# Appendices

## A Diffusion Kalman Filter

Assuming that the gradients in (3.8) are (approximately) constant, [STS20] define a state-space model for the diffusion coordinates using a Kalman filter ( $x_t$  is the measurement and  $\psi_t$  diffusion coordinates):

$$\begin{aligned}\psi_t &= (I - \Lambda)\psi_{t-1} + w_{t-1} \\ x_t &= \mathbf{H}\psi_t + v_t\end{aligned}$$

where  $\Lambda$  is the transition matrix for the linear dynamics containing the mapped eigenvalues  $-\varepsilon^{-1} \log \kappa_1, \dots, -\varepsilon^{-1} \log \kappa_\ell$  on its diagonal, and  $\mathbf{H}$  is the lifting operator. Note that  $w$  and  $v$  are Gaussian noises with covariance matrices  $\mathbf{Q}$  and  $\mathbf{V}$  respectively. Denote  $\hat{\psi}_t = \mathbb{E}[\psi_t | \mathcal{F}_{t-1}]$ , where  $\mathcal{F}_{t-1} = \{x_0, \dots, x_{t-1}\}$ , and  $P_t = \text{Cov}(\psi_t | \mathcal{F}_{t-1})$

The Diffusion Kalman Filter (DKF) update equations are (with  $\mathbf{A} = I - \Lambda$ ):

$$\begin{aligned}\hat{\psi}_t &= \mathbf{A}\hat{\psi}_{t-1} + K_t (x_t - \mathbf{H}\mathbf{A}\hat{\psi}_{t-1}) \\ P_t &= (I - K_t\mathbf{H}) (\mathbf{A}P_{t-1}\mathbf{A}^T + \mathbf{Q}) \\ K_t &= (\mathbf{A}P_{t-1}\mathbf{A}^T + \mathbf{Q}) \mathbf{H}^T \times (\mathbf{H}\mathbf{A}P_{t-1}\mathbf{A}^T\mathbf{H}^T + \mathbf{H}\mathbf{Q}\mathbf{H}^T + \mathbf{V})^{-1}\end{aligned}$$

## B Joint Diffusion Kalman Filter Explanatory Power

The figures below show respectively the individual  $R^2$  from regressing each time series of stock returns against the full and reduced sets of factors. Note the significant loss in explanatory power from using the DKF diffusion coordinates, this is to be expected since their estimation process does not jointly consider the variation in the dependent variables.

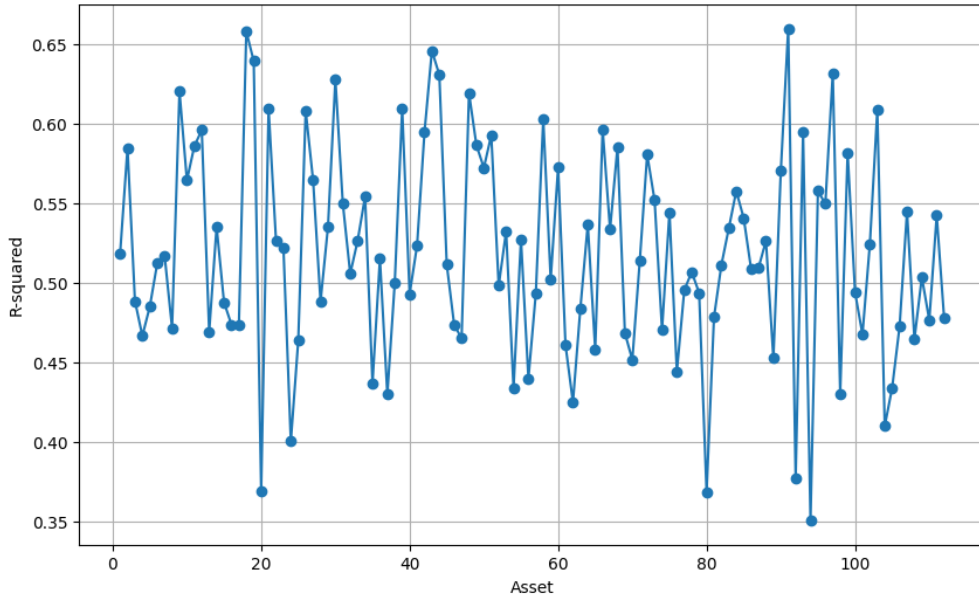


Figure B.1: Plot of the  $R^2$  from the individual stock return time series regressions directly from the JDKF state-space fitted observation equation

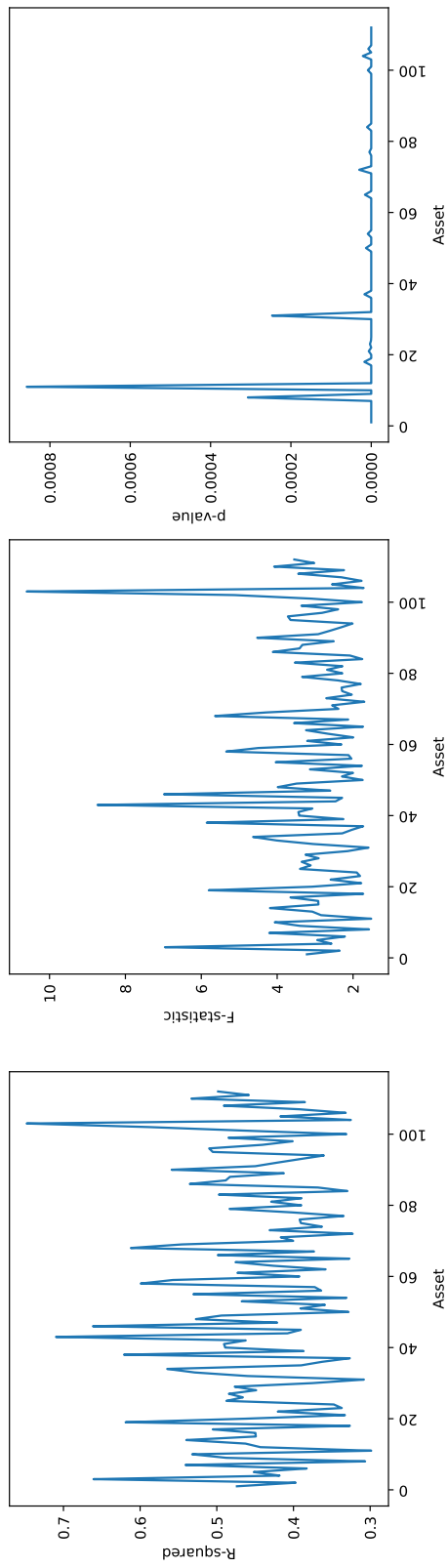


Figure B.2: Plot of the  $R^2$  from the OLS Regressions of Individual Stocks vs Original Set of 132 Macro Variables

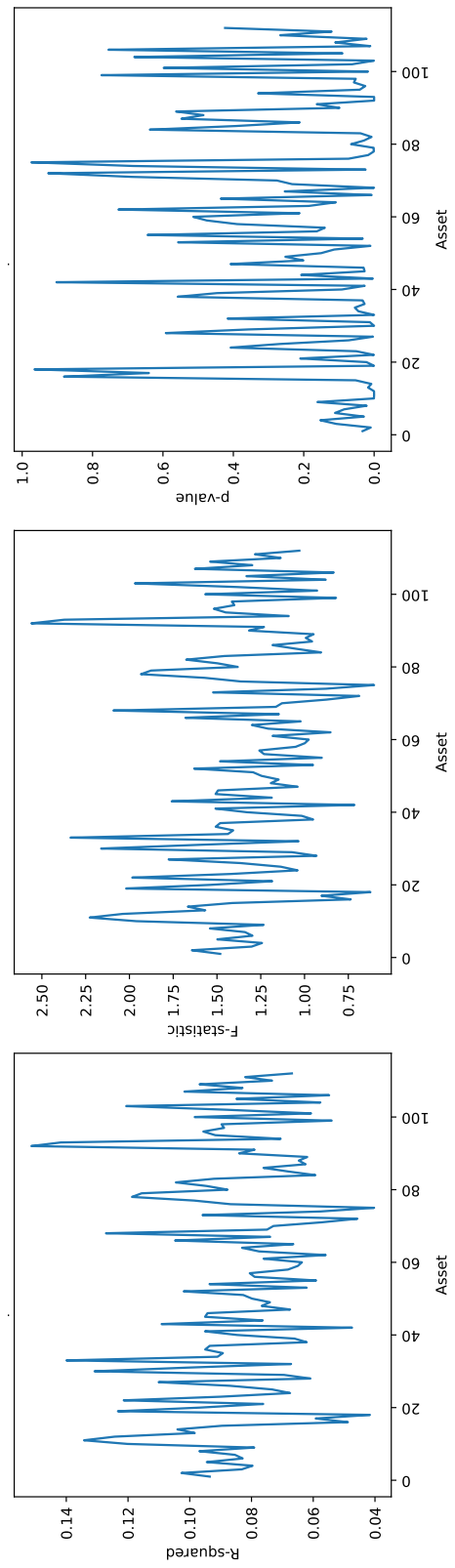


Figure B.3: Plot of the  $R^2$  from OLS Regressions of Individual Stocks vs Reduced Set of 39 DKF Diffusion Coordinates

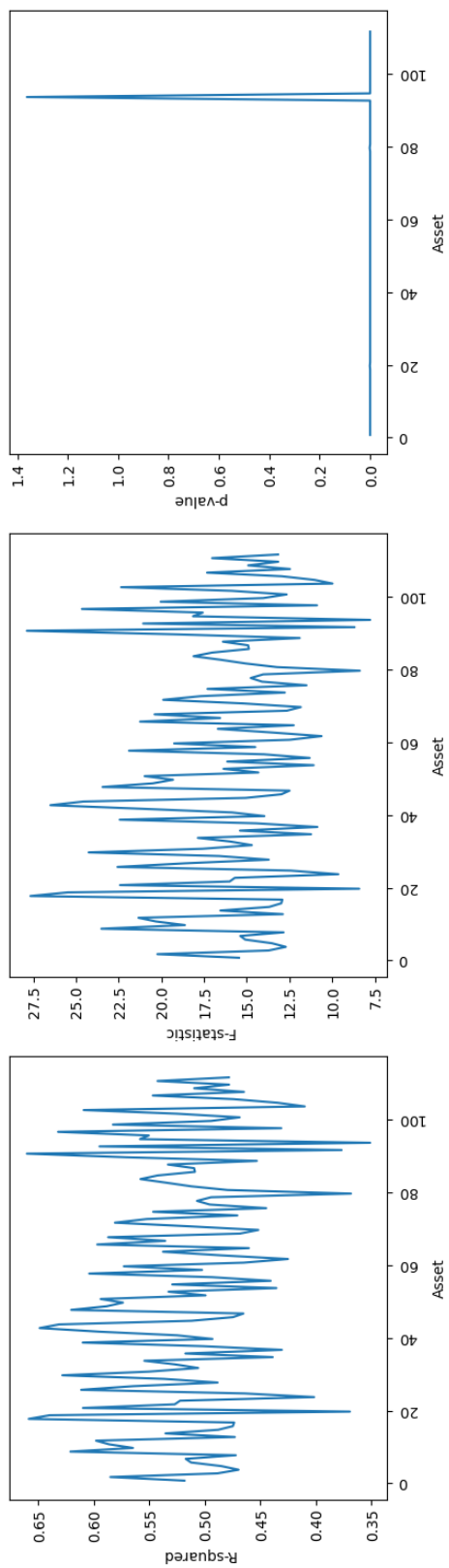


Figure B.4: Plot of the  $R^2$  from OLS Regressions of Individual Stocks vs Reduced Set of 39 JDKF Diffusion Coordinates

## C Second Moment Computation

We provide the full computation for the second moment of  $V$  from the proof of Theorem 4.3. A Taylor approximation following [SC08, Equation (28)] yields

$$\begin{aligned}\mathbb{E}_\mu[u] &= (2\pi\varepsilon)^{d/2}\{p(w)f(w) + \frac{\varepsilon}{2}[E(w)p(w)f(w) + \Delta(p(w)f(w))] + O(\varepsilon^2)\} \\ \mathbb{E}_\mu[v] &= (2\pi\varepsilon)^{d/2}\{p(w) + \frac{\varepsilon}{2}[E(w)p(w) + \Delta p(w)] + O(\varepsilon^2)\} \\ \mathbb{E}_\mu[u^2] &= (\pi\varepsilon)^{d/2}\{p(w)f^2(w) + \frac{\varepsilon}{4}[E(w)p(w)f(w)^2 + \Delta(p(w)f^2(w))] + O(\varepsilon^2)\} \\ \mathbb{E}_\mu[v^2] &= (\pi\varepsilon)^{d/2}\{p(w) + \frac{\varepsilon}{4}[E(w)p(w) + \Delta p(w)] + O(\varepsilon^2)\} \\ \mathbb{E}_\mu[uv] &= (\pi\varepsilon)^{d/2}\{p(w)f(w) + \frac{\varepsilon}{4}[E(w)p(w)f(w) + \Delta(p(w)f(w))] + O(\varepsilon^2)\}\end{aligned}$$

where  $E$  is a scalar function (see [SC08, Paragraph following Equation (28)]) which will cancel out in the following computation. In what follows, we will suppress dependence on  $w$ , and all expectations will be taken with respect to the invariant measure  $\mu$ .

Now, we define the variable  $Y_j$  to be the numerator of  $V(\theta(t_j))$ :

$$Y_j = \mathbb{E}[v]u(\theta(t_j)) - \mathbb{E}[u]v(\theta(t_j)) + \alpha\mathbb{E}[v](\mathbb{E}[v] - v(\theta(t_j)))$$

The second moment is given by

$$\begin{aligned}\mathbb{E}[Y_j^2] &= \mathbb{E}[v]^2\mathbb{E}[u^2] - 2\mathbb{E}[v]\mathbb{E}[u]\mathbb{E}[uv] + \mathbb{E}[u]^2\mathbb{E}[v^2] \\ &\quad + 2\alpha\mathbb{E}[v]\{\mathbb{E}[u]\mathbb{E}[v^2] - \mathbb{E}[v]\mathbb{E}[uv]\} + \alpha^2\mathbb{E}[v]^2\{\mathbb{E}[v^2] - \mathbb{E}[v]^2\}\end{aligned}$$

We are interested in the regime where  $\alpha \ll \varepsilon$ , hence we neglect the terms with  $\alpha$  and  $\alpha^2$  when we substitute in the expressions for the moments of  $u$  and  $v$ . We then have:

$$\begin{aligned}\mathbb{E}Y_j^2 &= \\ (2\pi\varepsilon)^d\{p + \frac{\varepsilon}{2}[Ep + \Delta p] + O(\varepsilon^2)\}^2(\pi\varepsilon)^{d/2}\{pf^2 + \frac{\varepsilon}{4}[Epf^2 + \Delta(pf^2)] + O(\varepsilon^2)\} \\ &\quad - 2(2\pi\varepsilon)^d(\pi\varepsilon)^{d/2}\{pf + \frac{\varepsilon}{2}[Epf + \Delta(pf)] + O(\varepsilon^2)\}\{p + \frac{\varepsilon}{2}[Ep + \Delta p] + O(\varepsilon^2)\}\{pf + \frac{\varepsilon}{4}[Epf + \Delta(pf)] + O(\varepsilon^2)\} \\ &\quad + (2\pi\varepsilon)^d(\pi\varepsilon)^{d/2}\{pf + \frac{\varepsilon}{2}[Epf + \Delta(pf)] + O(\varepsilon^2)\}^2\{p + \frac{\varepsilon}{4}[Ep + \Delta p] + O(\varepsilon^2)\}\end{aligned}$$

To shorten notation, set  $H(g) = Eg + \Delta g$  for any given  $g$ . We then have:

$$\begin{aligned}\mathbb{E}Y_j^2 &= 2^d(\pi\varepsilon)^{3d/2}\left(\{p + \frac{\varepsilon}{2}H(p)\}^2\{pf^2 + \frac{\varepsilon}{4}H(pf^2)\} - 2\{p + \frac{\varepsilon}{2}H(p)\}\{pf + \frac{\varepsilon}{2}H(pf)\}\{pf + \frac{\varepsilon}{4}H(pf)\}\right. \\ &\quad \left. + \{pf + \frac{\varepsilon}{2}H(pf)\}^2\{p + \frac{\varepsilon}{4}H(p)\}\right) + \text{h.o.t.} \\ &= 2^d(\pi\varepsilon)^{3d/2}\left(\{p^2\frac{\varepsilon}{4}H(pf^2) + 2p^2f^2\frac{\varepsilon}{2}H(p)\} - 2\{p^2f^2 + \frac{\varepsilon}{2}H(p) + p^2f\frac{\varepsilon}{2}H(pf) + p^2f\frac{\varepsilon}{4}H(pf)\}\right. \\ &\quad \left. + \{2p^2f\frac{\varepsilon}{2}H(pf) + p^2f^2\frac{\varepsilon}{4}H(p)\}\right) + \text{h.o.t.} \\ &= 2^d(\pi\varepsilon)^{3d/2}\left(\frac{\varepsilon}{4}p^2H(pf^2) + (\varepsilon - \varepsilon + \frac{\varepsilon}{4})p^2f^2H(p) + (-\varepsilon - \frac{\varepsilon}{2} + \varepsilon)p^2fH(pf)\right) + \text{h.o.t.} \\ &= 2^d(\pi\varepsilon)^{3d/2}\frac{\varepsilon}{4}(p^2H(pf^2) + p^2f^2H(p) - 2p^2fH(pf)) + \text{h.o.t.}\end{aligned}$$

Looking at the term in parenthesis and using the identity  $\Delta(gh) = g\Delta h + h\Delta g + 2\nabla g \cdot \nabla h$  gives

$$\begin{aligned}
& p^2 H(pf^2) + p^2 f^2 H(p) - 2p^2 f H(pf) \\
&= p^2 (Epf^2 + \Delta(pf^2) + Epf^2 + f^2 \Delta p - 2Epf^2 - 2f\Delta(pf)) \\
&= p^2 (\Delta(pf^2) - 2f\Delta(pf) + f^2 \Delta p) \\
&= p^2 (p\Delta f^2 + f^2 \Delta p + 2\nabla p \cdot \nabla f^2 + f^2 \Delta p - 2f(p\Delta f + f\Delta p + 2\nabla p \cdot \nabla f)) \\
&= p^2 (p\Delta f^2 - 2fp\Delta f + 2\nabla p \cdot \nabla f^2 - 4f\nabla p \cdot \nabla f) \\
&= p^2 (\Delta(pf^2) - f^2 \Delta p - 2f(\Delta(pf) - f\Delta p))
\end{aligned}$$

So that

$$\mathbb{E}[Y_j^2] = 2^d (\pi\varepsilon)^{3d/2} \frac{\varepsilon}{4} p^2 (\Delta(pf^2) - 2f\Delta(pf) + f^2 \Delta p) + \text{h.o.t.}$$

Noting now that  $\Delta f^2 = 2f\Delta f + 2\nabla f \cdot \nabla f$  and  $\nabla f^2 = 2f\nabla f$ , we have that:

$$\Delta(pf^2) = p\Delta f^2 + f^2 \Delta p + 2\nabla p \cdot \nabla f^2 = 2pf\Delta f + 2p\nabla f \cdot \nabla f + f^2 \Delta p + 4f\nabla p \cdot \nabla f$$

and

$$2f\Delta(pf) = 2f^2 \Delta p + 2fp\Delta f + 4f\nabla p \cdot \nabla f$$

Hence,

$$\mathbb{E}[Y_j^2] = 2^d (\pi\varepsilon)^{3d/2} \left( \frac{\varepsilon}{2} p^3 \|\nabla f\|^2 + O(\varepsilon^2) \right)$$

Finally, we divide by  $\mathbb{E}[v]^4$  to obtain

$$\mathbb{E}_{\theta_i \sim \mu}[V(\theta_i)^2] = \frac{2^d (\pi\varepsilon)^{3d/2} \left( \frac{\varepsilon}{2} p^3 \|\nabla f\|^2 + O(\varepsilon^2) \right)}{(2\pi\varepsilon)^{2d} p^4} = \frac{2^{-d} \pi^{-d/2} \varepsilon^{-d/2} \left( \varepsilon \|\nabla f(w)\|^2 + O(\varepsilon^2) \right)}{p(w)}$$

## D Dynamic PCA Kalman Filter Equations

We provide the standard EM algorithm procedure and Kalman filter equations for the Dynamic PCA benchmark outlined in Section 5.1.3 below:

### D.1 E-Step: Kalman Filter with Joint Observations

The Kalman filter is used to estimate the latent state  $\mathbf{Z}_t$  and the corresponding state covariance  $P_{t|t}$ . Note that for Dynamic PCA we utilize the standard Kalman filter and EM algorithm formulations where we only observe a single set of measurements  $\mathbf{X}_t$ . The transition matrix  $\mathbf{A}$  is known and estimated by fitting a VAR(1) process to the empirical PC components computed from the data, and the state covariance matrix  $\mathbf{Q}$  is computed as the empirical covariance matrix of these PC components. The observation equation is:

$$\mathbf{X}_t = \mathbf{\Gamma} \mathbf{Z}_t + \varepsilon_t \sim \mathcal{N}(0, \mathbf{R})$$

and the state transition equation is:

$$\mathbf{Z}_t = \mathbf{A} \mathbf{Z}_{t-1} + \eta_t, \quad \eta_t \sim \mathcal{N}(0, \mathbf{Q})$$

The steps of the Kalman filter are as follows:

1. Prediction Step:

$$\hat{\psi}_{t|t-1} = \mathbf{A}\hat{\mathbf{Z}}_{t-1|t-1}, \quad P_{t|t-1} = \mathbf{A}P_{t-1|t-1}\mathbf{A}^\top + \mathbf{Q}$$

2. Innovation (Residual):

$$\text{innovation}_t = \mathbf{X}_t - \mathbf{\Gamma}\hat{\mathbf{Z}}_{t|t-1}$$

3. Innovation Covariance:

$$S_t = \mathbf{\Gamma}P_{t|t-1}\mathbf{\Gamma}^\top + \mathbf{R}$$

4. Kalman Gain:

$$K_t = P_{t|t-1}\mathbf{\Gamma}^\top S_t^{-1}$$

5. Update Step:

$$\hat{\mathbf{Z}}_{t|t} = \hat{\mathbf{Z}}_{t|t-1} + K_t \text{innovation}_t, \quad P_{t|t} = (I - K_t\mathbf{\Gamma})P_{t|t-1}$$

6. Log-Likelihood Contribution:

$$\mathcal{L}_t = -\frac{1}{2} \left( \log |S_t| + \text{innovation}_t^\top S_t^{-1} \text{innovation}_t + p \log 2\pi \right)$$

where  $p$  is the dimension of  $\mathbf{X}_t$

After running the Kalman filter, we apply the Rauch-Tung-Striebel (RTS) smoother:

1. Initialize at  $T$ :

$$\hat{\mathbf{Z}}_{T|T} = \hat{\mathbf{Z}}_{T|T}, \quad P_{T|T} = P_{T|T}$$

2. Backward pass for  $t = T - 1, \dots, 1$ :

$$J_t = P_{t|t}\mathbf{A}^\top P_{t+1|t}^{-1}$$

$$\hat{\mathbf{Z}}_{t|T} = \hat{\mathbf{Z}}_{t|t} + J_t \left( \hat{\mathbf{Z}}_{t+1|T} - \hat{\mathbf{Z}}_{t+1|t} \right)$$

$$P_{t|T} = P_{t|t} + J_t (P_{t+1|T} - P_{t+1|t}) J_t^\top$$

## D.2 M-Step: Parameter Updates

After running the Kalman filter, we update the parameter  $\mathbf{R}$  based on the current estimates of  $\mathbf{Z}_t$ .

1. Update  $\mathbf{R}$  using the residuals from the smoothed estimates  $\hat{\mathbf{Z}}_{t|T}$ :

$$\mathbf{R} = \frac{1}{T} \sum_{t=1}^T \left( \mathbf{X}_t - \mathbf{\Gamma}\hat{\mathbf{Z}}_t \right) \left( \mathbf{X}_t - \mathbf{\Gamma}\hat{\mathbf{Z}}_t \right)^\top$$

### D.3 EM Algorithm

---

**Algorithm 7** EM Algorithm Iteration
 

---

```

1: Initialize the parameter  $\mathbf{R}$ .
2: Set tolerance  $\varepsilon$  and maximum iterations  $N_{\max}$ .
3: Initialize log-likelihood  $\mathcal{L}^{(0)} \leftarrow -\infty$ , iteration counter  $k \leftarrow 0$ .
4: while not converged and  $k < N_{\max}$  do
5:   E-step: Run Joint Diffusion Kalman filter using current estimate  $\mathbf{R}$ .
6:   Output: Estimate  $\psi_t$  and compute the log-likelihood  $\mathcal{L}^{(k+1)}$ .
7:   M-step: Update  $\mathbf{R}$  using the smoothed estimates of  $\mathbf{Z}_t$ .
8:   Convergence check:
9:   if  $|\mathcal{L}^{(k+1)} - \mathcal{L}^{(k)}| < \varepsilon$  then
10:    Converged: Stop the algorithm.
11:  else
12:     $k \leftarrow k + 1$ 
13:  end if
14: end while

```

---

## E Macroeconomic Factors Data

We use the macroeconomic factors from FRED-MD by [MN16] plus the eight factors found by [GW08]. We use the version of this data that was curated in [CPZ20] and the following transformations were applied:

Table E.1: Transformations (tCodes) for Macroeconomic Variables

tCode	Transformation Description
1	No transformation
2	$\Delta x_t$
3	$\Delta^2 x_t$
4	$\log(x_t)$
5	$\Delta \log(x_t)$
6	$\Delta^2 \log(x_t)$
7	$\Delta(x_t/x_{t-1} - 1.0)$

Table E.2: Macroeconomic Variables (based on table IA.XVI of [CPZ20])

Variable Name	Description	Source	tCode
RPI	Real Personal Income	Fred-MD	5
W875RX1	Real personal income ex transfer receipts	Fred-MD	5
DPCERA3M086SBEA	Real personal consumption expenditures	Fred-MD	5
CMRMTSPLx	Real Manu. and Trade Industries Sales	Fred-MD	5
RETAILx	Retail and Food Services Sales	Fred-MD	5
INDPRO	IP Index	Fred-MD	5
IPFPNSS	IP: Final Products and Nonindustrial Supplies	Fred-MD	5
IPFINAL	IP: Final Products (Market Group)	Fred-MD	5
IPCONGD	IP: Consumer Goods	Fred-MD	5

<b>Variable Name</b>	<b>Description</b>	<b>Source</b>	<b>tCode</b>
IPDCONGD	IP: Durable Consumer Goods	Fred-MD	5
IPNCONGD	IP: Nondurable Consumer Goods	Fred-MD	5
IPBUSEQ	IP: Business Equipment	Fred-MD	5
IPMAT	IP: Materials	Fred-MD	5
IPDMAT	IP: Durable Materials	Fred-MD	5
IPNMAT	IP: Nondurable Materials	Fred-MD	5
IPMANSICS	IP: Manufacturing (SIC)	Fred-MD	5
IPB51222S	IP: Residential Utilities	Fred-MD	5
IPFUELS	IP: Fuels	Fred-MD	5
CUMFNS	Capacity Utilization: Manufacturing	Fred-MD	2
HWI	Help-Wanted Index for United States	Fred-MD	2
HWIURATIO	Ratio of Help Wanted/No. Unemployed	Fred-MD	2
CLF16OV	Civilian Labor Force	Fred-MD	5
CE16OV	Civilian Employment	Fred-MD	5
UNRATE	Civilian Unemployment Rate	Fred-MD	2
UEMPMEAN	Average Duration of Unemployment (Weeks)	Fred-MD	2
UEMPLT5	Civilians Unemployed - Less Than 5 Weeks	Fred-MD	5
UEMP5TO14	Civilians Unemployed for 5-14 Weeks	Fred-MD	5
UEMP15OV	Civilians Unemployed - 15 Weeks & Over	Fred-MD	5
UEMP15T26	Civilians Unemployed for 15-26 Weeks	Fred-MD	5
UEMP27OV	Civilians Unemployed for 27 Weeks and Over	Fred-MD	5
CLAIMSx	Initial Claims	Fred-MD	5
PAYEMS	All Employees: Total nonfarm	Fred-MD	5
USGOOD	All Employees: Goods-Producing Industries	Fred-MD	5
CES1021000001	All Employees: Mining and Logging: Mining	Fred-MD	5
USCONS	All Employees: Construction	Fred-MD	5
MANEMP	All Employees: Manufacturing	Fred-MD	5
DMANEMP	All Employees: Durable goods	Fred-MD	5
NDMANEMP	All Employees: Nondurable goods	Fred-MD	5
SRVPRD	All Employees: Service-Providing Industries	Fred-MD	5
USTPU	All Employees: Trade, Transportation & Utilities	Fred-MD	5
USWTRADE	All Employees: Wholesale Trade	Fred-MD	5
USTRADE	All Employees: Retail Trade	Fred-MD	5
USFIRE	All Employees: Financial Activities	Fred-MD	5
USGOVT	All Employees: Government	Fred-MD	5
CES0600000007	Avg Weekly Hours : Goods-Producing	Fred-MD	1
AWOTMAN	Avg Weekly Overtime Hours : Manufacturing	Fred-MD	2
AWHMAN	Avg Weekly Hours : Manufacturing	Fred-MD	1
HOUST	Housing Starts: Total New Privately Owned	Fred-MD	4
HOUSTNE	Housing Starts, Northeast	Fred-MD	4
HOUSTMW	Housing Starts, Midwest	Fred-MD	4
HOUSTS	Housing Starts, South	Fred-MD	4
HOUSTW	Housing Starts, West	Fred-MD	4
PERMIT	New Private Housing Permits (SAAR)	Fred-MD	4
PERMITNE	New Private Housing Permits, Northeast (SAAR)	Fred-MD	4
PERMITMW	New Private Housing Permits, Midwest (SAAR)	Fred-MD	4
PERMITS	New Private Housing Permits, South (SAAR)	Fred-MD	4
PERMITW	New Private Housing Permits, West (SAAR)	Fred-MD	4
AMDMNOx	New Orders for Durable Goods	Fred-MD	5
AMDMUOx	Unfilled Orders for Durable Goods	Fred-MD	5
BUSINVx	Total Business Inventories	Fred-MD	5

<b>Variable Name</b>	<b>Description</b>	<b>Source</b>	<b>tCode</b>
ISRATIOx	Total Business: Inventories to Sales Ratio	Fred-MD	2
M1SL	M1 Money Stock	Fred-MD	6
M2SL	M2 Money Stock	Fred-MD	6
M2REAL	Real M2 Money Stock	Fred-MD	5
AMBSL	St. Louis Adjusted Monetary Base	Fred-MD	6
TOTRESNS	Total Reserves of Depository Institutions	Fred-MD	6
NONBORRES	Reserves Of Depository Institutions	Fred-MD	7
BUSLOANS	Commercial and Industrial Loans	Fred-MD	6
REALLN	Real Estate Loans at All Commercial Banks	Fred-MD	6
NONREVSL	Total Nonrevolving Credit	Fred-MD	6
CONSPI	Nonrevolving consumer credit to Personal Income	Fred-MD	2
S&P 500	S&P's Common Stock Price Index: Composite	Fred-MD	5
S&P: indust	S&P's Common Stock Price Index: Industrials	Fred-MD	5
S&P div yield	S&P's Composite Common Stock: Dividend Yield	Fred-MD	2
S&P PE ratio	S&P's Composite Common Stock: Price-Earnings Ratio	Fred-MD	5
FEDFUNDS	Effective Federal Funds Rate	Fred-MD	2
CP3Mx	3-Month AA Financial Commercial Paper Rate	Fred-MD	2
TB3MS	3-Month Treasury Bill	Fred-MD	2
TB6MS	6-Month Treasury Bill	Fred-MD	2
GS1	1-Year Treasury Rate	Fred-MD	2
GS5	5-Year Treasury Rate	Fred-MD	2
GS10	10-Year Treasury Rate	Fred-MD	2
AAA	Moody's Seasoned Aaa Corporate Bond Yield	Fred-MD	2
BAA	Moody's Seasoned Baa Corporate Bond Yield	Fred-MD	2
COMPAPFFx	3-Month Commercial Paper Minus FEDFUNDS	Fred-MD	1
TB3SMFFM	3-Month Treasury C Minus FEDFUNDS	Fred-MD	1
TB6SMFFM	6-Month Treasury C Minus FEDFUNDS	Fred-MD	1
T1YFFM	1-Year Treasury C Minus FEDFUNDS	Fred-MD	1
T5YFFM	5-Year Treasury C Minus FEDFUNDS	Fred-MD	1
T10YFFM	10-Year Treasury C Minus FEDFUNDS	Fred-MD	1
AAAFFM	Moody's Aaa Corporate Bond Minus FEDFUNDS	Fred-MD	1
BAAFFM	Moody's Baa Corporate Bond Minus FEDFUNDS	Fred-MD	1
EXSZUSx	Switzerland / U.S. Foreign Exchange Rate	Fred-MD	5
EXJPUSx	Japan / U.S. Foreign Exchange Rate	Fred-MD	5
EXUSUKx	U.S. / U.K. Foreign Exchange Rate	Fred-MD	5
EXCAUSx	Canada / U.S. Foreign Exchange Rate	Fred-MD	5
WPSFD49207	PPI: Finished Goods	Fred-MD	6
WPSFD49502	PPI: Finished Consumer Goods	Fred-MD	6
WPSID61	PPI: Intermediate Materials	Fred-MD	6
WPSID62	PPI: Crude Materials	Fred-MD	6
OILPRICEx	Crude Oil, spliced WTI and Cushing	Fred-MD	6
PPICMM	PPI: Metals and metal products	Fred-MD	6
CPIAUCSL	CPI : All Items	Fred-MD	6
CPIAPPSL	CPI : Apparel	Fred-MD	6
CPITRNSL	CPI : Transportation	Fred-MD	6
CPIMEDSL	CPI : Medical Care	Fred-MD	6
CUSR0000SAC	CPI : Commodities	Fred-MD	6
CUSR0000SAD	CPI : Durables	Fred-MD	6
CUSR0000SAS	CPI : Services	Fred-MD	6
CPIULFSL	CPI : All Items Less Food	Fred-MD	6
CUSR0000SA0L2	CPI : All items less shelter	Fred-MD	6

<b>Variable Name</b>	<b>Description</b>	<b>Source</b>	<b>tCode</b>
CUSR0000SA0L5	CPI : All items less medical care	Fred-MD	6
PCEPI	Personal Cons. Expend.: Chain Index	Fred-MD	6
DDURRG3M086SBEA	Personal Cons. Exp: Durable goods	Fred-MD	6
DNDGRG3M086SBEA	Personal Cons. Exp: Nondurable goods	Fred-MD	6
DSERRG3M086SBEA	Personal Cons. Exp: Services	Fred-MD	6
CES0600000008	Avg Hourly Earnings : Goods-Producing	Fred-MD	6
CES2000000008	Avg Hourly Earnings : Construction	Fred-MD	6
CES3000000008	Avg Hourly Earnings : Manufacturing	Fred-MD	6
MZMSL	MZM Money Stock	Fred-MD	6
DTCOLNVHFNM	Consumer Motor Vehicle Loans Outstanding	Fred-MD	6
DTCTHFNM	Total Consumer Loans and Leases Outstanding	Fred-MD	6
INVEST	Securities in Bank Credit at All Commercial Banks	Fred-MD	6
VXOCLSx	CBOE S&P 100 Volatility Index: VXO	Fred-MD	1
dp	Dividend-price ratio	W & G	2
ep	Earnings-price ratio	W & G	2
bm	Book-to-market ratio	W & G	5
ntis	Net equity expansion	W & G	2
tbl	Treasury-bill rate	W & G	2
tms	Term spread	W & G	1
dfy	Default spread	W & G	2
svar	Stock variance	W & G	5